University of Miami
Scholarly Repository

Open Access Dissertations | Electronic Theses and Dissertations

2009-06-16

Physicochemical Studies of the Grb2-Sos1 Interaction

Caleb Benton McDonald
University of Miami, cmcdonald@med.miami.edu

Follow this and additional works at: http://scholarlyrepository.miami.edu/oa_dissertations

Recommended Citation
McDonald, Caleb Benton, "Physicochemical Studies of the Grb2-Sos1 Interaction" (2009). *Open Access Dissertations.* Paper 260.

This Open access is brought to you for free and open access by the Electronic Theses and Dissertations at Scholarly Repository. It has been accepted for inclusion in Open Access Dissertations by an authorized administrator of Scholarly Repository. For more information, please contact repository.library@miami.edu.

UNIVERSITY OF MIAMI

PHYSICOCHEMICAL STUDIES OF THE GRB2-SOS1 INTERACTION

By

Caleb B. McDonald

A DISSERTATION

Submitted to the Faculty
of the University of Miami
in partial fulfillment of the requirements for
the degree of Doctor of Philosophy

Coral Gables, Florida

June 2009

©2009
Caleb B. McDonald
All Rights Reserved

UNIVERSITY OF MIAMI

A dissertation submitted in partial fulfillment of
the requirements for the degree of
Doctor of Philosophy

PHYSICOCHEMICAL STUDIES OF THE GRB2-SOS1 INTERACTION

Caleb B. McDonald

Approved:

Thomas K. Harris, Ph.D. Associate Professor of Biochemistry & Molecular Biology	Terri A. Scandura, Ph.D. Dean of the Graduate School
Amjad Farooq, Ph.D. Assistant Professor of Biochemistry & Molecular Biology	Joyce M. Slingerland, M.D. Ph.D. Professor of Medicine
Kerry L. Burnstein, Ph.D. Professor of Molecular & Cellular Pharmacology	Andrew C. Terentis, Ph.D. Assistant Professor of Chemistry Florida Atlantic University Boca Raton, Florida

McDONALD, CALEB B. (Ph.D., Biochemistry & Molecular Biology)

Physicochemical Studies of the Grb2-Sos1 Interaction (June 2009)

Abstract of a dissertation at the University of Miami.

Dissertation supervised by Assistant Professor Amjad Farooq.
No. of pages in text. (139)

Grb2, a modular protein comprised of a central SH2 domain flanked between a N-terminal SH3 (nSH3) domain and a C-terminal SH3 (cSH3) domain, is a component of cell signaling networks involved in the transmission of extracellular information in the form of growth factors and cytokines to downstream targets such as transcription factors within the nucleus. The Grb2-Sos1 interaction is mediated through the combinatorial binding of nSH3 and cSH3 domains of Grb2 to various sites — designated S1, S2, S3, and S4 — containing PXψPXR motifs within Sos1. Here, using a diverse array of biophysical techniques, including in particular isothermal titration calorimetry coupled with molecular modeling and semi-empirical analysis, I provide new insights into the Grb2-Sos1 interaction in thermodynamic and structural terms.

My data show that Grb2 exists in monomer-dimer equilibrium in solution and that the dissociation of dimer into monomers is entropically-driven. The heat capacity change observed was much smaller than that expected from the rather large molecular surfaces becoming solvent-occluded upon dimerization, implying that monomers undergo conformational rearrangement upon dimerization. 3D structural models suggest strongly that such conformational rearrangement may arise from domain swapping. I further show that the nSH3 domain of Grb2 binds to the S1 site containing the proline-rich consensus motif PXψPXR with an affinity that is nearly three-fold greater than that observed for the binding of the cSH3 domain. It is also demonstrated that such differential binding of the nSH3 domain relative to the cSH3 domain is largely due to the requirement of a specific

acidic residue, in the RT loop, to engage in the formation of a salt bridge with the arginine residue in the consensus motif PXψPXR. The data further reveal that, while binding of both SH3 domains to Sos1 is under enthalpic control, the nSH3 binding suffers from entropic penalty in contrast to entropic gain accompanying the binding of cSH3, implying that the two domains employ differential thermodynamic mechanisms for Sos1 recognition. Additionally, my data reveal that while the nSH3 domain of Grb2 binds with affinities in the physiological range to all four sites S1-S4, the cSH3 domain can only do so at the S1 site. Further scrutiny of these sites yields rationale for the recognition of various PXψPXR motifs by the SH3 domains in a discriminate manner. Unlike the PXψPXR motifs at S2, S3 and S4 sites, the PXψPXR motif at S1 site is flanked at its C-terminus with two additional arginine residues that are absolutely required for high-affinity binding of the cSH3 domain. In contrast, these two additional arginine residues augment the binding of the nSH3 domain to the S1 site but their role is not critical for the recognition of S2, S3 and S4 sites. Molecular modeling is employed to rationalize my new findings in structural terms.

Taken together, this thesis provides novel insights into the physicochemical basis of a key protein-protein interaction pertinent to cellular signaling and cancer. My studies bear the potential for the development of novel therapies with less toxicity but more effectiveness for the treatment of disease.

ACKNOWLEDGEMENTS

I would like to offer my deepest thanks to Dr. Amjad Farooq for his brilliant mentorship. I could not have asked for a better mentor throughout this process. Amjad has been a good a source of knowledge, help, constructive criticism, and enthusiasm for the work and science in general. He provided a superb laboratory setting that made my work possible. Without the organization, equipment, and level of technology his laboratory provided, I would not have been able to achieve nearly to the level that I did. Furthermore, Amjad's drive for perfection was an inspiration to me, and motivated me to excel in my work and develop into a better scientist than I would have otherwise. I cannot thank Amjad enough for taking the time, effort and patience to mentor me throughout this process.

I owe a lot to the other members of the Farooq Laboratory. Without the help of Kenneth Seldeen and Brian Deegan on a daily basis my project would not have been possible. Everything in the laboratory was done as a team effort from making buffers to discussing important aspects of everyone's projects. Without this team atmosphere my work would have been much more difficult. I am grateful to have worked with two great laboratory members that have helped to make this an enjoyable process.

I would like to acknowledge the members of my committee. I would like to thank Dr. Thomas Harris for being the chairman of my committee, and giving useful insight into my work. I thank Dr. Joyce Slingerland for all of her help as a member of my committee and through the Braman Family Breast Cancer Institute. Furthermore, I would like to thank Dr. Kerry Burnstein for helping to critically evaluate my work and provide helpful input. Lastly, I would like to thank Dr. Andrew Terentis for agreeing to be my external examiner, and traveling down from Florida Atlantic University for my

dissertation. I have benefited greatly from the knowledge that my committee members have helped to impart to me and I am grateful for their time, participation, and help in this process.

I would like to acknowledge the National Institutes of Health, the American Heart Association, and the Braman Family Breast Cancer Institute for helping to fund my work. Without funding from these organizations, my work would not have been possible.

Lastly, I would like to thank my family. Without the constant love and support of my parents David and Tracy, and brother, Zachary, this process would have been much more difficult. My family has always been there when I needed them, whether it be for advice, support, or just to talk. For that I am deeply grateful.

TABLE OF CONTENTS

LIST OF FIGURES

LIST OF TABLES

1 Chapter 1: Introduction to Grb2, Sos1, and Mitogenic Signaling

1.1 Grb2 is a ubiquitously expressed modular adaptor protein

Growth factor receptor binder 2 (Grb2) is a ubiquitous component of cell signaling networks that couples activated receptor tyrosine kinases (RTKs) to downstream effectors and regulators (Figure 1-2). The critical role of Grb2 in cellular signaling is exquisitely demonstrated through defects in mice embryos upon the disruption of *grb2* gene [1].

Grb2 is a modular protein comprised of a central SH2 domain flanked between a N-terminal (nSH3) domain and a C-terminal (cSH3) domain, giving it an overall modular architecture of nSH3-SH2-cSH3 (Figure 1-1) [2]. Grb2 recognizes activated RTKs by virtue of its SH2 domain to bind to phosphotyrosine (pY) sequences in the context of the consensus motif pYXN located within the cytoplasmic tails of a diverse array of receptors, including epidermal growth factor (EGF) and platelet-derived growth factor (PDGF) receptors [3, 4]. Alternatively, Grb2 can also indirectly dock onto activated RTKs through the binding of its SH2 domain to pY sequences within the adaptor protein p52Shc [5, 6]. Given a much broader spectrum of RTKs recognized by p52Shc, Grb2 is more often seen to fulfill this latter role instead of directly binding to RTKs upon receptor stimulation.

For its part, p52Shc contains at least two well-conserved YXN motifs at positions Y239 and Y317 that are subject to phosphorylation by a diverse array of protein tyrosine kinases, including the Src kinase family, upon its recruitment to receptor tails in response to extracellular mitogenic stimuli [7-9]. It has been shown that phosphorylation of both Y239 and Y317 in p52Shc is required for efficient recruitment of Grb2 to the inner-

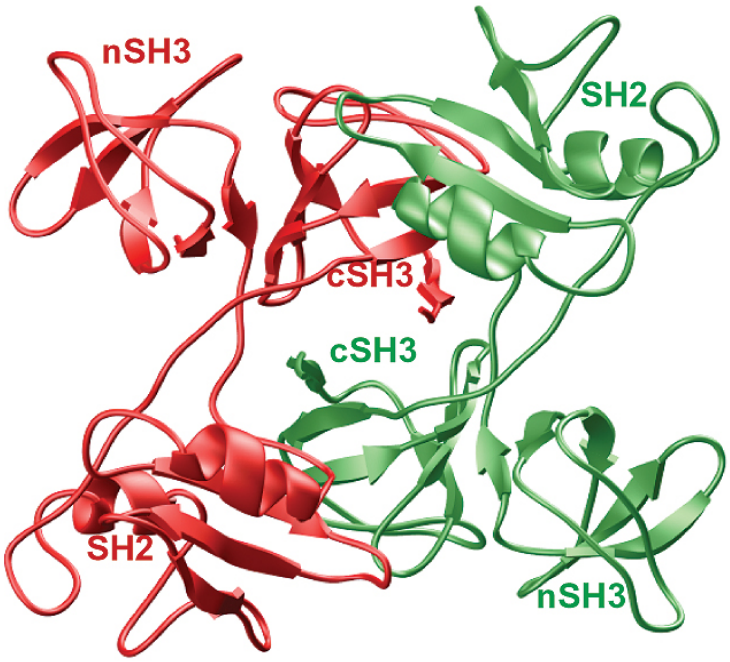

Figure 1-1: 3D structure of Grb2 dimer. One monomer is shown in red and the other in green. The three domains nSH3, SH2 and cSH3 are labeled. The protein crystallized as a dimer with two-fold axis of symmetry; the SH2 domain of one monomer docks against the cSH3 domain of the other and vice versa in a head-to-tail fashion [10].

membrane surface [11]; could this necessity be explained by the ability of Grb2 to participate in cellular signaling as a dimer?

1.2 Grb2 may participate as a dimer in cellular signaling

Grb2 is architecturally one of the simplest and smallest adaptor proteins with an overall modular architecture of nSH3-SH2-cSH3 [2]. The availability of its complete 3D structure has rendered Grb2 a prototype for understanding the function of other adaptor proteins in cellular signaling [10]. In the 3D crystal structure of Grb2, the protein crystallized as a dimer with two-fold axis of symmetry; the SH2 domain of one monomer docks against the cSH3 domain of the other and vice versa in a head-to-tail fashion (Figure 1-1) [10]. In this manner, the ligand binding sites in the SH2 and the SH3 domains remain fully exposed to solution and thereby rendering Grb2 in an active state and fully primed to participate in cellular signaling within the dimeric assembly. To

paraphrase this slightly, the role of Grb2 dimerization appears to activate the protein further rather than providing a negative regulatory switch that may need to be invoked upon receptor stimulation. Such a dimeric assembly of Grb2 is also expected to eliminate the need for any conformational change prior to interaction with upstream RTKs or downstream effector molecules. The extent to which Grb2 dimerization prevails in solution and the extent to which the monomers may have to undergo conformational change upon dimerization is not clear. Does Grb2 dimerize in solution? Do the monomers come together as rigid bodies to generate the Grb2 dimer or do they have to undergo some sort of conformational change upon dimerization?

1.3 Grb2 plays a key role in mitogenic signaling

Upon the recruitment of Grb2 to RTKs directly or indirectly, the SH3 domains of Grb2 present a placid opportunity for a wide variety of proteins, containing proline-rich sequences, to be recruited to the inner membrane surface and thus engage in downstream cellular signaling cascades (Figure 1-2). Some of the best characterized downstream partners of Grb2 SH3 domains are the guanine nucleotide exchange factor Son of sevenless 1 (Sos1) [12, 13], the adaptor protein Grb2-associated binding protein 1 (Gab1) [14, 15], the endocytic GTPase dynamin1 [16, 17], the ubiquitin ligase casitas B-lineage lymphoma proto-oncogene (Cbl) [15, 18, 19] and the cell cycle inhibitor cyclin-dependent kinase inhibitor 1B (p27kip1) [20].

Upon recruitment to the inner membrane surface, these downstream effectors of Grb2 exert a wide multitude of biological responses. For example, Sos1 facilitates the GDP-GTP exchange within the small membrane-bound GTPase Ras and thereby switches on a key signaling circuit that involves the activation of the MAP kinase (MAPK) cascade central to cellular proliferation, survival and differentiation [21, 22].

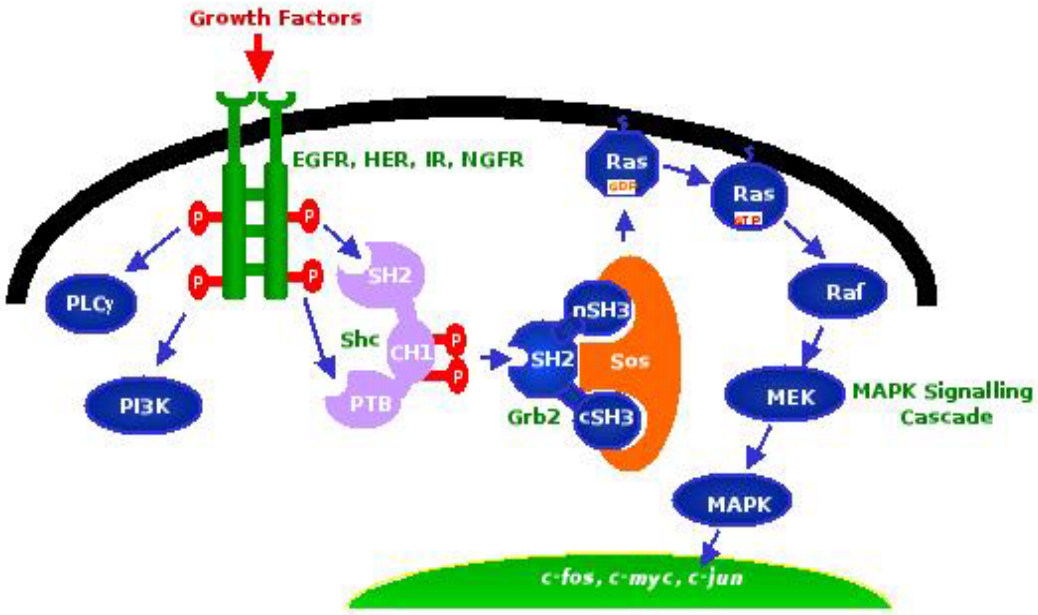

Figure 1-2: Grb2 mediates transmission of information from activated receptors to downstream targets through the Ras and Akt pathways. Upon the interaction of Grb2 to RTKs directly or indirectly, the SH3 domains of Grb2 present a placid opportunity for a wide variety of proteins, containing proline-rich sequences, to be recruited to the inner membrane surface and thus engage in downstream cellular signaling cascades. Some of the best characterized downstream partners of Grb2 SH3 domains are Sos1 [12, 13], Gab1 [14, 15], dynamin1 [16, 17], Cbl [15, 18, 19] and p27kip1 [20].

Likewise, the recruitment of Gab1 provides docking platforms for the protein tyrosine phosphatase Shp2 and the lipid kinase PI3K, which respectively account for further amplification of Ras activity. Sustained activation of Ras requires both the Sos1-dependent and Gab1-dependent pathways [23-25] as well as the activation of the serine-threonine kinase Akt/PKB, which plays a pivotal role in cell growth and survival [26].

The recruitment of dynamin1 to the inner membrane surface is believed to trigger clathrin-mediated receptor endocytosis of EGFR, a key mechanism for initiating intracellular signaling [27, 28]. In contrast, the recruitment of Cbl to the p52Shc-Grb2 signaling complex at the inner membrane surface results in ubiquitination of EGFR and its subsequent degradation, a step critical for negating the oncogenic potential of EGFR

[29]. Finally, the recruitment of p27kip1 to the Shc-Grb2 signaling complex appears to negatively regulate the activity of Ras by virtue of its ability to compete with Sos1 for binding to Grb2 [20].

1.4 The Grb2-Sos1 interaction is critical to mitogenic signaling

Early studies revealed that Grb2 binds to the proline-rich (PR) domain of Sos1 and recruits Sos1 to activated RTKs [30]. The recruitment of Sos1 to the plasma membrane is necessary for the activation of Ras [31-33]. The PR domain can bind to Grb2 which recruits it to the membrane [34]. Sos1 contains four distinct sites within its PR domain for binding to the SH3 domains of Grb2. These sites, designated S1, S2, S3 and S4, conform to the PXψPXR canonical consensus motif, where X is any residue and ψ is valine, leucine or isoleucine (Figure 1-5). Although site-directed mutagenesis studies suggest that PXψPXR is the minimal motif required for high-affinity binding to the nSH3 domain [35], the extent to which residues flanking this motif may be non-redundant for binding to the cSH3 domain is not understood. Furthermore, several studies have shown that the requirement of both SH3 domains of Grb2 is mandatory for full and sustained activation of Ras [6, 12, 13, 36]. However, biophysical analysis of the binding of the SH3 domains of Grb2 to the Sos1-derived S1 peptide suggests that the affinity of the nSH3 domain for Sos1 is several-fold greater than that observed for the cSH3 domain [37].

Structural studies of the nSH3 domain of Grb2 in complex with peptides derived from the S1 site in Sos1 indicate the nSH3 domain folds into a characteristic β-barrel architecture resulting in the formation of a hydrophobic cleft on one face of the domain for accommodating the incoming peptide (Figure 1-4) [35, 38-40]. While the β-barrel is comprised of a pair of nearly-orthogonal β-sheets, with each β-sheet containing three

anti-parallel β-strands, the peptide adopts a relatively open left-handed polyproline type II (PPII) helical conformation upon binding. Studies suggest that the cSH3 domain of Grb2 is likely to bind to S1 peptide in a manner akin to that observed for the nSH3 domain [41].

In comparison with the binding modes of proline-rich ligands to other SH3 domains, the residues in the S1 peptide that account for its specificity to the nSH3 domain of Grb2 appear to be V_{+2} and R_{+5} within the consensus motif PPVPPR, according

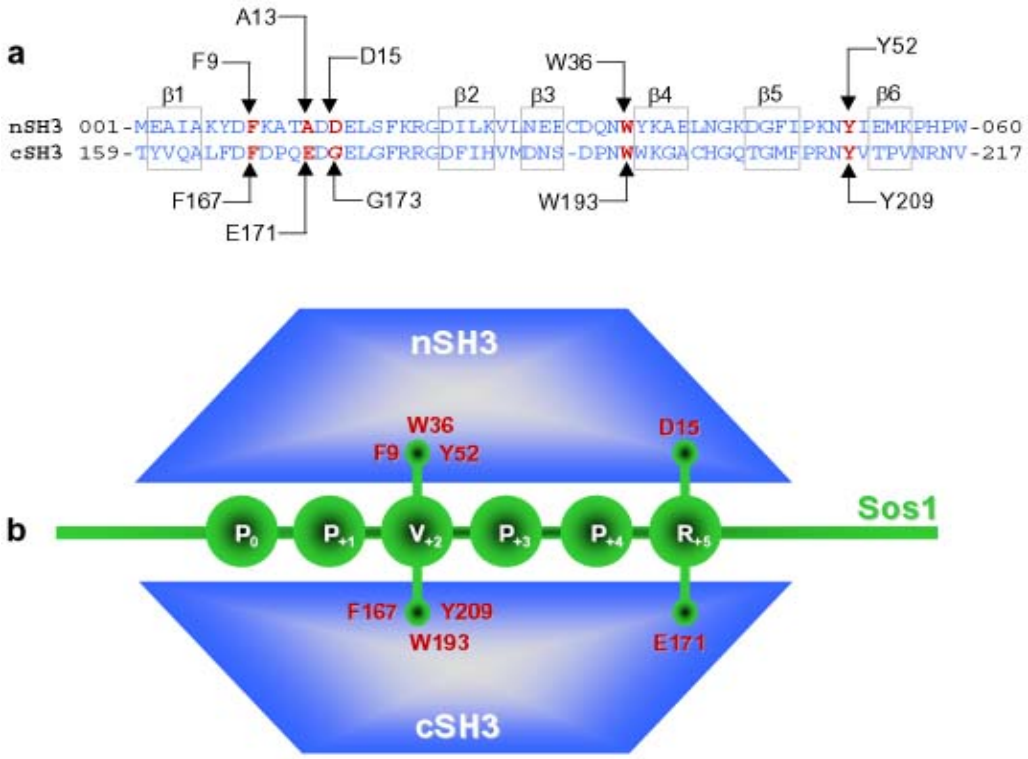

Figure 1-3: Sequence analysis of SH3 domains of Grb2 and the proline-rich motif PPVPPR within the Sos1 peptide. (a) Sequence alignment of nSH3 and cSH3 domains of Grb2 highlighting the structurally equivalent residues. The residues in each of the six strands β1-β6, as observed in the 3D structure of the nSH3 domain [35, 38-40], constituting the β-barrel fold are boxed. The residues in the SH3 domains predicted to be involved in stabilizing hydrophobic and electrostatic interactions respectively due to the valine and the arginine in the Sos1 proline-rich motif PPVPPR are colored red. Note that the C32 in the β3-β4 loop of the nSH3 domain is deleted in the cSH3 domain. (b) A cartoon diagram showing the residues in the SH3 domains predicted to be involved in stabilizing hydrophobic and electrostatic interactions respectively due to the valine and the arginine in the Sos1 proline-rich motif PPVPPR.

to the nomenclature suggested by Schreiber and co-workers [42], with the first proline within this motif designated zero. Alanine substitution of V_{+2} and R_{+5} individually indeed reduces the affinity of the Sos1 peptide for the nSH3 domain by about 10-20 fold [35]. Due to lower binding affinity, structural analysis of cSH3 domain in complex with a Sos1 peptide has not hitherto been possible but NMR analysis suggests that Sos1 binds to the cSH3 domain in a manner akin to that observed for its interaction with the nSH3 domain [37].

Pair-wise amino acid sequence alignment of nSH3 and cSH3 domains illustrates that V_{+2} and R_{+5} within the consensus motif PPVPPR account for the binding specificity of Sos1 to nSH3 domain (Figure 1-3a) [35]. Structural analysis of nSH3 domain in complex with the S1 peptide containing the consensus motif PPVPPR has previously indicated that V_{+2} inserts into a deep hydrophobic pocket formed by residues F9, W36 and Y52 within the nSH3 domain, while R_{+5} very likely engages in the formation of an energetically favorable salt bridge with acidic residues D15 and/or E16 located within the β1-β2 loop of the nSH3 domain [35, 38]. The β1-β2 loop is more widely known as the RT loop in the context of the β-barrel fold of SH3 domains due to the observation that the mutations of arginine and threonine residues within this loop of the SH3 domain of Src tyrosine kinase are important determinants of its transforming potential [43]. Analysis of the amino acid sequence alignment reveals that the triplet of F9/W36/Y52 in the nSH3 domain is absolutely conserved in the cSH3 domain with the structurally equivalent residues being F167/W193/Y209 (Figure 1-3a). Thus, the differential binding of nSH3 and cSH3 domains to Sos1 could not be explained in terms of the requirement of specific residues within the SH3 domain for stabilizing V_{+2} within the consensus motif PPVPPR.

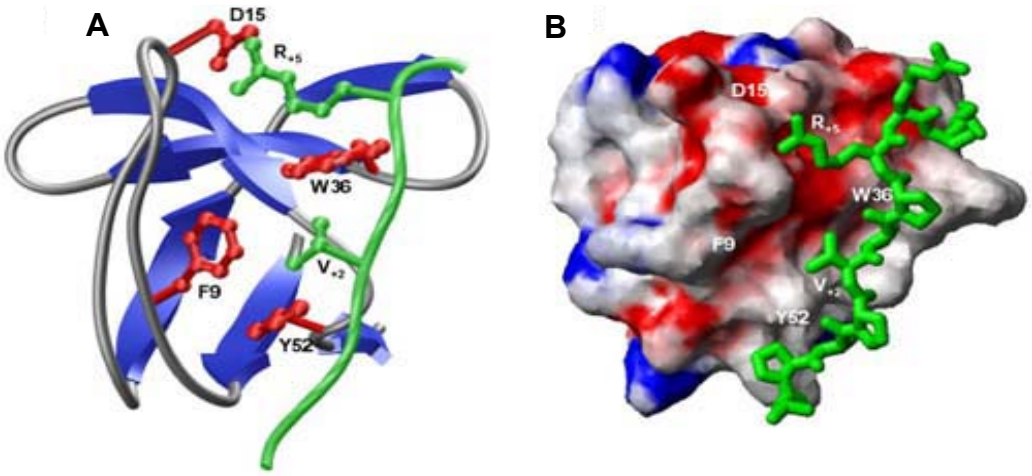

Figure 1-4: 3D structures of wildtype SH3 domains of Grb2 in complex with the Sos1 peptide PVPPPVPPRRRP. (a) Ribbon representation of nSH3 domain bound to Sos1 peptide. The nSH3 domain is shown in blue with loops depicted in gray and the sidechains of residues that stabilize the V_{+2} and R_{+5} residues in the Sos1 peptide are colored red. The Sos1 peptide, including the sidechains of V_{+2} and R_{+5} residues, is colored green. (b) Electrostatic surface potential view of nSH3 domain. The blue and red colors respectively denote the density of positive and negative charges, while the hydrophobic and neutral surfaces are indicated by white/gray color. The Sos1 peptide, including the sidechain of all residues, is shown in green.

Also phosphorylation of Y209 in the cSH3 has been demonstrated to abrogate binding [44]. In contrast, while E16 in the nSH3 domain is absolutely conserved by the structurally equivalent E174 in the cSH3 domain, the same is not true for D15 in the nSH3 domain, which is substituted by the structurally equivalent G173 in the cSH3 domain. Assuming that it is D15 and not E16 in the nSH3 domain that salt bridges with R_{+5} within the consensus motif PPVPPR, this scenario could easily explain the differential binding of nSH3 and cSH3 domains to Sos1 as the substitution of a glycine for an aspartate at a critical salt bridging position would likely result in the partial loss of binding affinity. Although the cSH3 domain lacks an acidic residue at the structurally equivalent position occupied by D15 in the nSH3 domain, the residue E171 lies within close proximity to G173 within the RT loop and thus could be a strong candidate for fulfilling the role of a salt bridging partner for R_{+5} within the consensus motif PPVPPR. In light of the foregoing argument, we hypothesize that the differential binding of nSH3

and cSH3 domains to a Sos1 peptide containing the consensus motif PPVPPR is likely due to the ability of D15 within the nSH3 domain to salt bridge with R_{+5}, while this role may only partially be fulfilled by a chemically distinct and structurally non-equivalent residue E171 in the cSH3 domain due to the absence of an acidic residue at the structurally equivalent position D15 (Figure 4-1b).

1.5 Sos1 is a large multi-domain protein capable of signaling in several critical cellular pathways

Human Sos1 is a large multi-domain protein of 1333 residues (Figure 1-5) [12]. A central 500 residue catalytic module is sufficient for the Ras-specific nucleotide exchange activity. This segment of Sos1 includes a core region known as the CDC25 domain (residues 750 to 1050), so named because of sequence homology to CDC25, a Ras-specific nucleotide exchange factor in *Saccharomyces cerevisiae* [45, 46]. Sos1 also contains an additional domain, known as the Ras exchanger motif (REM) domain, located N-terminal to the CDC25 domain [47]. The C-terminal segment of Sos1 contains a proline rich (PR) domain containing canonical recognition sites for SH3 domains, PxxP motifs, and mediates the interaction of Sos1 with Grb2, which recruits Sos1 to the membrane upon receptor activation (Figure 1-5). Sos1 also contains a Dbl-homology (DH) domain and a pleckstrin homology (PH) domain, located upstream or N-terminal to the catalytic module. The DH and PH domains are implicated in the ability of Sos1 to activate Rac, a small GTPase of the Rho/cdc42 family (Figure 1-5) [48].

At the N-terminus of Sos1, there are two histone-like folds (HF) comprising the HF domain (Figure 1-5). It is unprecedented for such nucleotide-binding domains to exist outside of the nucleus, making it difficult to predict their function. Computational modeling techniques predict the formation of ion pair interactions between aspartic acid

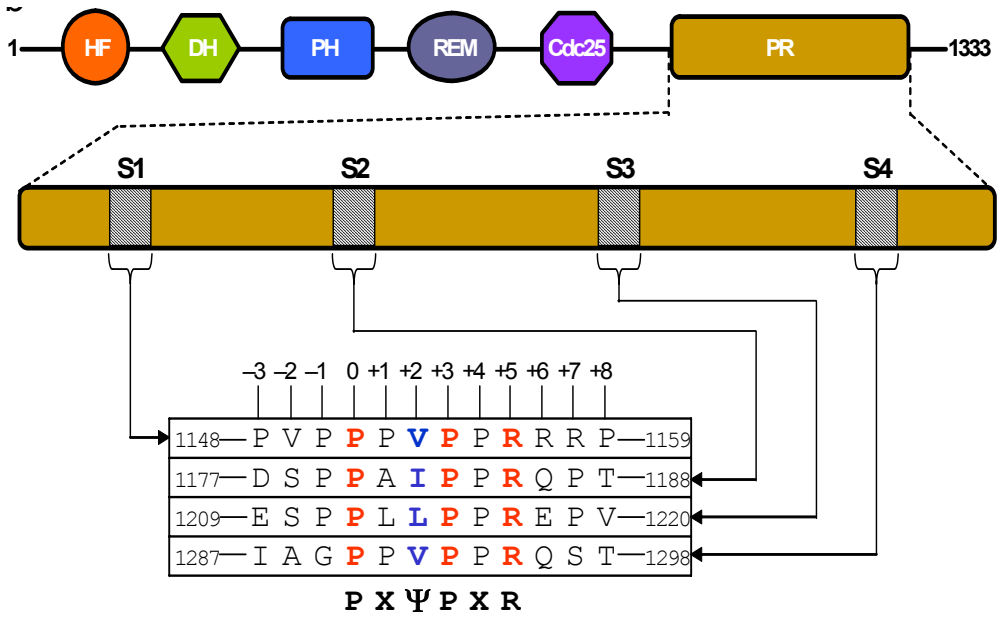

Figure 1-5: Domain organization and sequence analysis of Sos1. The proline-rich (PR) domain of Sos1 lies at the extreme C-terminal end. The PR domain contains four distinct sites (designated S1, S2, S3 and S4) characterized by the PXψPXR consensus motif. The complete sequences of these sites are shown. The position of various residues relative to the first proline within the PXψPX motif, which is designated zero, is also indicated. Other domains within Sos1 shown are HF (histone fold), DH (Dbl homology), PH (pleckstrin homology), REM (Ras exchange motif) and CDC25.

residues within the HF domain and arginines in the helical linker that connects the DH and PH domains of Sos1 to the REM domain [49]. Consistent with this, mutation of D140 in the HF domain or R552 in the linker region completely abolished the interaction between the isolated HF domain and a DH-PH-REM-CDC25 protein fragment in vitro. This suggests that association of the HF domain with the PH-REM linker may keep Sos1 in an inactive conformation prior to cellular stimulation.

C-terminal to the somewhat mysterious HF Domain is the catalytic DH domain (Figure 1-5). The DH domain is the catalytic entity mediating the guanine nucleotide exchange on Rho GTPases [50]. Overexpression of the DH domain of Sos1 leads to the activation of Rac by enhancing the rate of guanine nucleotide exchange [50]. In addition, a molecular complex consisting of Sos1 and two signaling molecules, epidermal growth factor receptor kinase substrate 8 (Eps8) and Abelson interactor 1 (E3b1), has been

shown to possess a Sos1-dependent guanine nucleotide exchange activity toward Rac in vivo and in vitro [51]. Also, the activation of Rac by specific integrins is mediated by the DH domain of Sos1 [52].

Following the DH domain is the PH domain (Figure 1-5). The PH domain of Sos1 has long been known to play a role in the recruitment of Sos1 to the plasma membrane. However, the lipid responsible for this translocation was unclear [52]. It was recently found that, like Sos1, phospholipase D2 (PLD2) is recruited to growth factor receptors by Grb2 [13]. Once at the membrane, it produces phosphatidic acid (PA) that binds to the PH domain of Sos1 to further promote membrane binding and Ras activation [13]. Although Grb2 and PA could differentially regulate Sos1, possibly targeting Sos1 to different intracellular compartments, it is likely that they cooperate to activate Ras. Additionally, the ability of PA to bind to Raf may permit differential signaling through the Raf-MEK–ERK pathway rather than through other Ras effector pathways [53].

C-terminal to the PH domain of Sos1 is the REM/CDC25 catalytic complex (Figure 1-5). The CDC25 domain of Sos1 binds to Ras and promotes the release of GDP so that Ras can bind GTP and adopt an active conformation [53]. The crystal structure of nucleotide-free Ras in complex with the Sos1 REM and CDC25 domains has been determined, explaining how Sos1 facilitates nucleotide release from Ras (Figure 1-6) [54].

1.6 Sos1 facilitates GDP-GTP exchange in the small membrane-bound GTPase Ras

Sos1 functions by opening up and distorting the nucleotide binding site of Ras, expelling either GTP or GDP. Key features of the mechanism include the movement of Switch 1 of Ras away from the nucleotide binding site and a restructuring of Switch 2.

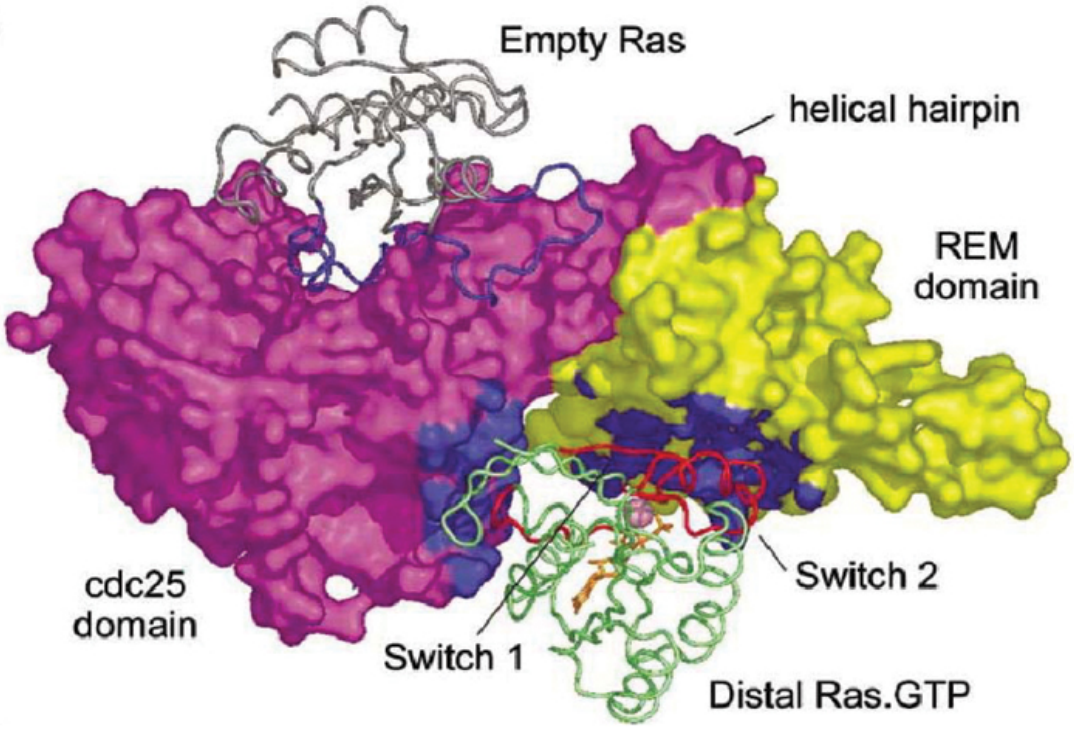

Figure 1-6: 3D structure of the CDC25 and REM domains of Sos1 in complex with GTP-Ras and empty Ras. The CDC25 domain is shown in purple and the REM domain in yellow. The empty Ras bound to the CDC25 domain is shown in grey and the allosterically bound GTP-Ras is shown in green. The two domains CDC25 and REM are labeled as well as the two bound Ras. Also the switch regions of the GTP-Ras and the helical hairpin of the CDC25 domain are indicated [55].

This results in the placement of the methyl group of A59 of Ras at the site where Mg^{2+} is normally bound (Figure 1-6). X-ray crystallographic analysis of Sos1 fragments initially revealed that, in addition to the presence of nucleotide-free Ras at the catalytic site, a second Sos1-bound Ras molecule is loaded with GTP and associated with the REM domain of Sos1 (Figure 1-6) [55]. The REM domain binds to a key helical hairpin loop structure in the core catalytic, CDC25 domain that is responsible for displacing the effector loop of Ras and releasing GDP. Comparison with a crystal structure lacking bound Ras establishes that allosteric regulation of Sos1 by the second Ras molecule occurs through a rotation of the Sos1 REM domain and, in turn, that of the hairpin at the catalytic site [56]. This motion relieves steric occlusion of the catalytic site and allows the binding of Ras and nucleotide release. Consequently, the introduction of a Ras Y64A

mutant that can bind to the allosteric site of Sos1 but not the active site increases the nucleotide release rate 75-fold over that catalyzed but unstimulated Sos1 [56]. Comparison with other available structures indicates that the helical hairpin loop of Ras protein–specific guanine nucleotide–releasing factor 1 (RasGRF1) is buttressed by projections extending from the CDC25 domain to prevent it from occupying an inhibitory conformation, whereas the helical hairpin loop of Epac2, a GEF for the GTPase Rap, might be regulated similarly to that of Sos1 [56]. A number of Rap GEFs, including Epac2, have Ras association (RA) domains, similar to those found in Ras effectors, located immediately N-terminal to their CDC25 domains [53]. Although the binding of Ras is known to influence the subcellular localization of these Rap GEFs [57, 58], Ras proteins have not been reported to allosterically activate them

1.7 Significance of these studies

Although the Grb2-Sos1 interaction mediates a diverse array of cellular processes, little is known about the physicochemical basis of this key protein-protein interaction in cellular signaling. By utilizing biophysical techniques, this thesis hopes to further our understanding of the biophysical parameters by which Grb2 signals downstream and also its dimeric potential. Unraveling the molecular mechanism of interaction of Grb2 with Sos1 as well as the dimerization of Grb2 in terms of biophysical forces will offer unparalleled insights into the biology of this key protein-protein interaction pertinent to cellular signaling and cancer. Such knowledge bears the potential for the development of novel therapies with less toxicity but more effectiveness for the treatment of pathological disorders such as cancer. In an attempt to further our understanding of how Grb2 binds to Sos1, in this thesis I set out to elucidate the physicochemical basis of this key protein-protein interaction.

2 Chapter 2: Materials and methods

2.1 Molecular cloning

Various constructs of human Grb2: full-length Grb2 (residues 1-217), Grb2 nSH3 domain (residues 1-56), Grb2 cSH3 domain (residues 156-217), were cloned into the pET102 bacterial expression vector using TOPO directional technology following the manufacturer's protocol (Invitrogen). The vector encodes an N-terminal thioredoxin (Trx)-tag and a C-terminal polyhistidine (His)-tag. The Trx-tag was included to maximize protein expression and help to keep the protein soluble — the His-tag was used to aid in protein purification using Ni-NTA affinity chromatography. Thrombin cleavage sites (LVPRGS) were introduced at both N- and C-termini of the protein to allow the removal of Trx and His-tags after protein purification.

2.2 Protein expression and purification

All Grb2 constructs were expressed in BL21* (DE3) (Invitrogen). The BL21* cells use the DE3 lysogen to express the recombinant protein and have a truncated RNase E to help maximize protein expression. The constructs were cultured in LB media, and purified using Ni-NTA affinity chromatography following standard procedures. Bacterial cells were grown at 37°C to an optical density of 0.7 at 600nm and induced with 0.5mM isopropyl β-D-1-thiogalactopyranoside (IPTG) for 3 hours at 37 ºC. The cells were harvested and disrupted using a Biospec Bead-Beater. The cell debris was separated from the lysate using high-speed centrifugation and the lysate was subjected to Ni-NTA column and washed with 20mM imidazole to remove non-specific binding of bacterial proteins to the column. The recombinant proteins were eluted with 200mM imidazole and

dialyzed into an appropriate physiological buffer. Constructs were further purified using Mono Q ion-exchange preceding further purification using a Superdex 200 gel filtration column coupled to a GE Akta FPLC system.

The treatment of recombinant proteins with thrombin protease significantly destabilized Grb2 constructs and rendered them proteolytically unstable. For this reason, all experiments reported herein were carried out on recombinant fusion constructs of Grb2 containing a Trx-tag at the N-terminus and a His-tag at the C-terminus. The tags were found to have no effect on the functional properties of the constructs. Protein concentrations were determined by both the fluorescence-based Quant-It assay (Invitrogen) and spectrophotometrically using extinction co-efficients of 52,160$M^{-1}cm^{-1}$ for Grb2, 24,075$M^{-1}cm^{-1}$ for Grb2 nSH3, and 28,085$M^{-1}cm^{-1}$ for Grb2 cSH3 at 280nm. The extinction co-efficients were calculated using the online software ProtParam at ExPASy Server [59]. Results from both methods were in excellent agreement. A more detailed and specific procedure can be found in Chapters: 3.4.1, 4.4.1 and 5.4.1.

2.3 SDS-PAGE analysis

Recombinant proteins were purified to apparent homogeneity as judged by SDS-PAGE analysis (Figures 2-1, 2-2). SDS-PAGE analysis was carried out by loading protein samples on a 12% (w/v) SDS-PAGE gel. The gel was run at 120 V for 50-60 minutes. The gel was visualized by staining with 0.1% (w/v) coomassie-blue solution containing 40% (v/v) methanol and 10% (v/v) acetic acid, and then destaining with a destain-solution containing 10% (v/v) acetic acid and 10% (v/v) methanol. Images of the gels were captured using a UVP MultiDoc-It Gel Imaging System. Protein yields were typically between 40-50mg of protein per liter of culture.

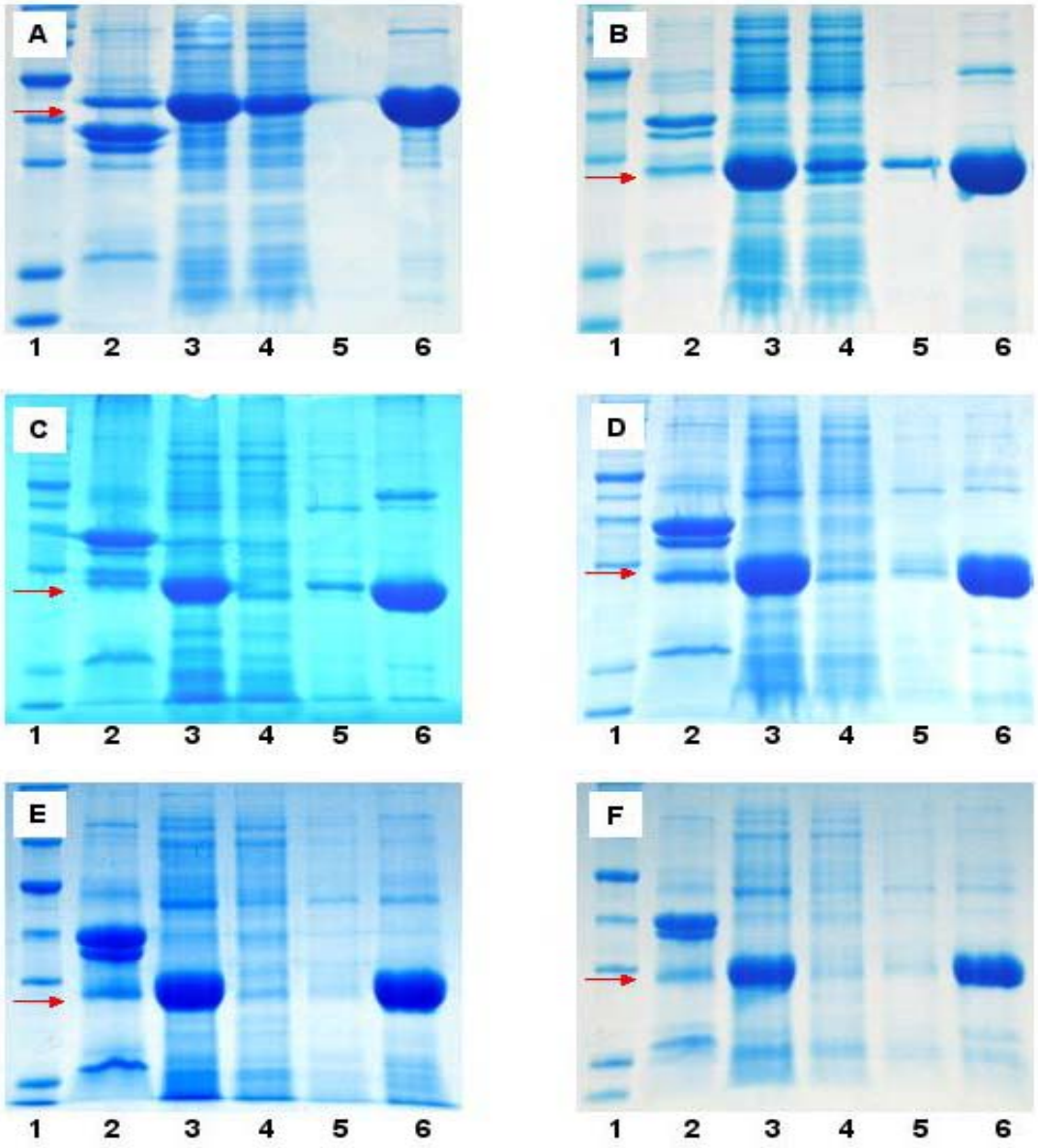

Figure 2-1: SDS-PAGE analysis of the Ni-NTA purification of recombinant proteins. Recombinant human: full-length Grb2 (A), Grb2 nSH3 (B), Grb2 nSH3 A13E (C), Grb2 nSH3 D15G (D), Grb2 nSH3 E31A (E), Grb2 nSH3 D33A (F), were expressed in the E. Coli strain BL21* (DE3) at 37ºC to an optical density of 0.7 at 600nm and induced with 0.5mM IPTG for 3 hours. The cells were harvested and disrupted using a Biospec Bead-Beater. After disruption the cell debris was separated from the lysate using high-speed centrifugation (32,000g) to form an inclusion body pellet and a soluble lysate supernatant fraction. The inclusion body was solubilized in 10% SDS and loaded on a 12% SDS-PAGE gel (lane 2). The lysate (Lane 3) was subjected to Ni-NTA column. The flow-through, the proteins that were not retained by the Ni column, was collected (lane 4). The column was washed with 20mM imidazole to remove non-specific binding of bacterial proteins to the column (lane 5). The recombinant proteins were eluted with 200mM imidazole (lane 6) and dialyzed into an appropriate physiological buffer. Promega Broad Range Protein Markers were loaded as a standard (lane 1). The gel was run at 120 V for 1 hour using a VWR AccuPower power supply and a Bio-Rad Protean Cell. The gel was then visualized by staining with coomassie-blue stain and destaining with a 10% acetic acid, 10% methanol solution. Images of the gels were captured using a UVP MultiDoc-It Gel Imaging System. A red arrow is used to indicate each protein of interest.

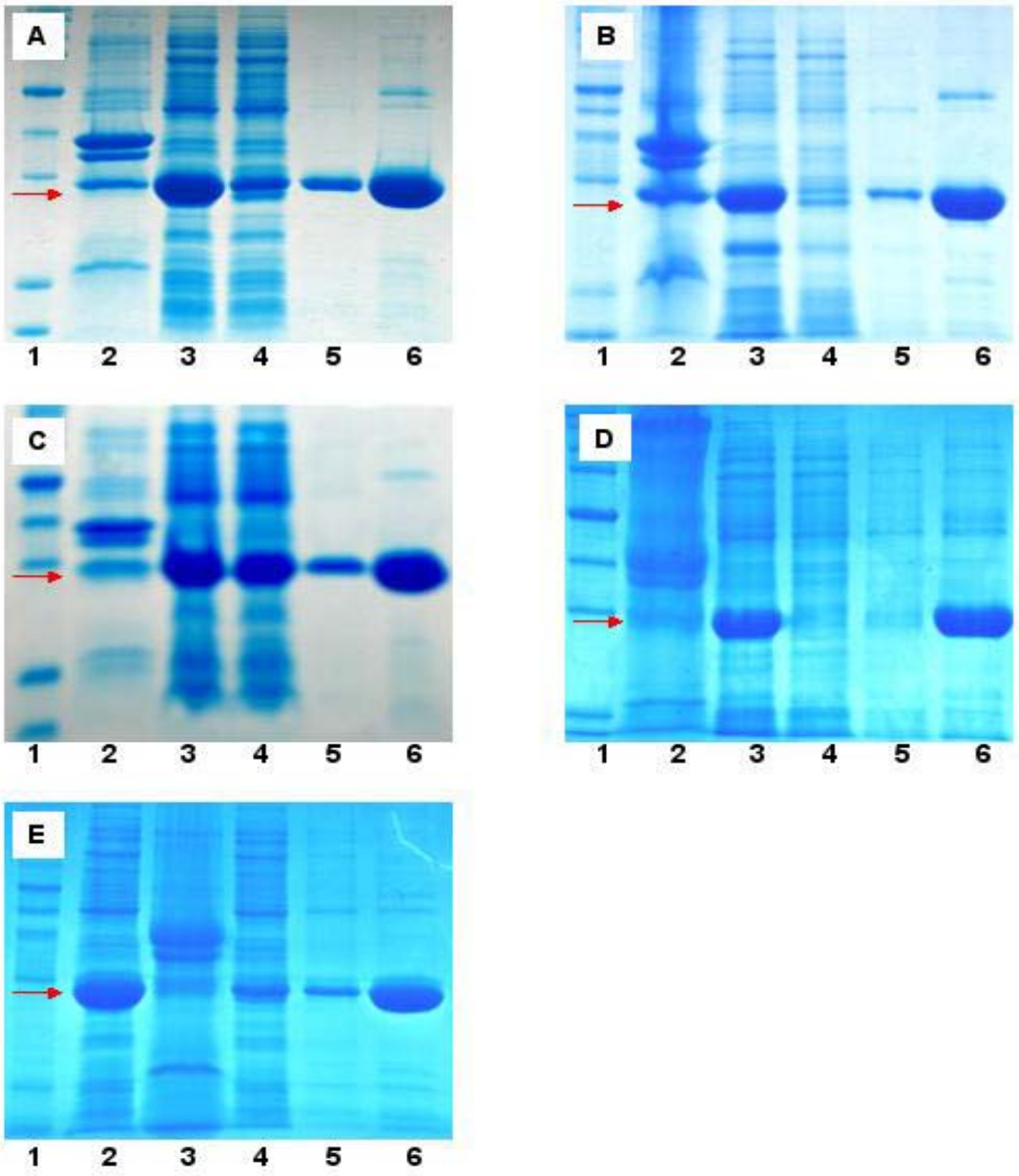

Figure 2-2: SDS-PAGE analysis of the Ni-NTA purification of recombinant proteins. Recombinant human: full-length Grb2 cSH3 (A), Grb2 cSH3 E171A (B), Grb2 cSH3 G173D (C), Grb2 cSH3 D187A (D), Grb2 cSH3 D190A (E), were expressed in the E. Coli strain BL21* (DE3) at 37ºC to an optical density of 0.7 at 600nm and induced with 0.5mM IPTG for 3 hours. The cells were harvested and disrupted using a Biospec Bead-Beater. After disruption the cell debris was separated from the lysate using high-speed centrifugation (32,000g) to form an inclusion body pellet and a soluble lysate supernatant fraction. The inclusion body was solubilized in 10% SDS and loaded on a 12% SDS-PAGE gel (lane 2). The lysate (Lane 3) was subjected to Ni-NTA column. The flow-through, the proteins that were not retained by the Ni column, was collected (lane 4). The column was washed with 20mM imidazole to remove non-specific binding of bacterial proteins to the column (lane 5). The recombinant proteins were eluted with 200mM imidazole (lane 6) and dialyzed into an appropriate physiological buffer. Promega Broad Range Protein Markers were loaded as a standard (lane 1). The gel was run at 120 V for 1 hour using a VWR AccuPower power supply and a Bio-Rad Protean Cell. The gel was then visualized by staining with coomassie-blue stain and destaining with a 10% acetic acid, 10% methanol solution. Images of the gels were captured using a UVP MultiDoc-It Gel Imaging System. A red arrow is used to indicate each protein of interest.

2.4 Site-directed mutagenesis

pET102 bacterial expression vectors expressing wildtype various Grb2 constructs were subjected to Stratagene Quickchange II site-directed mutagenesis to generate desired mutants. Mutations were carried out according to the manufacturer's protocol. All mutant proteins were expressed, purified and characterized as described above. When analyzed by size-exclusion chromatography (SEC) using a Superdex 200 column, all mutant SH3 domains exhibited virtually indistinguishable elution volumes to those observed for the wildtype SH3 domains, implying that the point substitution of specific residues did not lead to protein unfolding and that the mutant protein retained the compact globular fold characteristic of the wildtype protein. These observations were further confirmed by circular dichroism (CD) analysis (Figure 2-3). A more detailed and specific procedure can be found in Chapters: 4.4.2 and 5.4.1.

2.5 Peptide synthesis

HPLC-grade 12-residue peptides corresponding to sites S1, S2, S3, and S4 within human Sos1 protein and corresponding to the binding sites for the SH3 domains of Grb2 were commercially obtained from GenScript Corporation (Figure 1-5). The peptide concentration was measured gravimetrically. A more detailed and specific procedure can be found in Chapters: 4.4.3 and 5.4.1.

2.6 SEC analysis

Size-exclusion chromatography (SEC) on recombinant proteins was performed using a Hiload Superdex200 column coupled to a GE Akta FPLC system equipped with the UNICORN software for automatic operation. SEC is a technique that is commonly used to separate macromolecules, such as proteins, based upon hydrodynamic volume, or more simply size. The technique works by applying proteins to a column containing a

gel medium and running at low pressure. The gel medium is composed of porous "beads" of a fixed diameter. Molecules with a diameter smaller than the pores in the beads will enter them and this will thus impede their flow. Molecules with a diameter larger than that of the pore would be unable to enter the gel medium and their flow will thus be un-impeded. Because of this differential impedance, larger molecules will elute earlier than smaller molecules. However, since particles in solution do not have a completely fixed size, the change in the size will change the probability that the molecule will be able to enter the pore in the bead. This leads to a Gaussian distribution for the elution of the molecules. The benefit of this technique is that it can be performed under native conditions that do not alter the proteins. This allows protein-protein interactions and the oligomericity of proteins to be observed. However a major downfall of this technique is that since it is based upon the probability of a molecule entering a pore due to its size, the technique is very dependent on molecular shape. Thus a molecule that is not relatively spherical will appear to be a different size than it really is.

After purification to apparent homogeneity using Ni-NTA affinity chromatography and ion-exchange chromatography, recombinant proteins were extensively dialyzed in an appropriate buffer. The recombinant protein was concentrated to an appropriate concentration using Amicon Ultra-15 centrifugal filter units, prior to application on Superdex200 column pre-equilibrated in the same buffer at 4°C. The elution of protein was recorded using UV monitor at 280nm and automatically plotted as a function of elution volume in the UNICORN software. The identity of the protein in elution fractions was further confirmed by SDS-PAGE, Western blotting and MALDI-TOF mass spectrometry analysis. The apparent molecular mass was obtained by extrapolation of its recorded elution volume on a straight-line graph generated by plotting

the logarithm of the molecular mass of known protein markers versus their elution volumes on the Superdex200 column pre-equilibrated in the same buffer at 4°C. Control experiments involving the analysis of thioredoxin containing a C-terminal His-tag on the Superdex200 column confirmed that the tags possessed no oligomeric potential. A more detailed and specific procedure can be found in Chapter 3.4.2.

2.7 MALDI-TOF mass spectrometry

Matrix-assisted LASER desorption/ionization time of flight (MALDI-TOF) mass spectrometry is considered a "soft" type of ionization that can be used on fragile bio-molecules without fragmenting them. The process works by using a crystalline matrix to embed the protein to protect it from the laser and at the same type help to vaporize and ionize the protein upon excitation by the laser. Usually a nitrogen laser is used to ionize the protein. Once ionized the proteins are separated due to their mass to charge ratio by their time of flight. This works by the detector measuring how long it takes the protein to reach it from the ionization point. This is a good technique for analyzing proteins due to its gentle means of ionization. Proteins can be observed without fragmentation, and also under proper conditions larger macromolecular complexes such as dimers and oligomers can be observed without fragmentation.

MALDI-TOF mass spectrometry analysis of recombinant protein was performed on a Voyager-DE spectrometer with a linear detector coupled to v5.0 software from Applied Biosystems. Recombinant samples were extensively dialyzed in 10mM Tris and 5mM β-mercaptoethanol at pH 8.0. The dialyzed protein solution was mixed with an equal volume of matrix solution and the resulting mixture was air-dried on the sample plate prior to MALDI-TOF analysis. The matrix solution comprised of a saturated solution of 3,5-dimethoxy-4-hydroxycinnamic acid in acetonitrile:water (1:1). Molecular

masses were calibrated externally with bovine serum albumin. Molecular mass accuracy was within ±0.25%. All MALDI-TOF experiments were carried out at the Global Peptide Services, Fort Collins, CO. A more detailed and specific procedure can be found in Chapter 3.4.3.

2.8 AUC experiments

Protein oligomerization was analyzed by sedimentation equilibrium using analytical ultra-centrifugation (AUC). AUC is a process in which a sample is placed in a centrifuge and spun at an acceleration as high as 1,000,000 g and the sample can be monitored in real time using optical detection. In sedimentation equilibrium only the steady-state equilibrium is of concern and thus the concentration of the molecule is observed as a function of only the radius that it has traveled. From this information the exact mass of the molecule of interest can be determined. A benefit of this technique is that it can be performed under native conditions that do not perturb inter-molecular interactions. Thus binding of molecules can be observed as well as oligomerization. The binding constant between two molecules can also be calculated. Thus AUC is a very powerful technique for characterizing molecular interactions.

Analytical ultra-centrifugation (AUC) sedimentation equilibrium experiments were carried out in a Beckman-Coulter XL-A analytical ultracentrifuge at rotor speeds of 17,000rpm at 4°C. After purification to apparent homogeneity using Ni-NTA affinity chromatography and ion-exchange chromatography, recombinant proteins were extensively dialyzed in 50mM Tris and 200mM NaCl at pH 8.0 prior to transfer to an ultracentrifuge cell at various initial concentrations. The distribution of protein concentration, expressed as absorbance at 280 nm (A_r), as a function of radius (r) at

centrifugal equilibrium was analyzed using L-1 (robust) regression with the mathematical modeling system MLAB (Civilized Software, Silver Spring, MD). A more detailed and specific procedure can be found in Chapter 3.4.4.

2.9 CD analysis

Circular dichroism (CD) analysis was used to verify that the point substitution of specific residues in various domains and peptides did not lead to protein unfolding and that the mutant retained the characteristic fold of the wildtype protein or peptide (Figures 2-3 and 2-4). CD is a valuable technique that allows for the determination of secondary structure characteristics in macromolecules. It is a very useful technique to validate that no major structural changes are introduced in a protein when making a mutation. Also CD is capable of detecting structural changes in a macromolecule upon ligand binding.

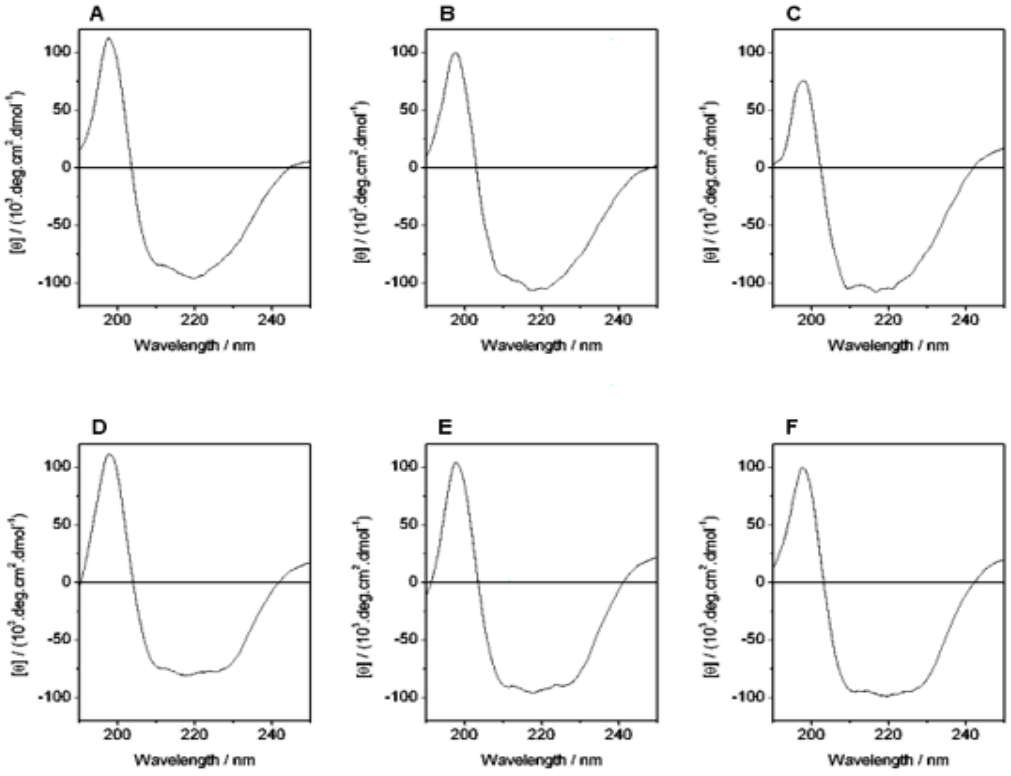

Figure 2-3: Far-UV CD analysis of various recombinant wildtype and mutant nSH3 and cSH3 domains of Grb2. Grb2 nSH3 (A), Grb2 nSH3 A13E (B), Grb2 nSH3 A13E (C), Grb2 cSH3 (D), Grb2 cSH3 E171A (E), Grb2 cSH3 G173D (F).

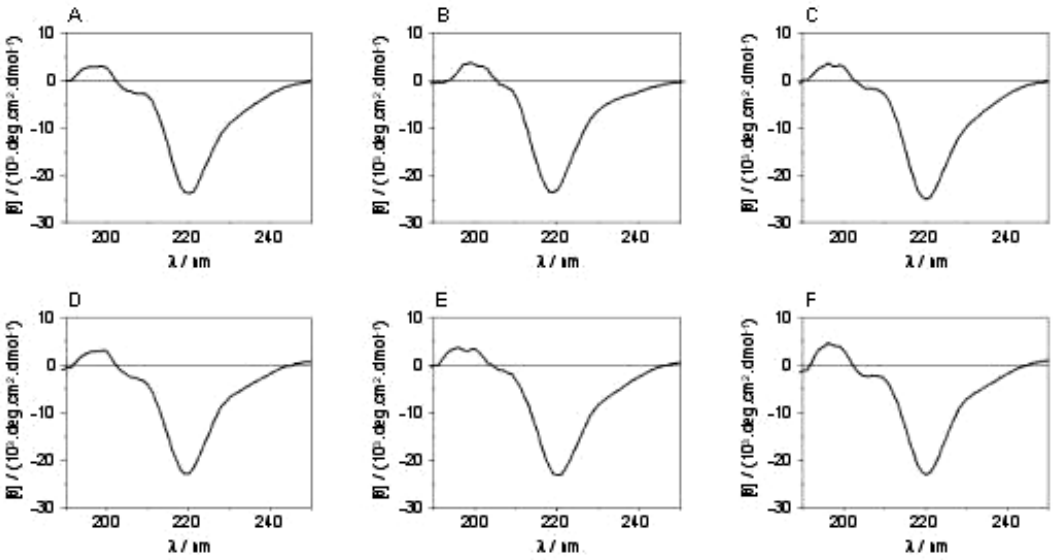

Figure 2-4: Far-UV CD analysis of wildtype (WT) and mutant S1 peptides. Sos1 S1 wild type (A), Sos1 S1 R+5A (B), Sos1 S1 R+6A (C), Sos1 S1 R+7A (D), Sos1 S1 AA (E), Sos1 S1 AAA (F).

CD measurements were conducted on Bio-Logic SFM400/MOS450 spectrometer equipped with a CD accessory. Samples were prepared in 10mM Sodium phosphate buffer at pH 8.0. All spectra were collected at 30°C using a quartz cuvette with a 2-mm pathlength over the interval 200-250nm. Data were recorded with a bandwidth of 2nm at a scan rate of 3nm/min. Each data set represents an average of 4-8 scans acquired at 1nm intervals and corrected for buffer signals.

2.10 ITC measurements

Isothermal titration calorimetry (ITC) is a powerful method for studying protein-ligand thermodynamics and provides molecular insight into the forces that stabilize protein-ligand complexes [60, 61]. ITC measures heat change associated with a chemical reaction triggered by the mixing of ligand with macromolecules such as proteins [60]. Thus, an ITC experiment can directly measure enthalpy (ΔH) and then calculate entropy (ΔS), Gibbs free energy (ΔG), binding constants (K_d) and stoichiometry (n). ITC can also determine whether a reaction between two components is under enthalpic or entropic

control. Reactions under enthalpic control are usually exothermic and the heat released, as a result of favorable contacts generated between protein and ligand due to hydrophobic forces and electrostatic interactions, drives the binding process. In contrast, reactions under entropic control are usually endothermic, or weakly exothermic, and the driving force is derived from a large positive entropy change of the system, which reflects ordering, disordering or conformational change in the macromolecule upon ligand binding.

ITC experiments were performed on Microcal VP-ITC instrument and data were acquired and processed using fully automized features in Microcal ORIGIN software. All measurements were repeated 3-4 times. Briefly, after purification to apparent homogeneity using a combination of Ni-NTA affinity chromatography, ion-exchange chromatography and size-exclusion chromatography, recombinant proteins were extensively dialyzed in either Tris buffer (50mM Tris, 200mM NaCl, 1mM EDTA and 5mM β-mercaptoethanol at pH 8.0), or alternatively, in Phosphate buffer (50mM Sodium phosphate, 200mM NaCl, 1mM EDTA and 5mM β-mercaptoethanol at pH 8.0). The protein samples were subsequently de-gassed using the ThermoVac accessory for 10min. The experiments were initiated by injecting 25 x 10µl injections from the syringe into the calorimetric cell, at a fixed temperature. The change in thermal power as a function of each injection was automatically recorded using Microcal ORIGIN software and the raw data were further processed to yield binding isotherms of heat uptake per injection as a function of concentration. The heats of mixing and dilution were subtracted from the heat of binding per injection. A more detailed procedure and specific can be found in Chapters: 3.4.5, 4.4.4 and 5.4.2.

2.11 SASA calculations

The magnitude of polar and apolar solvent-accessible surface area (SASA) becoming occluded upon binding was calculated from thermodynamic data and compared to that determined from the 3D structures. A more detailed and specific procedure can be found in Chapter 3.4.6.

2.12 Molecular modeling

3D structures were modeled using the MODELLER software based on homology modeling [62]. Briefly, MODELLER employs molecular dynamics and simulated annealing protocols to optimize the modeled structure through satisfaction of spatial restraints derived from amino acid sequence alignment with a corresponding template in Cartesian space. The modeled structures should be expected to adopt 3D folds similar to the template structure except for the sidechain conformations of specific amino acids due to the introduction of specific hydrogen bonding, the rearrangement of domains spatially to one-another or the modeling of loops not rendered in template structures. Such hydrogen bonding restraints being introduced herein are necessary to bring the sidechain atoms of respective residues within optimal hydrogen bonding distance in agreement with our thermodynamic data reported. The atomic distances set for hydrogen bonding restraints between a specific pair of oxygen and nitrogen atoms were 2.8±0.5Å. Thus, MODELLER will force the sidechain oxygen and nitrogen atoms of specific hydrogen bonding partners to lie within approximately 2.8Å of each other through the rotation of backbone N-Cα and Cα-C' bonds with little effect on the overall global fold. In each case, a total of 100 structural models were calculated and the structure with the lowest energy, as judged by the MODELLER Objective Function, was selected for further energy minimization in MODELLER prior to analysis. The modeled structures were

rendered using RIBBONS [63]. All calculations were performed on the lowest energy structural model. A more detailed procedure and specific can be found in Chapters: 3.4.7, 4.4.5 and 5.4.3.

3 Chapter 3: Grb2 adaptor undergoes conformational change upon dimerization

3.1 Summary

Grb2 is an adaptor protein that couples activated receptor tyrosine kinases to downstream effector molecules such as Ras and Akt. Despite being a central player in mitogenic signaling and a target for therapeutic intervention, the role of Grb2 oligomerization in cellular signaling is not well understood. Here, using the techniques of size exclusion chromatography, mass spectrometry, analytical ultra-centrifugation and isothermal titration calorimetry, we demonstrate that Grb2 exists in monomer-dimer equilibrium in solution and that the dissociation of dimer into monomers is entropically-driven without an unfavorable enthalpic change at physiological temperatures. Our data indicate that enthalpy and entropy of dimer dissociation are highly temperature-dependent and largely compensate each other resulting in negligible effect of temperature on the overall free energy. From the plot of enthalpy change versus temperature, the magnitude of heat capacity change derived is much smaller than that expected from the rather large molecular surfaces becoming solvent-occluded upon Grb2 dimerization, implying that Grb2 monomers undergo conformational rearrangement upon dimerization. 3D structural models of Grb2 dimer and monomers suggest strongly that such conformational rearrangement upon dimerization may arise from domain swapping. Taken together, our study provides novel insights into the role of Grb2 as an adaptor in cellular signaling circuitry and how Grb2 dimerization may impart high fidelity in signal transduction as well as lead to rapid signal amplification upon receptor stimulation.

3.2 Abbreviations

AUC	Analytical Ultra-Centrifugation
EGF	Epidermal Growth Factor
Grb2	Growth factor Receptor Binder 2
ITC	Isothermal Titration Calorimetry
MALDI-TOF	Matrix-Assisted LASER Desorpton/Ionization Time of Flight
MAPK	Mitogen-Activated Protein Kinase
MMCO	Molecular Mass Cut-Off
PDGF	Platelet-Derived Growth Factor
RTK	Receptor Tyrosine Kinase
SASA	Solvent-Accessible Surface Area
SEC	Size Exclusion Chromatography
SH2	Src Homology 2
SH3	Src Homology 3
Shc	Src Homology Containing

3.3 Background

Grb2 is a ubiquitous component of cell signaling networks that couples activated receptor tyrosine kinases (RTKs) to downstream effectors and regulators. The critical role of Grb2 in cellular signaling is exquisitely demonstrated through defects in mice embryos upon the disruption of *grb2* gene [1]. Grb2 is a modular protein comprised of a central SH2 domain flanked between an N-terminal SH3 (nSH3) domain and a C-terminal SH3 (cSH3) domain, giving it an overall modular architecture of nSH3-SH2-cSH3 [2]. Grb2 recognizes activated RTKs by virtue of its SH2 domain to bind to tyrosine-phopshorylated (pY) sequences in the context of the consensus motif pYXN located

within the cytoplasmic tails of a diverse array of receptors, including EGF and PDGF receptors [3, 4]. Alternatively, Grb2 can also indirectly dock onto activated RTKs through the binding of its SH2 domain to pY sequences within the adaptor protein p52Shc [5, 6]. Given a much broader spectrum of RTKs recognized by p52Shc, Grb2 is more often seen to fulfill this latter role instead of directly binding to RTKs upon receptor stimulation. For its part, p52Shc contains at least two well-conserved YXN motifs at positions Y239 and Y317 that are subject to phosphorylation by a diverse array of protein tyrosine kinases, including the Src kinase family, upon its recruitment to receptor tails in response to extracellular mitogenic stimuli [7-9]. It has been shown that phosphorylation of both Y239 and Y317 in p52Shc is required for efficient recruitment of Grb2 to the inner membrane surface [11]. Could this necessity be explained by the ability of Grb2 to participate in cellular signaling as a dimer?

Upon the interaction of Grb2 to RTKs directly or indirectly, the SH3 domains of Grb2 present a placid opportunity for a wide variety of proteins, containing proline-rich sequences, to be recruited to the inner membrane surface and thus engage in downstream cellular signaling cascades. Some of the best characterized downstream partners of Grb2 SH3 domains are the guanine nucleotide exchange factor Sos1 [12, 13], the adaptor protein Gab1 [14, 15], the endocytic GTPase dynamin1 [16, 17], the ubiquitin ligase Cbl [15, 18, 19] and the cell cycle inhibitor p27kip1 [20]. Upon recruitment to the inner membrane surface, these downstream effectors of Grb2 exert a wide multitude of biological responses. For example, Sos1 catalyzes the GDP-GTP exchange within the small membrane-bound GTPase Ras and thereby switches on a key signaling circuit that involves the activation of MAPK cascade central to cellular proliferation, survival and differentiation [21, 22]. Likewise, the recruitment of Gab1 provides docking platforms

for the protein tyrosine phosphatase Shp2 and the lipid kinase PI3K, which respectively account for further amplification of Ras activity, as sustained activation of Ras requires both the Sos1-dependent and Gab1-dependent pathways [23-25], and the activation of serine-threonine kinase Akt/PKB, which plays a pivotal role in cell growth and survival [26]. The recruitment of dynamin1 to the inner membrane surface is believed to trigger clathrin-mediated receptor endocytosis of EGFR — a key mechanism for initiating intracellular signaling [27, 28]. In contrast, the recruitment of Cbl to the p52Shc-Grb2 signaling complex at the inner membrane surface results in ubiquitination of EGFR and its subsequent degradation, a step that is critical for negating the oncogenic potential of EGFR [29]. Finally, the recruitment of p27kip1 to the Shc-Grb2 signaling complex appears to negatively regulate the activity of Ras by virtue of its ability to compete with Sos1 for binding to Grb2 [20].

Grb2 is architecturally one of the simplest and smallest adaptor proteins with an overall modular architecture of nSH3-SH2-cSH3 [2]. The availability of its complete 3D structure has rendered Grb2 a prototype for understanding the function of other adaptor proteins in cellular signaling [10]. In the 3D crystal structure of Grb2, the protein crystallized as a dimer with two-fold axis of symmetry such that the SH2 domain of one monomer docks against the cSH3 domain of the other and vice versa in a head-to-tail fashion [10]. In this manner, the ligand binding sites in the SH2 and the SH3 domains remain fully exposed to solution and thereby rendering Grb2 in an active state and fully primed to participate in cellular signaling within the dimeric assembly. To paraphrase this slightly, the role of Grb2 dimerization appears to stabilize the protein further rather than providing a negative regulatory switch that may need to be invoked upon receptor stimulation. Such a dimeric assembly of Grb2 is also expected to eliminate the need for

any conformational change prior to interaction with upstream RTKs or downstream effector molecules. The extent to which Grb2 dimerization prevails in solution and the extent to which the monomers may have to undergo conformational change upon dimerization is however not clear. Does Grb2 dimerize in solution? Do the monomers come together as rigid bodies to generate the Grb2 dimer or do they have to undergo some sort of conformational change upon dimerization?

To address these key issues, we undertook the present study. Here, using the techniques of size exclusion chromatography, mass spectrometry, analytical ultra-centrifugation and isothermal titration calorimetry, we demonstrate that Grb2 exists in monomer-dimer equilibrium in solution and that the dissociation of dimer into monomers is entropically-driven without an unfavorable enthalpic change at physiological temperatures. Our data further indicate that the heat capacity change is much smaller than that expected from the rather large molecular surfaces becoming solvent-occluded upon Grb2 dimerization, implying that Grb2 monomers undergo conformational rearrangement upon dimerization. 3D structural models of Grb2 dimer and monomers suggest strongly that such conformational rearrangement upon dimerization may arise from domain swapping. Taken together, our study provides novel insights into the role of Grb2 as an adaptor in cellular signaling circuitry and how Grb2 dimerization may impart high fidelity in signal transduction as well as lead to rapid signal amplification upon receptor stimulation.

3.4 Experimental procedures

3.4.1 Protein preparation

Full-length human Grb2 (residues 1-217; Expasy# P62993) was cloned into pET102 bacterial expression vector with an N-terminal thioredoxin (Trx)-tag followed by

a thrombin site (a total of 133 additional residues at the N-terminus) and a C-terminal polyhistidine (His)-tag preceded by a thrombin site (a total of 36 additional residues at the C-terminus) using Invitrogen TOPO technology. Trx-tag was included to maximize protein expression in soluble fraction, while the His-tag was added to aid in protein purification by Ni-NTA affinity chromatography. Additionally, thrombin protease sites were introduced at both the N- and C-termini of the protein to aid in the removal of tags after protein purification. Proteins were subsequently expressed in *Escherichia coli* BL21*(DE3) bacterial strain (Invitrogen) cultured in LB media and purified on Ni-NTA affinity column using standard procedures. Further treatment of the protein on a MonoQ ion-exchange column and a Hiload Superdex200 size-exclusion column coupled to GE Akta FPLC system led to purification of recombinant Grb2 to apparent homogeneity as judged by SDS-PAGE analysis (appendix 1-4). The identity of recombinant Grb2 was further confirmed by MALDI-TOF mass spectrometry analysis. Protein yield was typically between 20-30mg of recombinant Grb2 of apparent homogeneity per liter of bacterial culture. The treatment of recombinant protein with thrombin protease significantly destabilized Grb2 and rendered it proteolytically unstable. For this reason, all experiments reported herein were carried out on a 43-kD recombinant fusion Grb2 (386 residues) containing a Trx-tag at the N-terminus and a His-tag at the C-terminus. The tags were found to have no effect on the dimeric potential of Grb2. Protein concentrations were determined by both fluorescence using Invitrogen Quant-It assay and absorbance at 280nm using an extinction co-efficient of $52{,}160 M^{-1} cm^{-1}$ for the recombinant Grb2. The extinction co-efficient was calculated from amino acid sequence alone using the online software ProtParam at ExPasy Server [59]. Results from both methods were in an excellent agreement.

3.4.2 SEC analysis

Size-exclusion chromatography (SEC) on recombinant Grb2 was performed using a Hiload Superdex200 column coupled to a GE Akta FPLC system equipped with the UNICORN software for automatic operation. After purification to apparent homogeneity using Ni-NTA affinity chromatography and ion-exchange chromatography, recombinant Grb2 was extensively dialyzed in 50mM Tris, 200mM NaCl, 1mM EDTA and 5mM β-mercaptoethanol at pH 8.0. The recombinant protein was concentrated to 100-300μM using Amicon Ultra-15 centrifugal filter units (MMCO 30kD) prior to application on Superdex200 column pre-equilibrated in the same buffer at 4°C. The elution of protein was recorded using UV monitor at 280nm and automatically plotted as a function of elution volume in the UNICORN software. The identity of Grb2 in elution fractions was further confirmed by SDS-PAGE, Western blotting and MALDI-TOF mass spectrometry analysis. The apparent molecular mass of recombinant Grb2 was obtained by extrapolation of its recorded elution volume on a straight line graph generated by plotting the logarithm of the molecular mass of known protein markers versus their elution volumes on the Superdex200 column pre-equilibrated in the same buffer at 4°C. Control experiments involving the analysis of thioredoxin containing a C-terminal His-tag on the Superdex200 column confirmed that the tags possessed no oligomeric potential.

3.4.3 MALDI-TOF mass spectrometry

Matrix-assisted LASER desorption/ionization time of flight (MALDI-TOF) mass spectrometry analysis of recombinant Grb2 was performed on a Voyager-DE spectrometer with a linear detector coupled to v5.0 software from Applied Biosystems. Recombinant Grb2 was extensively dialyzed in 10mM Tris and 5mM β-mercaptoethanol

at pH 8.0. The dialyzed protein solution was mixed with an equal volume of matrix solution and the resulting mixture was air-dried on the sample plate prior to MALDI-TOF analysis. The matrix solution comprised of a saturated solution of 3,5-dimethoxy-4-hydroxycinnamic acid in acetonitrile:water (1:1). Molecular masses were calibrated externally with bovine serum albumin. Molecular mass accuracy was within ±0.25%. All MALDI-TOF experiments were carried out at the Global Peptide Services, Fort Collins, CO.

3.4.4 AUC experiments

Analytical ultra-centrifugation (AUC) sedimentation equilibrium experiments were carried out in a Beckman-Coulter XL-A analytical ultracentrifuge at rotor speeds of 17,000rpm at 4°C. After purification to apparent homogeneity using Ni-NTA affinity chromatography and ion-exchange chromatography, recombinant Grb2 was extensively dialyzed in 50mM Tris and 200mM NaCl at pH 8.0 prior to transfer to an ultracentrifuge cell at various initial concentrations in the range 0.1-10μM. The distribution of Grb2 concentration, expressed as absorbance at 280 nm (A_r), as a function of radius (r) at centrifugal equilibrium was analyzed using L-1 (robust) regression with the mathematical modeling system MLAB (Civilized Software, Silver Spring, MD) and was best fit to the following equation based on a reversible monomer-dimer equilibrium model [64]:

$$A_r = A_b\exp[M\omega^2(1-\bar{\nu}\rho)(r^2-r_b^2)/2RT] + A_b^2\exp[\ln K_a - \ln(\varepsilon/2) + 2M\omega^2(1-\bar{\nu}\rho)(r^2-r_b^2)/2RT] + \delta \quad [1]$$

where A_b is the absorbance at 280nm at the radial position r_b (at the cell bottom), ε is the molar extinction coefficient of the monomer at 280nm, M is the molecular mass of the monomer, ω is the angular velocity of the rotor, $\bar{\nu}$ is the partial specific volume of the monomer, ρ is the buffer density, R is the universal molar gas constant, T is the absolute

temperature, K_a is the equilibrium association constant for dimer formation and δ is the baseline offset. The above analysis was carried out globally for various monomer-equivalent concentrations of Grb2 in the range 0.1-10μM.

3.4.5 ITC measurements

Isothermal titration calorimetry (ITC) experiments were performed on Microcal VP-ITC instrument and data were acquired and processed using fully automized features in Microcal ORIGIN software. All measurements were repeated 3-4 times. Briefly, after purification to apparent homogeneity using a combination of Ni-NTA affinity chromatography, ion-exchange chromatography and size-exclusion chromatography, recombinant Grb2 was extensively dialyzed in either Tris buffer (50mM Tris, 200mM NaCl, 1mM EDTA and 5mM β-mercaptoethanol at pH 8.0), or alternatively, in Phosphate buffer (50mM Sodium phosphate, 200mM NaCl, 1mM EDTA and 5mM β-mercaptoethanol at pH 8.0). The protein samples were subsequently concentrated to 100-300μM using the Amicon Ultra-15 centrifugal filter units (MMCO 30kD) and degassed using the ThermoVac accessory for 10min. The experiments were initiated by injecting 25 x 10μl injections of 100-300μM of recombinant Grb2 from the syringe into the calorimetric cell containing 1.8ml of the same buffer, used for protein dialysis, at a fixed temperature in the narrow range 10-30°C. The change in thermal power as a function of each injection was automatically recorded using Microcal ORIGIN software and the raw data were further processed to yield binding isotherms of heat uptake per injection as a function of monomer concentration. The heats of mixing and dilution were subtracted from the heat of dimer dissociation per injection by carrying out a control experiment in which the appropriate buffer in the calorimetric cell was titrated against concentrated thioredoxin containing a C-terminal His-tag (Trx-His) from the syringe in an identical

manner. Control experiments involving the injection of concentrated Trx-His into the appropriate buffer alone or containing Grb2 in the calorimetric cell produced similar heats to those observed for the injection of buffer into buffer, implying that neither Trx-tag nor His-tag interacts with Grb2. To extract various thermodynamic parameters, the binding isotherms were iteratively fit in Microcal Origin using non-linear least squares regression analysis to the following sigmoidal function:

$$q(i) = \Delta H / \{1+\exp[(C-K_d)/f]\} \quad [2]$$

where q(i) is the heat uptake (kcal/mol) for the ith injection (the Y-axis variable), C is the total monomer-equivalent concentration of the dimer (μM) injected into the calorimetric cell after ith injection (the X-axis variable), ΔH is the total enthalpy of dimer dissociation (kcal/mol), K_d is the apparent equilibrium dissociation constant of the dimer (μM) and f is the steepness factor (μM), related to the number of moles of dimer injected per unit volume of the calorimetric cell for the ith injection, of the sigmoidal curve for the dissociation of Grb2 dimer into monomers. The above model is the simplest mathematical function that best describes our data and the resulting fit directly generated the thermodynamic parameters K_d and ΔH for the dissociation of Grb2 dimer into monomers. The free energy change (ΔG) upon dimer dissociation was calculated from the relationship:

$$\Delta G = -RT\ln K_d \quad [3]$$

where R is the universal molar gas constant (1.99 cal/K/mol), T is the absolute temperature in Kelvins and K_d is in the units of mol/L. The entropic contribution (TΔS) to the free energy of binding was calculated from the relationship:

$$T\Delta S = \Delta H - \Delta G \quad [4]$$

where ΔH and ΔG are as defined above. Heat capacity change (ΔC_p) upon dimer dissociation was calculated by measuring ΔH as a function of temperature (T) in the narrow range 10-30°C with the slope of the ΔH versus T plot yielding the value of ΔC_p.

3.4.6 SASA calculations

The magnitude of polar and apolar solvent-accessible surface area (SASA) becoming occluded upon the formation of Grb2 dimer from monomers was calculated from thermodynamic data and compared to that determined from the 3D structures of Grb2 dimer and monomers [10].

For calculation of change in polar SASA ($\Delta SASA_{polar}$) and apolar SASA ($\Delta SASA_{apolar}$) upon Grb2 dimerization from thermodynamic data, it was assumed that ΔC_p and ΔH at 60°C (ΔH_{60}) are additive and linearly depend on the change in $\Delta SASA_{polar}$ and $\Delta SASA_{apolar}$ as embodied in the following empirically-derived expressions [65-68]:

$$\Delta C_p = a[\Delta SASA_{polar}] + b[\Delta SASA_{apolar}] \quad [5]$$

$$\Delta H_{60} = c[\Delta SASA_{polar}] + d[\Delta SASA_{apolar}] \quad [6]$$

where a, b, c and d are empirically-determined co-efficients with values of –0.14 cal/mol/K/Å^2, +0.32 cal/mol/K/Å^2, +31.34 cal/mol/Å^2 and –8.44 cal/mol/Å^2, respectively. The co-efficients a and b are independent of temperature, while c and d refer to a temperature of 60°C, which equates to the median melting temperature of the proteins from which these constants are derived [65-67]. ΔC_p for the dissociation of Grb2 dimer was calculated from the slope of a plot of ΔH versus T in the narrow temperature range 10-30°C using ITC instrument. ΔH_{60} for the dissociation of Grb2 dimer was calculated by extrapolation of a plot of ΔH versus T in the narrow temperature range 10-30°C, using ITC instrument, to 60°C. With ΔC_p and ΔH_{60} experimentally determined using ITC and

the knowledge of co-efficients a-d from empirical models [65-68], equations [5] and [6] were simultaneously solved to obtain the magnitudes of $\Delta SASA_{polar}$ and $\Delta SASA_{apolar}$ independent of structural information upon the dissociation of Grb2 dimer into monomers.

Changes in $\Delta SASA_{polar}$ and $\Delta SASA_{apolar}$ upon Grb2 dimerization from 3D structural data were calculated using the following relationships:

$$\Delta SASA_{polar} = [SASA_{dp}] - 2[SASA_{mp}] \quad [7]$$

$$\Delta SASA_{apolar} = [SASA_{da}] - 2[SASA_{ma}] \quad [8]$$

where $SASA_{dp}$ and $SASA_{da}$ are the polar and apolar SASA of Grb2 dimer, and $SASA_{mp}$ and $SASA_{ma}$ are the polar and apolar SASA of Grb2 monomer. $SASA_{dp}$ and $SASA_{da}$ were calculated from the 3D structural model of Grb2 dimer (see below), $SASA_{mp}$ and $SASA_{ma}$ were calculated from the 3D structural model of Grb2 monomer assuming it retained the same conformation as that observed in the dimer for the Rigid Body model (see below), while $SASA_{mp}$ and $SASA_{ma}$ were calculated from the 3D structural model of Grb2 monomer assuming it adopted a different conformational when in isolation for the Flexible Body model (see below). All SASA calculations were performed using the online software GETAREA with a probe radius of 1.4Å [69].

3.4.7 Structural modeling

3D structures of Grb2 monomers alone and as a dimer were modeled using the MODELLER software based on homology modeling [62]. The model of Grb2 dimer was obtained using the crystal structure of Grb2, but lacking residues 28-33 in a loop in the nSH3 domain as a result of lack of electron density, as a template (with a PDB code of 1GRI). The Rigid Body model of Grb2 monomer, assuming it retained the same conformation as that observed in the dimer, was obtained using atomic coordinates of

only one monomer in the crystal structure of Grb2 (with a PDB code of 1GRI). The Flexible Body model of Grb2 monomer, assuming it adopted a different conformation when in isolation, was obtained using atomic coordinates of nSH2 and cSH3 domains of one monomer and the atomic coordinates of SH2 domain from the other monomer in the crystal structure of Grb2 (with a PDB code of 1GRI). In the Flexible Body model of Grb2 monomer, the residues in the inter-domain loops were allowed to float freely without a template so as to enable them to adopt the energy-minimized conformations consistent with the re-arrangement of the SH2 domain relative to nSH3 and cSH3 domains. In each case, a total of 100 structural models were calculated and the structure with the lowest energy, as judged by the MODELLER Objective Function, was selected for further energy minimization in MODELLER prior to analysis. The structures were rendered using the RIBBONS software [63]. All calculations were performed on the lowest energy structural model.

3.5 Results and discussion

3.5.1 Grb2 exists in monomer-dimer equilibrium

In an attempt to determine the extent to which Grb2 may dimerize in solution, we analyzed the oligomeric state of full-length recombinant Grb2 on Superdex200 column using size-exclusion chromatography (SEC). Our SEC analysis reveals that Grb2 exists in two distinct species with apparent molecular masses of 43kD and 90kD (Figure 3-1a). The molecular mass of recombinant Grb2 obtained from its amino acid sequence analysis is 43.3kD. Thus, the most straightforward interpretation of our data is that the two species of Grb2, as observed in our SEC analysis, most likely represent the monomeric and dimeric states of the protein in agreement with the crystal structure of Grb2 [10]. To shed further light on the dimerization of Grb2, we analyzed the potential of monomeric and

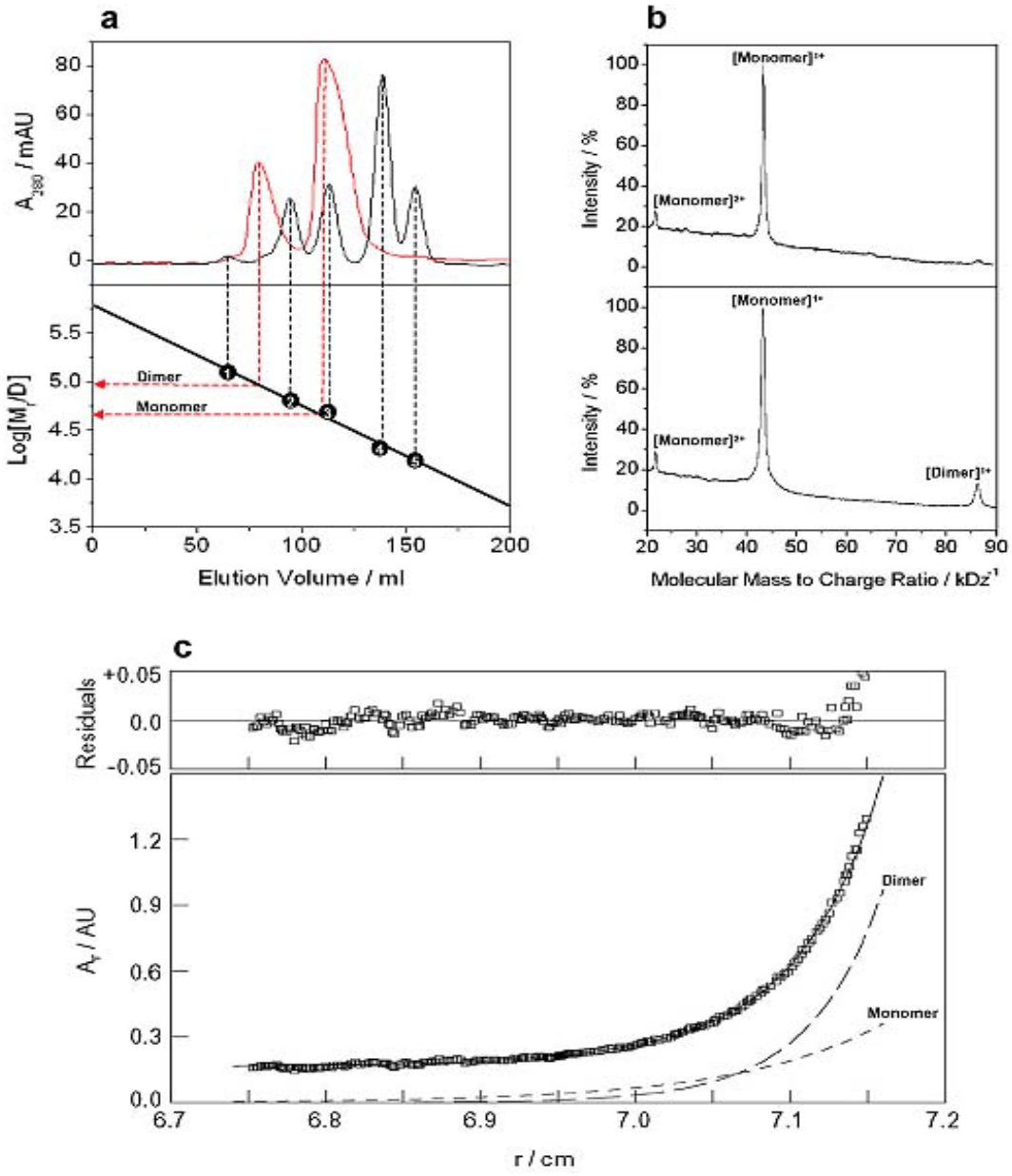

Figure 3-1: Biophysical analysis of monomer-dimer equilibrium in Grb2. (a) SEC analysis of Grb2 oligomerization. Protein markers of known molecular masses or recombinant Grb2 were applied onto a Hiload Superdex200 column coupled to a GE AKTA FPLC system. The proteins were eluted with the same buffer and the elution profiles for protein markers (black) and Grb2 (red) were recorded with a UV monitor at 280nm (top panel). A plot of the logarithm of the molecular mass of known protein markers versus their elution volume was fit to a straight line using linear regression analysis (bottom panel). The numerals indicate the elution volumes of protein markers of known molecular masses as follows: (1) 128-kD dimeric albumin; (2) 64-kD monomeric albumin; (3) 48-kD ovalbumin; (4) 20-kD chymotrypsinogen; and (5) 16-kD ribonuclease. Extrapolation of the elutions volumes of Grb2 peaks (red) observed in the elution profile (top panel) on the logarithmic plot (bottom panel) yielded apparent molecular masses of 90kD and 43kD — which are in remarkable agreement with the calculated molecular masses of dimeric (86.6kD) and monomeric (43.3kD) recombinant Grb2. (b) MALDI-TOF analysis of Grb2 oligomerization. SEC fractions eluting as an apparent monomer (top panel) and as an apparent dimer (bottom panel) were further subjected to MALDI-TOF mass spectrometry. The multiply charged ions of Grb2 monomer and dimer observed in the MALDI-TOF analysis are indicated. (c) AUC analysis of Grb2 oligomerization. Distribution of Grb2

concentration, expressed as absorbance at 280 nm (A_r) as a function of radius (r) at centrifugal equilibrium in the cell at a rotor speed of 17000 rpm at 4°C (open squares) is shown in the lower panel. The data shown are for the initial concentration of 10μM of Grb2 loaded into the centrifugal cell. The solid line in the lower panel shows the fit of the data to a reversible monomer-dimer model using equation [1]. The quality of the fit is indicated by the residuals shown in the upper panel. The net distribution of Grb2 observed experimentally was decomposed into the distribution of individual monomer (short dash) and dimer (long dash) as shown in the lower panel. The monomer and dimer distributions shown are not corrected for baseline offset The baseline correction was found to be approximately proportional to the initial loadings for all cells and thus appears to primarily represent non-sedimentable absorbance, although some may be artifactual. The contribution of non-sedimentable absorbance is apparent from its value at the initial point of the total gradient.

dimeric species to exchange with each other. The species eluting as an apparent dimer and as an apparent monomer were recovered and concentrated separately and then re-injected onto Superdex200 column. Both species generated elution profiles containing a mixture of monomeric and dimeric species, implying that Grb2 exists in reversible monomer-dimer equilibrium. Although SEC analysis is highly dependent upon molecular shape, the knowledge that Grb2 is a compact globular protein with a tightly packed 3D structure speaks volumes in support of our conclusion that the two species with apparent molecular masses of 43kD and 90kD observed here most likely represent Grb2 in its monomeric and dimeric conformation.

In support of the observation that Grb2 may exist in monomer-dimer equilibrium, we also performed MALDI-TOF analysis on the two species of Grb2 observed in SEC analysis (Figure 3-1b). MALDI-TOF analysis of the species eluting as an apparent monomer led to observation of a dominant ion of 43.3kD and a less dominant ion of 21.7kD, implying that these ions correspond to singly-charged Grb2 monomer and doubly-charged Grb2 monomer, respectively. In contrast, MALDI-TOF analysis of the species eluting as an apparent dimer led to observation of a dominant ion of 43.3kD and less dominant ions with molecular masses of 21.7kD and 86.5kD, implying that the dominant ion corresponds to singly-charged Grb2 monomer, while the less dominant ions correspond to doubly-charged Grb2 monomer and singly-charged Grb2 dimer,

respectively. Non-covalent protein dimers do not usually survive the MALDI-TOF process but the fact that we have been able to observe Grb2 dimer in such an analysis suggests that Grb2 dimer must be a highly stable species despite its rapid exchange with its monomeric counterpart.

To further analyze the ability of Grb2 to dimerize, we carried out sedimentation equilibrium experiments using analytical ultracentrifugation (AUC) at various concentrations of Grb2 in the range 0.1-10 μM (Figure 3-1c). The distribution of Grb2 concentration as a function of centrifugal radius in these experiments could not be described by either a homogeneous monomer or dimer but gave excellent fits to a reversible monomer-dimer equilibrium model. Our results thus demonstrate unequivocally that Grb2 exists in monomer-dimer equilibrium at all concentrations analyzed and that there is no evidence of the presence of any higher-order protein aggregate. The global analysis of the distribution of Grb2 at various protein concentrations in the ultracentrifuge cell at equilibrium using the monomer-dimer model, as described by equation [1], yielded a value of 5μM for the apparent dimer dissociation constant (K_d) at 4°C.

3.5.2 Entropy drives the dissociation of Grb2 dimer into monomers

To characterize the Grb2 monomer-dimer equilibrium in thermodynamic terms, we employed the powerful technique of isothermal titration calorimetry (ITC). Because thermodynamic parameters can be dependent upon the varying ionization of particular buffers, we performed our ITC measurements in both Tris and Phosphate buffers. Our ITC data indicate that the dissociation of Grb2 dimer into monomers is under entropic control and accompanied by an unfavorable gain of enthalpy (Figure 3-2). It has been suggested that the sigmoidal nature of ITC isotherms may result from the dissociation of

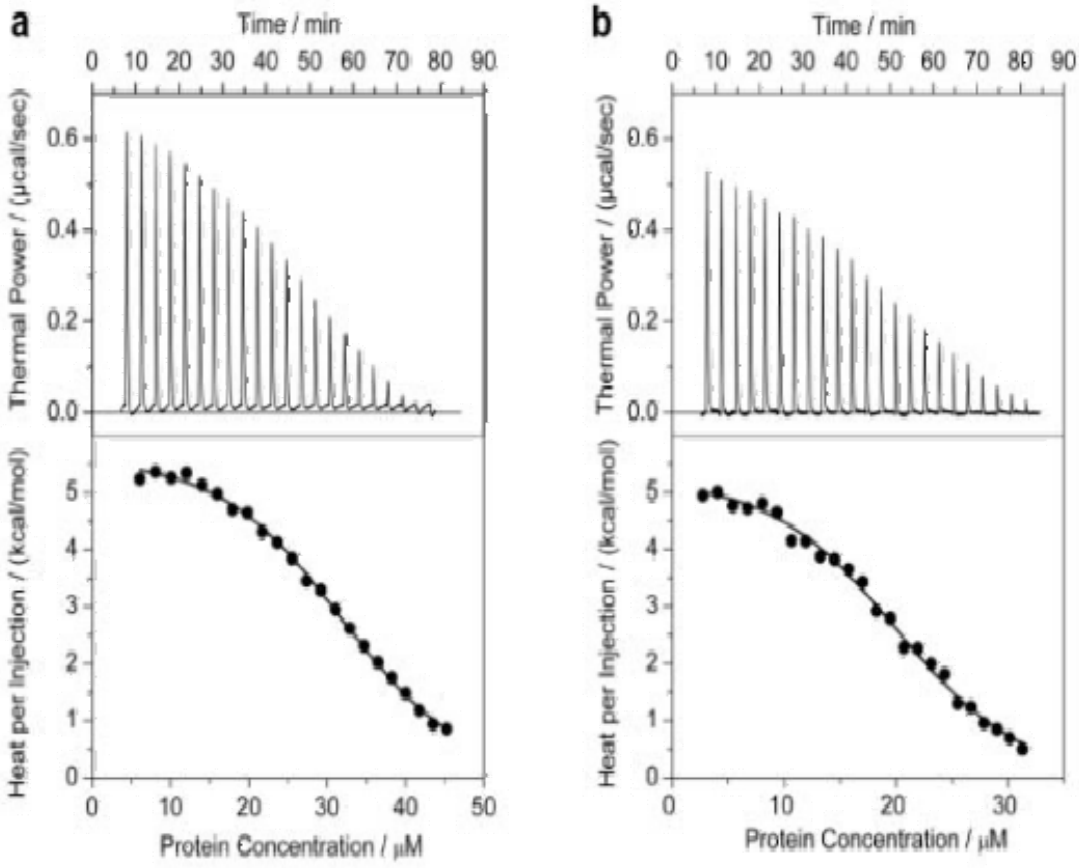

Figure 3-2: ITC analysis of the dissociation of Grb2 dimer into monomers. (a) 300µM of monomer-equivalent Grb2 in Tris buffer in the injection syringe were diluted by making 25 x 10µl injections into the calorimetric cell containing the same buffer at 25°C. (b) 200µM of monomer-equivalent Grb2 in Phosphate buffer in the injection syringe were diluted by making 25 x 10µl injections into the calorimetric cell containing the same buffer at 25°C. In each case, protein concentration on the x-axis is the monomer-equivalent of Grb2 monomers formed upon Grb2 dissociation. The first injection and the corresponding heat uptake are not shown due to systematic uncertainties in the measurement. The solid lines represent the fit of the data to the sigmoidal function given in expression [2].

higher-order multimers into dimers and monomers [70]. In light of the fact that Grb2 only exists in monomer-dimer equilibrium as evidenced by our SEC, MALDI-.TOF and AUC analysis (Figure 3-1), we attribute this sigmoidal behavior to the rather weak nature of Grb2 dimers. For such moderate dimers, the first few injections in an ITC experiment will be expected to result in similar heat uptake due to the fact that every dimer injected into the calorimetric cell will completely dissociate. However, as the concentration of the monomers in the calorimetric cell rises after the first few injections, the additional

injections will progressively result in the lowering of heat uptake due to the decreased tendency of dimers to dissociate into monomers. The heat uptake will eventually level out as the concentration of monomers reaches in excess of the dimer dissociation constant toward the final few injections. Such dissociation of weak dimers will be expected to generate a sigmoidal response curve. In contrast, the ITC isotherms will be expected to obey hyperbolic behavior for the dissociation of strong dimers — each successive injection at the start of an ITC experiment will be expected to result in a slightly lower heat uptake due to the tendency of dimers not to fully dissociate even at lower monomer concentrations in the calorimetric cell. The heat uptake will continue to decrease slowly with further injections and eventually level out as the concentration of monomers in the calorimetric cell reaches beyond the dimer dissociation constant

To extract various thermodynamic parameters, the ITC isotherms were best fit to a sigmoidal function given in equation [2], assuming a model-independent approach to the analysis of dissociation of Grb2 dimer into monomers. Table 3-1 presents the results of such an analysis. As shown in Table 3-1, the dissociation of Grb2 dimer into monomers exhibits thermodynamic signatures in both Tris and Phosphate buffers that are virtually indistinguishable. Although the possibility that enthalpy change could also be a driving force cannot be ruled out, the dissociation of protein dimers into monomers has been hitherto observed to be an exclusively entropy-driven affair accompanied by unfavorable enthalpic changes [70-72]. Such unfavorable enthalpic changes are believed to result from the disruption of an extensive network of electrostatic interactions, hydrogen bonding and hydrophobic forces at the monomer-monomer interface upon dimer dissociation. The crystal structure of Grb2 dimer indeed shows the burial of large hydrophobic surface area upon dimerization and it is thus likely that the unfavorable gain

Table 3-1

Experimentally determined thermodynamic parameters for the dissociation of Grb2 dimer obtained from ITC measurements at 25°C in Tris and Phosphate buffers

	K_d / μM	ΔH / kcalmol^{-1}	TΔS / kcalmol^{-1}	ΔG / kcalmol^{-1}
Tris	31.0±0.9	+5.57±0.35	+11.73±0.35	–6.16± 0.02
Phosphate	19.6±0.4	+5.40±0.17	+11.80±0.17	-6.43±0.01

The values for the various parameters were obtained from the fit of the sigmoidal function given in equation [2] to the binding isotherms shown in Figure 3-2. Errors were calculated from 3-4 independent measurements. All errors are given to one standard deviation. Tris buffer was 50mM Tris, 200mM NaCl, 1mM EDTA and 5mM β-mercaptoethanol at pH 8.0. Phosphate buffer was 50mM Sodium phosphate, 200mM NaCl, 1mM EDTA and 5mM β-mercaptoethanol at pH 8.0.

in enthalpy observed here is due to the disruption of intermolecular interactions at the monomer-monomer interface [10].

What might be the molecular basis of favorable entropic contributions to the free energy upon the dissociation of Grb2 dimer into monomers? Net entropic changes upon the dissociation of protein dimer into monomers are likely to result from interplay between the following three major entropic forces ΔS_{solv}, ΔS_{conf} and ΔS_{mix}. ΔS_{solv} is the unfavorable entropy change due to reduction in the degrees of freedom of solvent molecules as a result of hydration of molecular surfaces, particularly around apolar groups, upon dimer dissociation. ΔS_{conf} is the favorable entropic change that arises from the enhancement of conformational degrees of freedom of the backbone and sidechain atoms upon the dissociation of dimer into monomers. The monomers may also undergo some degree of conformational change upon dissociation, which is also likely to contribute favorably to ΔS_{conf}. Finally, ΔS_{mix} is the favorable entropic change due to the enhancement in the translational, rotational and vibrational degrees of freedom of monomers upon dimer dissociation. Several lines of evidence suggest that ΔS_{mix} typically contributes no more than about –10 cal/mol/K of entropy penalty to the overall entropic

change upon molecular associations [73-76]. To reverse this statement, one could gain up to +10 cal/mol/K in entropy contributions to the free energy of molecular dissociations. In the case of Grb2 dimer dissociation, the entropic contribution to the free energy is approximately +80 cal/mol/K for the dissociation of each dimer — a value that is much larger than the favorable ΔS_{mix} contribution likely to result from the dissociation of two molecules. On the basis of the foregoing argument, we attribute the favorable entropy gain observed here upon the dissociation of Grb2 dimer into monomers to the increase in the conformational degrees of freedom of backbone and sidechain atoms as embodied in the term ΔS_{conf}.

3.5.3 Enthalpy and entropy have compensatory effects on the temperature-dependency of dimerization

Thermodynamic behavior of monomer-dimer equilibria can be highly dependent on the ambient temperature and knowledge of how thermodynamics vary as a function of temperature can provide invaluable insights into the mechanism of protein oligomerization. In an effort to determine the effect of temperature on the various thermodynamic parameters, we analyzed the dissociation of Grb2 dimer into monomers in the narrow temperature range 10-30°C (Figure 3-3). Our data indicate that both the enthalpic (ΔH) and entropic ($T\Delta S$) contributions to the overall free energy of dissociation (ΔG) show strong temperature-dependence and that both ΔH and $T\Delta S$ largely compensate for each other to generate ΔG that is virtually independent of temperature — while ΔH and $T\Delta S$ experience over 10 kcal/mol change in their contributions to dimer dissociation in going from 10°C to 30°C, ΔG gains no more than 0.5 kcal/mol over the same temperature range. Consistent with this observation is the relatively constant nature of the apparent dissociation constant (~20-30μM) over the same temperature range. We limited

our investigations of the effect of temperature on the thermodynamics of Grb2 dimer dissociation within this narrow temperature range due to a number of technical hurdles; below a temperature of 10°C, the low signal-to-noise ratio observed is highly undesirable, while above a temperature of 30°C, the ITC signal in the form of thermal power becomes significantly attenuated such that measurements become less reliable. Despite these limitations, our data suggest that within this temperature range, the dissociation of Grb2 dimer into monomers is overwhelmingly driven by favorable entropic changes accompanied by unfavorable enthalpic contributions to the overall free energy of dissociation.

The linear and opposing dependence of ΔH and $T\Delta S$ as a function of temperature, while maintaining a more or less constant ΔG, is a common feature observed in protein folding and binding reactions [66, 68, 77]. This phenomenon gives rise to two key temperature points T_H and T_S — the temperatures where enthalpic (ΔH) and entropic ($T\Delta S$) contributions to the free energy of binding or dissociation change sign, respectively. Thus, in the case of the dissociation of Grb2 dimer into monomers, ΔH will become negative and hence thermodynamically favorable above T_H, while $T\Delta S$ will become negative and hence thermodynamically unfavorable above T_S. Table 3-2 provides the values for T_H and T_S accompanying the dissociation of Grb2 dimer into monomers. As evidenced in Table 3-2, T_H for the dissociation of Grb2 into monomers is virtually equal to the physiological temperature of 37°C within the experimental error of these measurements. This salient observation implies that the dissociation of Grb2 dimer into monomers under physiological temperatures will not be accompanied by unfavorable enthalpic changes and that enthalpic contributions to the free energy of dissociation will

become favorable at temperatures above 37°C. In contrast, the entropic contributions to the free energy of Grb2 dissociation will remain highly favorable at physiological temperatures and may only act in an opposing manner at temperatures greater than about 55°C.

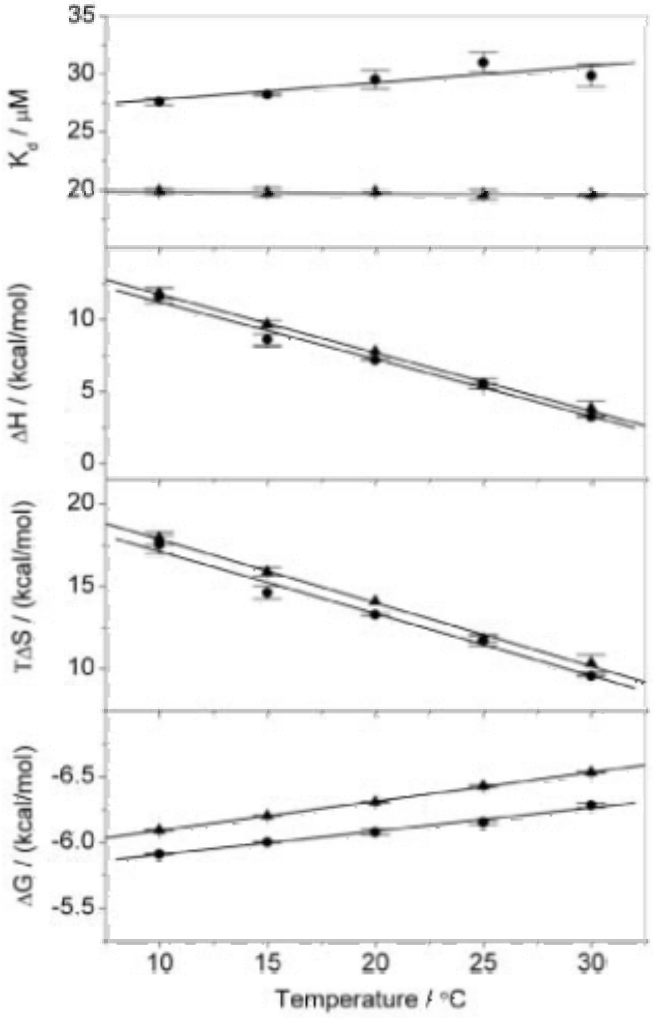

Figure 3-3: Dependence of thermodynamic parameters K_d, ΔH, TΔS and ΔG on temperature for the dissociation of Grb2 dimer into monomers. 100-300μM of monomer-equivalent Grb2 in Tris buffer (●) or Phosphate buffer (▲) in the injection syringe were diluted by making 25 x 10μl injections into the calorimetric cell containing an identical buffer at various temperatures in the range 10-30°C. To determine the various thermodynamic parameters, the ITC isotherms were fit to the sigmoidal function given by the expression [2]. Each data point is the arithmetic mean of 2-3 experiments. All error bars are given to one standard deviation. The solid lines show linear fits to the data points.

It is thus interesting to note that while Grb2 dimer dissociation is enthalpically unfavorable at room temperature, the enthalpic contribution to the free energy will become favorable at temperatures above the physiological temperature of 37°C. At temperatures above 55°C, enthalpy change will be the sole factor favoring the dissociation of Grb2 dimer into monomers, while at the same time, compensating the unfavorable contributions from entropic changes. The favorable enthalpic contributions to the free energy of dissociation at higher temperatures are likely to result from the increase in the kinetic energy of the system due to lowering of the activation energy for the disruption of intermolecular interactions at the monomer-monomer interface. On the same token, the unfavorable entropic contributions to the free energy of dissociation at higher temperatures most likely arise from the change in the ΔS_{conf} component of the overall entropy change of the system. Unlike at room temperature, the change in ΔS_{conf} is unlikely to be the major factor behind favorable entropic contributions at higher temperatures due to an increase in the kinetic energy of the system; this is likely to cancel out any advantage of monomers over the dimer in terms of the conformational degrees of freedom available to backbone and sidechain atoms at higher temperatures. As a consequence of decreased or negligible contributions from changes in the conformational degrees of freedom available to backbone and sidechain atoms upon dimer dissociation, the hydration of molecular surfaces at the monomer-monomer interface upon dissociation may provide the major source of entropic penalty at higher temperatures.

3.5.4 Grb2 monomers undergo domain swapping upon dimerization

The temperature-dependence of ΔH is related to heat capacity of binding (ΔC_p) by Kirchhoff's relationship $\Delta C_p = d(\Delta H)/dT$; the slope of a plot of ΔH versus temperature equates to ΔC_p. Heat capacity is an important thermodynamic parameter in that it is

related to the extent of the burial, occlusion and dehydration of molecular surfaces from surrounding solvent molecules upon intermolecular association. This is technically referred to as the change in solvent-accessible surface area (ΔSASA) [66, 78-80]. As such, this information is critical to understanding the mechanism of molecular recognition and, in the context of protein oligomerization, such information can further help us pinpoint any conformational changes involved in the association of protein monomers into dimer.

In an attempt to understand how the association of monomers into dimer affects SASA, we calculated values for ΔC_p in the neighborhood of around – 400 cal/mol/K from the slope of ΔH versus temperature plots obtained for the dissociation of Grb2 dimer into monomers (Figure 3-3 and Table 3-2). What might be the significance of such small negative values of ΔC_p observed here? A positive value of ΔC_p implies that the occlusion of polar surfaces dominates the intermolecular association over apolar surfaces [66, 81, 82]. The fact that ΔC_p possesses small negative values suggests that the occlusion of

Table 3-2

Experimentally determined thermodynamic parameters for the dissociation of Grb2 dimer obtained from ITC measurements at various temperatures in the range 10-30°C in Tris and Phosphate buffers

	T_H / °C	T_S / °C	ΔH_{60} / kcalmol^{-1}	ΔC_p / kcalmol^{-1}K^{-1}
Tris	+38.35±1.10	+55.48±2.50	-8.61±1.13	-0.40±0.03
Phosphate	+39.11±1.79	+58.51±3.36	-8.52±1.45	-0.41±0.03

The values for T_H, the temperature at which ΔH is zero, were obtained from the extrapolation of linear fits to the ΔH versus temperature plots (Figure 3-3). The values for T_S, the temperature at which TΔS is zero, were obtained from the extrapolation of linear fits to the TΔS versus temperature plots (Figure 3-3). The values for ΔH_{60}, the enthalpy at 60°C, were obtained from the extrapolation of linear fits to the ΔH versus temperature plots (Figure 3-3). The values for ΔC_p, the heat capacity change, were obtained from the slopes of linear fits to the ΔH versus temperature plots (Figure 3-3). Errors were calculated from 3-4 independent measurements. All errors are given to one standard deviation. Tris buffer was 50mM Tris, 200mM NaCl, 1mM EDTA and 5mM β-mercaptoethanol at pH 8.0. Phosphate buffer was 50mM Sodium phosphate, 200mM NaCl, 1mM EDTA and 5mM β-mercaptoethanol at pH 8.0.

apolar surfaces does not play a significant role in the dimerization of Grb2. This thermodynamic observation is in stark contrast to the 3D crystal structure of Grb2 dimer, in which protein monomers appear to bury a rather large hydrophobic surface area upon dimerization [10]. Could this discrepancy be due to some sort of protein conformational changes in the monomers upon dimerization? Experimental determination of the magnitude of ΔC_p combined with ΔH_{60} (enthalpy change at 60°C), as listed in Table 3-2, has been widely used to quantitatively calculate changes in polar SASA ($\Delta SASA_{polar}$), apolar SASA ($\Delta SASA_{apolar}$) and total SASA ($\Delta SASA_{total}$) upon intermolecular associations [65-68, 76, 83]. Such changes in SASA upon the dimerization of Grb2 from our thermodynamic measurements are reported in Table 3-3.

In accordance with the crystal structure of Grb2, whereby the protein crystallized as a dimer with two-fold axis of symmetry [10], the monomers would adopt a rather open conformation particularly with respect to the orientation of the SH2 domain relative to the SH3 domains assuming no conformational change upon dimer dissociation. Given the rather large inter-domain loops (between 13-24 residues), the scenario of Grb2 not undergoing any conformational change upon dimer dissociation would be very unrealistic. Rather, a more likely scenario would be the one where the domains undergo some degree of rearrangement relative to each other such that the monomeric protein adopts a more compact and globular shape. To test that this is so, we also determined changes in SASA upon the dimerization of Grb2 from structural data independent of our thermodynamic measurements. To calculate changes in SASA upon the dimerization of Grb2 from structural data, we assumed two models of dimerization — the Rigid Body model and the Flexible Body model. In the Rigid Body model, it was assumed that the monomers do not undergo any conformational change whatsoever upon dimerization and

that the domains within each monomer and dimer retain the same conformations relative to each other as those observed in the crystal dimeric unit with two-fold axis of symmetry [10]. In the Flexible Body model, it was assumed that the monomers undergo domain swapping upon dimerization so as to preserve the cSH3-SH2 domain-domain interactions.

The Grb2 dimer is largely held together by two major monomer-monomer contacts at the cSH3(A)-SH2(B) and cSH3(B)-SH2(A) interfaces, where A and B in the parenthesis refer to monomers A and B within Grb2 dimer. Given the large and flexible nature of inter-domain loops in Grb2 [84], we reasoned that the cSH3(A)-SH2(B) and cSH3(B)-SH2(A) inter-monomer contacts could be swapped by cSH3(A)-SH2(A) and cSH3(B)-SH2(B) inter-domain contacts within monomers A and B, respectively, upon Grb2 dimer dissociation. In other words, the cSH3-SH2 inter-monomer contacts, between cSH3 domain of one monomer and the SH2 domain of the other monomer and vice versa, that hold the two monomers together to form a dimer could re-establish their respective interactions between cSH3 and SH2 domains within the same monomer due to the flexibility of the inter-domain loops upon Grb2 dimer dissociation. The fact that the cSH3 and SH2 domains are tethered together via a flexible loop (23 residues) implies that the cSH3-SH2 interactions within the same monomer could in fact be much stronger — due to entropic advantage — than the interactions between cSH3 domain of one monomer and SH2 domain of the other monomer and vice versa. Thus, the dimerization of Grb2 would require that the cSH3-SH2 interactions within the same monomer be disrupted and then re-established in an inter-monomer context. The energetic cost of re-building such cSH3-SH2 contacts in an inter-monomer context would then have to be recovered and it may well be that the functional benefits of dimerization outweigh this energetic penalty.

Protein dimerization imparts additional advantages, such as enhanced stability and greater specificity, and as such, what may seem Grb2's extravagant pursuit in search of becoming dimerized, could in fact be a blessing in disguise in the context of attaining high fidelity in cellular signaling.

If the Grb2 monomers were to undergo above-mentioned cSH3-SH2 domain swapping, that would involve breaking up of cSH3-SH2 contacts within each monomer and then re-establishing these contacts between the cSH3 domain of one monomer and the SH2 domain of the other monomer, upon dimerization, the extent of the burial of surface area would be expected to be different from the situation where they do not undergo domain swapping and simply come together as rigid bodies. Table 3-3 summarizes and compares values for $\Delta SASA_{polar}$, $\Delta SASA_{apolar}$ and $\Delta SASA_{total}$ upon the dimerization of Grb2, as calculated from our thermodynamic measurements using ITC

Table 3-3

Changes in polar SASA ($\Delta SASA_{polar}$), apolar SASA ($\Delta SASA_{apolar}$) and total SASA ($\Delta SASA_{total}$) upon the dimerization of Grb2 obtained from thermodynamic and structural data

Method →	Thermodynamic		Structural	
Buffer/Model →	Tris	Phosphate	Rigid Body	Flexible Body
$\Delta SASA_{polar}$ / Å^2	-693	-699	-2070	-964
$\Delta SASA_{apolar}$ / Å^2	-1553	-1587	-2711	-1432
$\Delta SASA_{total}$ / Å^2	-2246	-2286	-4781	-2396

ΔSASA values based on thermodynamic data were obtained from the measurement of ΔC_p and ΔH_{60} for the dimer dissociation of Grb2 in Tris and Phosphate buffers (Figure 3-3) using expressions [4] and [5], while ΔSASA values based on structural data were derived from 3D structural models of Grb2 dimer and monomer (Figure 3-4) using expressions [6] and [7]. For ΔSASA values calculated from structural data, two models were assumed — the Rigid Body model and the Flexible Body model. In the Rigid Body model, it was assumed that the monomers undergo no conformational change upon dimerization and that the two monomers essentially come into contact with each other as rigid bodies. In the Flexible Body model, it was assumed that the monomers undergo conformational change and domain swapping upon dimerization (see text for full explanation). ΔSASA values calculated from thermodynamic data make no assumptions and are thus model-independent. Tris buffer was 50mM Tris, 200mM NaCl, 1mM EDTA and 5mM β-mercaptoethanol at pH 8.0. Phosphate buffer was 50mM Sodium phosphate, 200mM NaCl, 1mM EDTA and 5mM β-mercaptoethanol at pH 8.0.

and structural data obtained from 3D structural models based on the known crystal structure of Grb2 [10]. Our analysis shows that there are significant deviations between the values calculated from thermodynamic data and the Rigid Body model of dimerization. In contrast, the values determined from thermodynamic data agree par excellence with those calculated from the Flexible Body model. While the changes in SASA determined from thermodynamic data deviate by more than 100% relative to those determined from structural data assuming the Rigid Body model, these values agree within about 10% to those calculated from structural data assuming the Flexible Body model. The small anomalies in the values for changes in SASA between those obtained from thermodynamic data versus those calculated from structural data assuming the Flexible Body model are likely due to errors in the atomic coordinates of the structural models of the monomers; although somewhat similar, the SH2 and SH3 domains may not exactly adopt the orientations relative to each other in the monomers as described by our Flexible Body model. An alternative explanation for the discrepancy observed between the values for changes in SASA between those obtained from thermodynamic data versus those calculated from structural data assuming the Flexible Body model may also be due to poor parameterization of the empirical models that couple heat capacity changes to changes in SASA upon intermolecular associations [65-68, 76, 83].

In short, we believe that the significant overestimation of changes in SASA calculated from structural data assuming the Rigid Body model are due to the unrealistic assumption that the monomers do not experience any conformational change or domain swapping upon dimerization. This is particularly significant in light of the large flexible inter-domain loops, which are likely to favor cSH3-SH2 domain swapping once the

dimer contacts at the monomer-monomer interface are removed. This likely scenario bears fruit in our Flexible Body model, which seems to fully account for our thermodynamic data reported here.

3.5.5 Structural modeling allows rationalization of thermodynamic data

In an attempt to rationalize our thermodynamic data in structural terms, we modeled 3D structures of Grb2 as a dimer and as a monomer that adopts the same conformation as that observed in the dimer structure as well as an alternative conformation consistent with our thermodynamic data discussed above (Figure 3-4). All three structures were modeled using the crystal structure of Grb2 dimer as a template [10]. The necessity for modeling the structure of Grb2 dimer arose due to the absence of residues 28-33 in a loop in the nSH3 domain as a result of lack of electron density for these residues in the crystal structure. As evident, in the Grb2 dimer, the two monomers are related by a two-fold axis of symmetry and pack tightly against each other burying a total surface area of about 4800Å^2 at the monomer-monomer interface (Figure 3-4a). The monomers are largely held together by molecular interaction provided by cSH3 domain of one monomer and SH2 domain of the other monomer at the cSH3(A)-SH2(B) and cSH3(B)-SH2(A) interfaces, where A and B in the parenthesis refer to monomers A and B within Grb2 dimer. Furthermore, the dimer is also stabilized by domain-domain interactions between cSH3 domains from each monomer. However, the nSH3 domains are positioned well away from the monomer-monomer interface and thus do not participate in the dimerization process. Furthermore, such exquisite packing of monomers ensures that the ligand binding pockets of all three domains — nSH3, SH2 and cSH3 — in each monomer are solvent-exposed and thus fully accessible to engage in protein-protein interactions with the cellular partners of Grb2.

It has been suggested that the monomers may maintain the same conformation and the relative orientation of their domains when in isolation [10]. However, a quick survey of the monomer conformation suggests that at least some degree of conformational change is likely to occur upon the dissociation of Grb2 dimer. Thus, while the SH3 domains within the monomer are somewhat packed against each other, the SH2 domain makes no contact with either SH3 domain and it is simply held at an interfacial distance of about 30Å by the nSH3-SH2 loop (13 residues) and the SH2-cSH3 loop (24 residues) (Figure 3-4b). If the monomers were to adopt this conformation when in isolation, the flexibility of the inter-domain loops would imply that the SH2 domain is able to adopt multiple orientations and that it could also yo-yo relative to the SH3 domains. This hypothesis is further supported by our heat capacity measurements, which suggest that the total surface area buried upon Grb2 dimerization is close to 2300Å^2 instead of 4800Å^2 obtained from structural analysis alone assuming no conformational changes in the monomers upon Grb2 dimerization (Table 3-3). In light of the foregoing argument, the most straightforward interpretation of this discrepancy is that the SH2 domain is unlikely to be fully solvent-exposed and most likely packs against either the nSH3 domain or the cSH3 domain or both in the isolated monomers. Given that the cSH3-SH2 domain-domain interactions appear to be the dominant force holding the monomers together into a dimer, it is plausible to speculate that the cSH3 and SH2 domains could also re-establish such contact in the context of an isolated monomer (Figure 3-4c). To paraphrase this slightly, the SH2 domain may pack against the cSH3 domain within the same isolated monomer in a manner akin to the domain-domain interactions observed between the SH2 domain of one monomer and the cSH3 domain of the other monomer within the Grb2 dimer. To accomplish such domain swapping, the

SH2 domain will have to undergo two spatial transformations; to rotate clockwise by ~180° about an axis parallel to the nSH3-cSH3 plane followed by a second clockwise rotation of ~180° about an axis perpendicular to the nSH3-cSH3 plane (Figures 4b and 4c).

The large and flexible nature of inter-domain loops nSH3-SH2 and SH2-cSH3 would ensure that this is not only kinetically feasible but the tethering of SH2 and cSH3 domains within the same isolated monomer would also be entropically more favorable than the coming together of SH2 domain of one monomer and the cSH3 domain of the other monomer in the context of a dimer.

In so doing, the SH2-cSH3 packing within each isolated monomer would bury surface area of approximately 1200Å^2 at the domain-domain interface, or a total surface area of about 2400Å^2 between two isolated monomers. Thus, upon Grb2 dimerization, the disruption of SH2-cSH3 contacts within both isolated monomers would initially result in the exposure of surface area of about 2400Å^2 and hence a deficit of surface area of about 2400Å^2 prior to re-establishing the SH2-cSH3 contacts across each monomer to generate the dimer in order to pay for this deficit. The total surface area buried upon Grb2 dimerization is about 4800Å^2 assuming no conformational change in the monomers. However, after paying a deficit of surface area of about 2400Å^2 exposed upon the disruption of SH2-cSH3 contacts within each isolated monomer, the overall surface area buried upon Grb2 dimerization would equate to about 4800Å^2 minus 2400Å^2. Thus, a

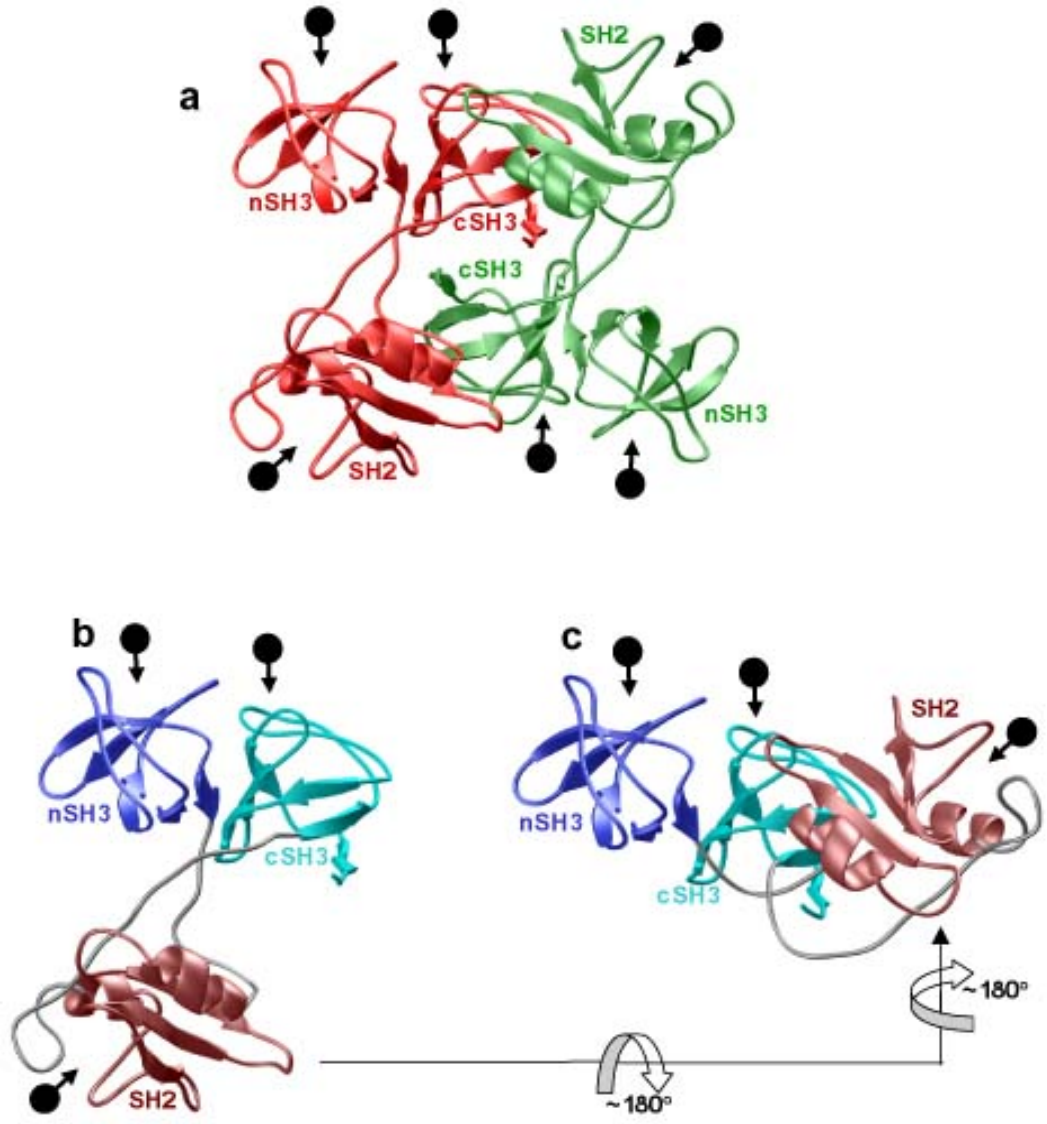

Figure 3-4: 3D modeled structures of Grb2 in dimeric and monomeric forms with arrow-headed black spheres directing the ligand binding sites within SH2 and SH3 domains. (a) Modeled structure of Grb2 dimer. One monomer is shown in red and the other in green. The three domains nSH3, SH2 and cSH3 are labeled. The structure was modeled using the crystal structure of Grb2 dimer as a template (with a PDB code of 1GRI). The only notable difference in the modeled structure and the crystal structure is the construction of a loop in the nSH3 domain (residues 28-33) that was missing in the crystal structure due to poor electron density. (b) Modeled structure of Grb2 monomer assuming no conformational change upon dimer dissociation. The nSH3 domain is shown in blue, the SH2 domain in brown and the cSH3 domain in cyan. The inter-domain loops nSH3-SH2 and SH2-cSH3 are colored gray. The structure was modeled using only the monomeric unit in the crystal structure of Grb2 dimer as a template (with a PDB code of 1GRI). Additionally, residues 28-33 missing in the crystal structure due to poor electron density were built. (c) Modeled structure of Grb2 monomer assuming conformational change upon dimer dissociation as a result of cSH3-SH2 domain swapping. The nSH3 domain is shown in blue, the SH2 domain in brown and the cSH3 domain in cyan. The inter-domain loops nSH3-SH2 and SH2-cSH3 are colored gray. The structure was modeled using the crystal structure of Grb2 dimer as a template (with a PDB code of 1GRI) but with atomic coordinates derived from only the nSH3 and cSH3 domains of one monomer and the SH2 domain of the other monomer. The residues in the inter-domain loops were allowed to float freely so as enable them to adopt optimal conformations during the modeling process.

value of 2400Å^2 would be expected to be the overall burial of surface area being recorded in our heat capacity measurements reported here. A value of about 2300Å^2 deduced from such measurements is in an excellent agreement with a value of 2400Å^2 derived from structural data for Grb2 dimerization on the basis of the assumption that such dimerization proceeds via cSH3-SH2 domain swapping. Such conformational change that Grb2 may have to undergo upon dimerization, in agreement with our thermodynamic data reported here, can be best visualized in the form of a movie accessible @ http://labs.med.miami.edu/farooq/movies/Grb2Dimer.

It should be noted here that the isolated SH2 domain of Grb2 can also dimerize by virtue of its ability to undergo domain swapping [85-87]. Here, the dimerization is achieved through the ability of the C-terminal α-helix from each SH2 domain to swap in an inter-domain manner so as to generate an intertwined SH2 dimer that exhibits lower affinity for cognate ligands relative to SH2 monomer. This observation is in contrast to the model presented above for the dimerization of Grb2 in which the SH2 domain simply swaps its interactions with the cSH3 domain from being in an intra-molecular contact in the context of Grb2 monomer to being in an inter-molecular contact in the Grb2 dimer without blocking access to ligand binding sites. Although ligand binding affinity to SH2 and SH3 domains has not been measured in the context of full-length protein, it is unlikely that Grb2 dimerization would lower the ligand binding affinity in a manner akin to that observed for the SH2 domain-swapped dimer. On the contrary, the SH2 and SH3 domains in the context of Grb2 dimer are likely to bind with much higher affinity to multivalent ligands due to entropic advantage. That such a scenario may prevail warrants further studies on the role of Grb2 dimerization in cellular signaling.

3.6 Concluding remarks

Elucidating protein-protein interactions in thermodynamic terms offers molecular insights into the mechanisms of life at a level second to none. Although Grb2 has been perceived as a central player in cellular signaling since its discovery over a decade ago [2, 4, 10], little is known about the role of oligomerization in the biological function of Grb2. This is particularly significant given that Grb2 is one of only a handful of adaptor modular proteins for which complete 3D structure has been solved to atomic resolution and it is often tipped as the best characterized adaptor protein in cellular signaling [10]. The ability of proteins to undergo oligomerization comes at a price but that is worth paying for in exchange for functional advantages that include but are not limited to enhanced stability, greater specificity and selectivity toward cognate ligands, and increased ability to participate in signal amplification — a feature that is a hallmark of cellular signaling and perturbations to which can make the difference between a healthy and diseased cell.

In this study, using an array of biophysical methods, we have shown that Grb2 exists in a dynamic equilibrium between dimer and monomers with the equilibrium well in favor of the latter species under low protein concentrations that are likely to be encountered under normal functioning of the cellular machinery. Allthough the Grb2 monomer-dimer equilibrium is likely to be in favor of the monomer in quiescent cells, rapid expression and rise in Grb2 concentration upon mitogenic stimulation is likely to shift this equilibrium in favor of the dimer. Other factors within the cell are also likely to affect the Grb2 monomer-dimer equilibrium. Studies on cultured mammalian cells indicate that phosphorylation of both Y239 and Y317 in p52Shc is required for efficient formation of p52Shc-Grb2-Sos complex [11]. Thus, the requirement of two rather than

one phosphorylation site in p52Shc for Grb2 recruitment may shift the Grb2 monomer-dimer equilibrium in favor of the dimer due to the fact that SH2 domains in dimeric Grb2 are likely to bind to two phosphorylation sites in p52Shc with much greater affinity and specificity than a single SH2 domain in monomeric Grb2 and as a consequence of this differential binding, the existence of Grb2 dimer over monomers will be highly favored over both thermodynamic and kinetic grounds not to mention the functional advantages that such a mechanism may impart upon cellular signaling.

Our study also demonstrates exquisitely how thermodynamic information can be employed to corroborate or refute structural data. Although Grb2 crystallizes as a dimer with a two-fold axis of symmetry [10], the assumption that the monomers within this dimer may retain the same conformation in isolation is unlikely to bear fruit due to the large and flexible inter-domain loops. Our thermodynamic data indeed suggest strongly that the monomers are likely to undergo cSH3-SH2 domain swapping and thus adopt a more compact structure than that observed in the Grb2 dimer. Given that the structure of Grb2 in its monomeric state is not available and that it may not be practically surmountable in the foreseeable future due to the requirement of protein at high concentrations, conditions under which it predominantly exists as a dimer, for structural analysis by both the X-ray and NMR methodologies, the relevance of our thermodynamic studies presented here could not be overemphasized.

In short, our data demonstrate unequivocally that Grb2 exists in monomer-dimer equilibrium in solution and that it is likely to undergo cSH3-SH2 domain swapping upon dimerization. This salient observation has profound impacts for furthering our understanding of the role of Grb2 in cellular signaling and for the possible therapeutic intervention of Grb2 in signaling cascades that result in oncogenic transformation of

cells. Many drugs are designed to interfere with protein oligomerization or lead to disruption of protein-protein interfaces. Our demonstration that Grb2 exists in monomer-dimer equilibrium may open up new avenues of drug design for disrupting Grb2 dimerization, such as targeting the monomeric conformation of Grb2 so as to prevent its dimerization, and thus could lead to the development of novel anti-cancer drugs with low toxicity coupled with more effectiveness.

4 Chapter 4: Structural Basis of the Differential Binding of the SH3 Domains of Grb2 Adaptor to the Guanine Nucleotide Exchange Factor Sos1

4.1 Summary

Grb2-Sos1 interaction, mediated by the canonical binding of N-terminal SH3 (nSH3) and C-terminal SH3 (cSH3) domains of Grb2 to a proline-rich sequence in Sos1, provides a key regulatory switch that relays signaling from activated receptor tyrosine kinases to downstream effector molecules such as Ras. Here, using isothermal titration calorimetry in combination with site-directed mutagenesis, we show that the nSH3 domain binds to a Sos1-derived peptide containing the proline-rich consensus motif PPVPPR with an affinity that is nearly three-fold greater than that observed for the binding of cSH3 domain. We further demonstrate that such differential binding of nSH3 domain relative to the cSH3 domain is largely due to the requirement of a specific acidic residue in the RT loop of the β-barrel fold to engage in the formation of a salt bridge with the arginine residue in the consensus motif PPVPPR. While this role is fulfilled by an optimally positioned D15 in the nSH3 domain, the chemically distinct and structurally non-equivalent E171 substitutes in the case of the cSH3 domain. Additionally, our data suggest that salt tightly modulates the binding of both SH3 domains to Sos1 in a thermodynamically distinct manner. Our data further reveal that, while binding of both SH3 domains to Sos1 is under enthalpic control, the nSH3 binding suffers from entropic penalty in contrast to entropic gain accompanying the binding of cSH3, implying that the two domains employ differential thermodynamic mechanisms for Sos1 recognition. Our new findings are rationalized in the context of 3D structural models of SH3 domains in complex with the Sos1 peptide. Taken together, our study provides structural basis of the differential binding of SH3 domains of Grb2 to Sos1 and a detailed thermodynamic profile of this key protein-protein interaction pertinent to cellular signaling and cancer.

4.2 Abbreviations

CD	Circular dichroism
EGF	Epidermal Growth Factor
Grb2	Growth factor Receptor Binder 2
ITC	Isothermal Titration Calorimetry
MALDI-TOF	Matrix-assisted LASER Desorption/Ionization-Time of Flight
MAPK	Mitogen-Activated Protein Kinase
NMR	Nuclear Magnetic Resonance
PDGF	Platelet-Derived Growth Factor
RTK	Receptor Tyrosine Kinase
SEC	Size Exclusion Chromatography
SH2	Src Homology 2
SH3	Src Homology 3
Shc	Src Homology Containing
Sos1	Son of sevenless 1

4.3 Background

Adaptor proteins play a central role in mediating cellular signaling within and across cells. Grb2 is one such adaptor that couples activated receptor tyrosine kinases (RTKs) to downstream effectors and regulators such as Ras [2, 13, 36, 50]. The critical role of Grb2 in cellular signaling is exquisitely demonstrated through defects in mice embryos upon the disruption of *grb2* gene [1]. Grb2 is a modular protein comprised of a central SH2 domain flanked between an N-terminal SH3 (nSH3) domain and a C-terminal SH3 (cSH3) domain, giving it an overall modular architecture of nSH3-SH2-cSH3 [2]. Grb2 recognizes activated RTKs by virtue of its SH2 domain to bind to

tyrosine-phosphorylated (pY) sequences in the context of the consensus motif pYXN located within the cytoplasmic tails of a diverse array of receptors, including EGF and PDGF receptors [3, 4]. Alternatively, Grb2 can also indirectly dock onto activated RTKs through the binding of its SH2 domain to pY sequences within the adaptor protein p52Shc [5, 6]. Upon the interaction of Grb2 to RTKs directly or indirectly, the SH3 domains of Grb2 present a vast opportunity for a wide variety of proteins, containing proline-rich sequences, to be recruited to the inner membrane surface and thus engage in downstream cellular signaling cascades [12-20]. Among them, the guanine nucleotide exchange factor Sos1 is by far the best characterized downstream partner of Grb2 [12, 13]. Upon recruitment to the inner membrane surface, Sos1 catalyzes the GDP-GTP exchange within the membrane-bound GTPase Ras and thereby switches on a key signaling circuit that involves the activation of MAPK cascade central to cellular proliferation, survival and differentiation [21, 22].

Several studies have shown that the requirement of both SH3 domains of Grb2 is de rigueur for full and sustained activation of Ras [6, 12, 13, 36]. However, biophysical analysis of the binding of SH3 domains of Grb2 to a Sos1-derived peptide containing the proline-rich consensus motif PPVPPR suggests that the affinity of the nSH3 domain for Sos1 is several-fold greater than that observed for the cSH3 domain [37]. Structural analysis reveals that the nSH3 domain of Grb2 binds to a Sos1 peptide containing the consensus motif PPVPPR in a canonical fashion [35, 38-40]. The nSH3 domain adopts a characteristic β-barrel fold comprised of a pair of nearly-orthogonal β-sheets with each β-sheet containing three anti-parallel β-strands. The incoming Sos1 peptide docks against a largely hydrophobic binding cleft located on one face of the β-barrel. Upon binding to this cleft in the nSH3 domain, the Sos1 peptide adopts the relatively open left-handed

polyproline type II helical conformation. In comparison with the binding modes of proline-rich ligands to other SH3 domains, the residues in the Sos1 peptide that account for its specificity to the nSH3 domain of Grb2 appear to be V_{+2} and R_{+5} within the consensus motif PPVPPR, according to the nomenclature suggested by Schreiber and co-workers [42], with the first proline within this motif designated zero. Alanine substitution of V_{+2} and R_{+5} individually indeed reduces the affinity of the Sos1 peptide for the nSH3 domain by about 10-20 fold [35]. Due to lower binding affinity, structural analysis of cSH3 domain in complex with a Sos1 peptide has not hitherto been possible but NMR analysis suggests that Sos1 binds to the cSH3 domain in a manner akin to that observed for its interaction with the nSH3 domain [37].

To address the structural basis of the differential binding of SH3 domains of Grb2 to Sos1, we performed pair-wise amino acid sequence alignment of nSH3 and cSH3 domains (Figure 4-1a). Given that V_{+2} and R_{+5} within the consensus motif PPVPPR account for the binding specificity of Sos1 to nSH3 domain [35], we reasoned that the residues within the nSH3 domain in close spatial contact with V_{+2} and R_{+5} may hold the clue to unraveling the differential binding of nSH3 domain versus cSH3 domain to Sos1. Structural analysis of nSH3 domain in complex with a Sos1 peptide containing the consensus motif PPVPPR has previously indicated that V_{+2} inserts into a deep hydrophobic pocket formed by residues F9, W36 and Y52 within the nSH3 domain, while R_{+5} very likely engages in the formation of an energetically favorable salt bridge with acidic residues D15 and/or E16 located within the β1-β2 loop of the nSH3 domain [35, 38]. The β1-β2 loop is more widely known as the RT loop in the context of the β-barrel fold of SH3 domains due to the observation that the mutations of arginine and threonine residues within this loop of the SH3 domain of Src tyrosine kinase are

important determinants of its transforming potential [43]. Analysis of the amino acid sequence alignment reveals that the triplet of F9/W36/Y52 in the nSH3 domain is absolutely conserved in the cSH3 domain with the structurally equivalent residues being F167/W193/Y209 (Figure 4-1a). Thus, the differential binding of nSH3 and cSH3 domains to Sos1 could not be explained in terms of the requirement of specific residues within the SH3 domain for stabilizing V_{+2} within the consensus motif PPVPPR. In contrast, while E16 in the nSH3 domain is absolutely conserved by the structurally equivalent E174 in the cSH3 domain, the same is not true for D15 in the nSH3 domain, which is substituted by the structurally equivalent G173 in the cSH3 domain. Assuming that it is D15 and not E16 in the nSH3 domain that salt bridges with R_{+5} within the consensus motif PPVPPR, this scenario could easily explain the differential binding of nSH3 and cSH3 domains to Sos1 as the substitution of a glycine for an aspartate at a critical salt bridging position would likely result in the partial loss of binding affinity. Interestingly, our sequence analysis further suggests that there may be more to this story. Although the cSH3 domain lacks an acidic residue at the structurally equivalent position occupied by D15 in the nSH3 domain, the residue E171 lies within close proximity to G173 within the RT loop and thus could be a strong candidate for fulfilling the role of a salt bridging partner for R_{+5} within the consensus motif PPVPPR. In light of the foregoing argument, we hypothesize that the differential binding of nSH3 and cSH3 domains to a Sos1 peptide containing the consensus motif PPVPPR is likely due to the ability of D15 within the nSH3 domain to salt bridge with R_{+5}, while this role may only partially be fulfilled by a chemically distinct and structurally non-equivalent residue E171 in the cSH3 domain due to the absence of an acidic residue at the structurally equivalent position D15 (Figure 4-1b).

In an effort to test the above hypothesis, we have employed here isothermal titration calorimetry in combination with site-directed mutagenesis to determine complete thermodynamic signatures of the binding of various wildtype and mutant SH3 domains of Grb2 to a Sos1-derived peptide containing the consensus motif PPVPPR. Our data show that the nSH3 domain binds to a Sos1-derived peptide containing the proline-rich consensus motif PPVPPR with an affinity that is nearly three-fold greater than that observed for the binding of cSH3 domain. We further demonstrate that such differential binding of nSH3 domain relative to the cSH3 domain is largely due to the requirement of a specific acidic residue in the RT loop of the β-barrel fold to engage in the formation of a salt bridge with the arginine residue in the consensus motif PPVPPR. While this role is fulfilled by an optimally positioned D15 in the nSH3 domain, the chemically distinct and structurally non-equivalent E171 substitutes in the case of the cSH3 domain. Additionally, our data suggest that salt tightly modulates the binding of both SH3 domains to Sos1 in a thermodynamically distinct manner. Our data further reveal that, while binding of both SH3 domains to Sos1 is under enthalpic control, the nSH3 binding suffers from entropic penalty in contrast to entropic gain accompanying the binding of cSH3, implying that the two domains employ differential thermodynamic mechanisms for Sos1 recognition. Our new findings are rationalized in the context of 3D structural models of SH3 domains in complex with the Sos1 peptide. Taken together, our study provides structural basis of the differential binding of SH3 domains of Grb2 to Sos1 and a detailed thermodynamic profile of this key protein-protein interaction pertinent to cellular signaling and cancer.

4.4 Experimental procedures

4.4.1 Protein preparation

nSH3 (residues 1-56) and cSH3 (residues 156-217) domains of human Grb2 (Expasy# P62993) were cloned into pET102 bacterial expression vector — with an N-terminal thioredoxin (Trx)-tag followed by a thrombin site and a C-terminal polyhistidine (His)-tag preceded by a thrombin site — using Invitrogen TOPO technology. Trx-tag was included to maximize protein expression in soluble fraction, while the His-tag was added to aid in protein purification by Ni-NTA affinity chromatography. Additionally, thrombin protease sites were introduced at both the N- and C-termini of the protein to aid in the removal of tags after protein purification. The proteins were expressed in Escherichia coli BL21*(DE3) bacterial strain (Invitrogen) cultured in LB media and purified on Ni-NTA affinity column using standard procedures. Further treatment of the recombinant proteins on a MonoQ ion-exchange column and a Hiload Superdex 200 size-exclusion column coupled to GE Akta FPLC system led to purification of recombinant nSH3 and cSH3 domains to apparent homogeneity as judged by SDS-PAGE analysis. The identity of recombinant domains was further confirmed by MALDI-TOF mass spectrometry analysis. Protein yield was typically between 20-30mg of recombinant domain of apparent homogeneity per liter of bacterial culture. The treatment of recombinant domains with thrombin protease significantly destabilized them and rendered them proteolytically unstable. For this reason, all experiments reported herein were carried out on recombinant fusion nSH3 and cSH3 domains containing a Trx-tag at the N-terminus and a His-tag at the C-terminus. The tags were found to have no effect on the functional properties of either domain. Protein concentrations were determined by both fluorescence using Invitrogen Quant-It assay and absorbance at 280nm using an extinction coefficient

of 24,075$M^{-1}cm^{-1}$ for the nSH3 domains and 28,085$M^{-1}cm^{-1}$ for the cSH3 domains. The extinction co-efficients were calculated from amino acid sequence alone using the online software ProtParam at ExPasy Server [59]. Results from both methods were in an excellent agreement.

4.4.2 Site-directed mutagenesis

pET102 bacterial expression vectors expressing wildtype nSH3 (nSH3_WT) and wildtype cSH3 (cSH3_WT) domains of Grb2 were subjected to Stratagene Quickchange II site-directed mutagenesis to generate D15G (nSH3_D15G) and A13E (nSH3_A13E) mutants of the nSH3 domain and G173D (cSH3_G173D) and E171A (cSH3_E171A) mutants of the cSH3 domain. All mutant domains were expressed, purified and characterized as described above. When analyzed by size-exclusion chromatography (SEC) using Superdex 200 column, all mutant SH3 domains exhibited virtually indistinguishable elution volumes to those observed for the wildtype SH3 domains, implying that the point substitution of specific residues did not lead to protein unfolding and that the mutant SH3 domains retained the compact globular fold characteristic of wildtype SH3 domains. These observations were further confirmed by circular dichroism (CD) analysis.

4.4.3 Peptide synthesis

HPLC-grade 12-residue peptide PVPPPVPPRRRP spanning residues 1148-1159 within human Sos1 protein (Expasy# Q07889) and corresponding to the binding site for the SH3 domains of Grb2 was commercially obtained from GenScript Corporation. The peptide concentration was measured gravimetrically.

4.4.4 ITC measurements

Isothermal titration calorimetry (ITC) experiments were performed on Microcal VP-ITC instrument and data were acquired and processed using fully automized features in Microcal ORIGIN software. All measurements were repeated 3-4 times. Briefly, SH3 domain samples were prepared in Tris buffer (50mM Tris, 200mM NaCl, 1mM EDTA and 5mM β-mercaptoethanol at pH 8.0) or Phosphate buffer (50mM Sodium phosphate, 200mM NaCl, 1mM EDTA and 5mM β-mercaptoethanol at pH 8.0) or 50mM Tris, 1mM EDTA and 5mM β-mercaptoethanol containing 0-300mM NaCl at pH 8.0 and de-gassed using the ThermoVac accessory for 5min. The experiments were initiated by injecting 25 x 10μl injections of 1-4mM of Sos1 peptide from the syringe into the calorimetric cell containing 1.8ml of 50-200μM of an SH3 domain solution at 25°C. The change in thermal power as a function of each injection was automatically recorded using Microcal ORIGIN software and the raw data were further processed to yield binding isotherms of heat release per injection as a function of peptide to protein molar ratio. The heats of mixing and dilution were subtracted from the heat of binding per injection by carrying out a control experiment in which the same buffer in the calorimetric cell was titrated against the Sos1 peptide in an identical manner. Control experiments with scrambled peptides generated similar thermal power to that obtained for the buffer alone — as did the titration of Sos1 peptide against a protein construct containing thioredoxin with a C-terminal His-tag (Trx-His). Titration of concentrated Trx-His protein construct into the calorimetric cell containing an SH3 domain solution produced no observable signal, implying that neither Trx-tag nor His-tag interact with any of the wildtype or mutant SH3 domains. To extract binding affinity (K_d) and binding enthalpy (ΔH), the binding

isotherms were iteratively fit to the following built-in function by non-linear least squares regression analysis using the integrated Microcal ORIGIN software:

$$q(i) = (n\Delta HVP/2)\ \{[1+(L/nP)+(K_d/nP)] - [[1+(L/nP)+(K_d/nP)]^2 - (4L/nP)]^{1/2}\} \quad [1]$$

where q(i) is the heat release (kcal/mol) for the ith injection, n is the binding stoichiometry, V is the effective volume of protein solution in the calorimetric cell (1.46ml), P is the total protein concentration in the calorimetric cell (μM) and L is the total concentration of peptide ligand added (μM). The above equation is derived from the binding of a ligand to a macromolecule using the law of mass action assuming a 1:1 binding stoichiometry [88]. The free energy change (ΔG) upon ligand binding was calculated from the relationship:

$$\Delta G = RT\ln K_d \quad [2]$$

where R is the universal molar gas constant (1.99 cal/K/mol), T is the absolute temperature in Kelvins and K_d is in the units of mol/L. The entropic contribution (TΔS) to the free energy of binding was calculated from the relationship:

$$T\Delta S = \Delta H - \Delta G \quad [3]$$

where ΔH and ΔG are as defined above. The free energy change (ΔG) upon ligand binding can be dissected into two major constituent components by the following relationship:

$$\Delta G = \Delta G_{lig} + \Delta G_{ion} \quad [4]$$

where ΔG_{lig} is the contribution due to direct ligand binding and ΔG_{ion} is the contribution due to the indirect displacement of counterions upon ligand binding. ΔG_{ion} at a given NaCl concentration was calculated from the following relationship based on polyelectrolyte theory [89-92]:

$$\Delta G_{ion} = \psi RT \ln[NaCl] \quad [5]$$

where ψ is the fractional degree of net counterions displaced upon ligand binding. ψ was calculated from the slope of a plot of $\ln K_d$ versus ln[NaCl] assuming the following linear relationship based on thermodynamic linkage [89-92]:

$$\ln K_d = \psi \ln[NaCl] \quad [6]$$

With the knowledge of ΔG and ΔG_{ion}, equation [4] was re-arranged to obtain ΔG_{lig}.

4.4.5 Structural analysis

3D structures of SH3 domains of Grb2 in complex with the Sos1 peptide were modeled using the MODELLER software based on homology modeling [62]. In each case, the NMR structure of Grb2 nSH3 domain in complex with a Sos1-derived peptide containing the consensus motif PPVPPR (with a PDB code of 4GBQ) was used as a template. For the nSH3-Sos1 complex, hydrogen bonding restraints were added between the sidechain carboxylic oxygen atoms OD1 and OD2 of D15 in the nSH3 domain and sidechain guanidinium nitrogen atoms NH1 and NH2 of R_{+5} residue in the consensus motif PPVPPR. For the cSH3-Sos1 complex, hydrogen bonding restraints were added between the sidechain carboxylic oxygen atoms OE1 and OE2 of E171 in the cSH3 domain and sidechain guanidinium nitrogen atoms NH1 and NH2 of R_{+5} residue in the consensus motif PPVPPR. Hydrogen bonding restraints were necessary to bring the sidechains of respective residues within optimal hydrogen bonding distance in agreement with our thermodynamic data. In each case, a total of 100 structural models were calculated and the structure with the lowest energy, as judged by the MODELLER Objective Function, was selected for further energy minimization in MODELLER prior

to analysis. The structures were rendered using RIBBONS [63] and electrostatic surface potential views were generated using MOLMOL [93]. All calculations were performed on the lowest energy structural model.

4.5 Results and discussion

4.5.1 Residues D15 and E171 underlie the differential binding of SH3 domains to Sos1

To test the differential binding of SH3 domains of Grb2 to Sos1, we expressed and purified the wildtype nSH3 (nSH3_WT) and the wildtype cSH3 (cSH3_WT) domains of Grb2 and measured their binding to the 12-residue Sos1 peptide PVPPPVPPRRRP containing the consensus motif PPVPPR using ITC. Additionally, we also generated various mutants of SH3 domains to map critical residues within both the nSH3 and cSH3 domains and measured their binding to the Sos1 peptide as described above. Because ligand binding can be coupled to other events such as protonation/deprotonation which can contribute to the magnitude of thermodynamic parameters with varying extents depending on the nature of the buffer, we performed our measurements in both Tris and phosphate buffers. Figure 4-2 shows representative ITC data for the binding of wildtype SH3 domains of Grb2 to the Sos1 peptide in Tris buffer. The binding affinities and the various thermodynamic parameters calculated from such data are presented in Figure 4-1. The fact that various thermodynamic parameters are similar in both the Tris and phosphate buffers implies that the binding of SH3 domains to Sos1 peptide is not coupled to protonation/deprotonation events and that the thermodynamic parameters reported reflect actual values for the binding process.

As evidenced by our data in Figure 4-1, the nSH3 domain binds to Sos1 with an affinity that is nearly three-fold greater than that observed for the binding of cSH3 domain, implying that such differences arise from residues that are unique to each of the

two SH3 domains. In order to determine the extent to which D15 in the nSH3 domain is critical as a salt bridging partner of R_{+5} in the consensus motif PPVPPR, the D15G mutant of nSH3 (nSH3_D15G) domain was generated. The rationale for the substitution of D15 to glycine instead of conventional alanine becomes obvious in light of the knowledge that G173 is the structurally equivalent residue in the cSH3 domain to D15 in the nSH3 domain (Figure 4-1a). The fact that the D15G mutant reduces the binding of nSH3 domain to Sos1 by more than an order of magnitude suggests strongly that D15 plays the role of a salt bridging partner for R_{+5} and that the neighboring residues D14 and E16 cannot substitute for this role. In order to test the extent to which substitution of an aspartate for a glycine at position 173 in the cSH3 domain will restore its binding potential to a level similar to that observed for the nSH3 domain, the G173D mutant of cSH3 (cSH3_G173D) domain was generated. As expected, the G173D mutant augments the binding of the cSH3 domain to Sos1 to a level that is virtually indistinguishable from that of nSH3 domain. A corollary of our hypothesis is that E171 in the cSH3 domain may at least partially fulfill the role of D15 in the nSH3 domain. To test that this is so, we generated E171A mutant of cSH3 (cSH3_E171A) domain. The substitution of E171 to alanine may appear to be due to the relatively conservative and non-destructive properties of alanine but the logic for doing so here is of quite different nature. The residue that occupies structurally equivalent position to E171 in the nSH3 domain is A13 and thus the mutant E171A bears the potential to play a double act in not only reporting the significance of the role of a glutamate but also that of alanine at this position (Figure 4-1a). Consistent with our hypothesis, the E171A mutant reduces the binding of the cSH3 domain to Sos1 by nearly an order of magnitude, implying that this residue, at least in part, fulfills the role of D15 in the cSH3 domain in its ability to form a salt bridge with

R_{+5}. This salient observation also suggests that the neighboring residues D172 and E174 in the cSH3 domain cannot substitute for the role of salt bridging with R_{+5}. Finally, to test whether a glutamate at position 13 may further augment the binding of nSH3 domain to Sos1, we generated the A13E mutant of nSH3 (nSH3_A13E) domain. The finding that the A13E mutant does not further augment the binding of nSH3 domain to Sos1 suggests that R_{+5} has either acquired a preference for salt bridging with a counterpart at position 15 over position 13, or alternatively, prefers an aspartate over a glutamate within the RT loop of the β-barrel fold.

In sum, our binding data discussed above unequivocally demonstrate that the higher affinity binding of nSH3 domain relative to cSH3 domain to Sos1 is largely attributable to the single residue D15 located within the RT loop of the β-barrel fold wherein it acts as a salt bridging partner for R_{+5}. Furthermore, the lack of an acidic residue at the structurally equivalent position of D15 in the cSH3 domain accounts for its lower binding affinity to Sos1 relative to the nSH3 domain. Nonetheless, this lower affinity binding of the cSH3 domain to Sos1 is dependent on E171 located within the RT loop of the β-barrel fold wherein it most likely engages in the formation of a salt bridge with R_{+5} in the consensus motif PPVPPR.

4.5.2 SH3 domains employ differential thermodynamic mechanisms for binding to Sos1

One of the unique features of ITC is that it provides a complete thermodynamic signature of two binding partners. As shown in Figure 4-2 and Figure 4-1, the binding of nSH3 and cSH3 domains of Grb2 to Sos1 employs distinct thermodynamic mechanisms While both interactions are driven by favorable enthalpic changes, the binding of nSH3 domain to Sos1 is accompanied by entropic penalty in contrast to entropic gain for the binding of cSH3 domain to Sos1.

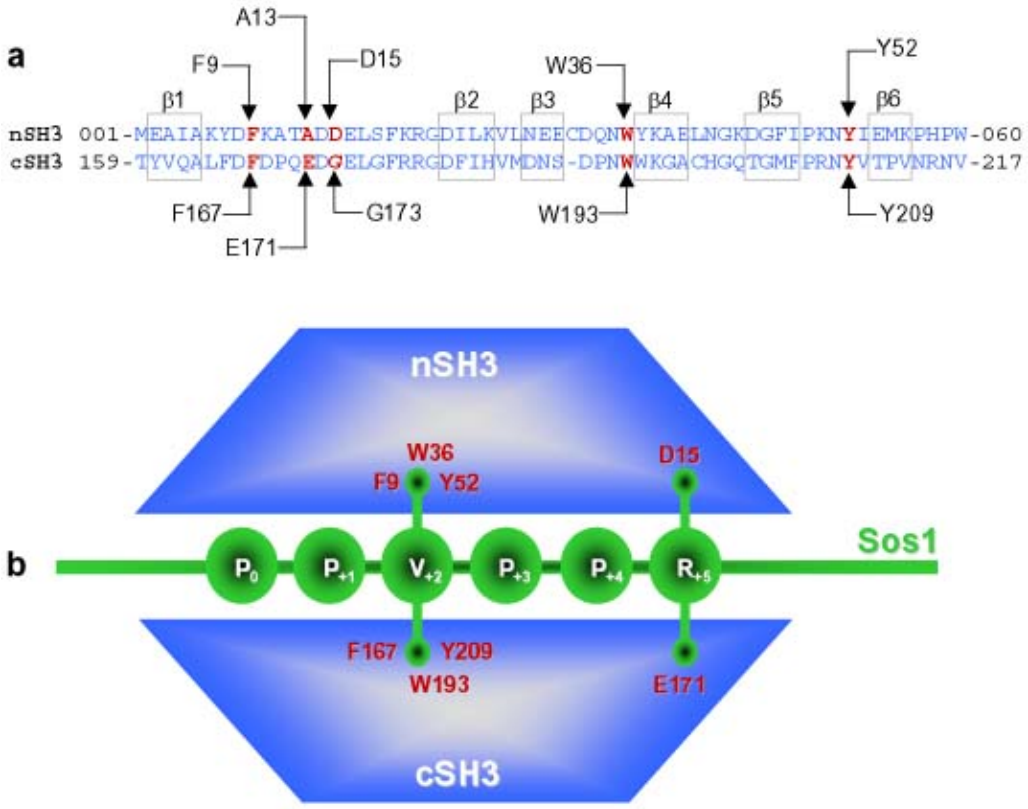

Figure 4-1: Sequence analysis of SH3 domains of Grb2 and the proline-rich motif PPVPPR within the Sos1 peptide. (a) Sequence alignment of nSH3 and cSH3 domains of Grb2 highlighting the structurally equivalent residues. The residues in each of the six strands β1-β6, as observed in the 3D structure of the nSH3 domain [35, 38-40], constituting the β-barrel fold are boxed. The residues in the SH3 domains predicted to be involved in stabilizing hydrophobic and electrostatic interactions respectively due to the valine and the arginine in the Sos1 proline-rich motif PPVPPR are colored red. Note that the C32 in the β3-β4 loop of the nSH3 domain is deleted in the cSH3 domain. (b) A cartoon diagram showing the residues in the SH3 domains predicted to be involved in stabilizing hydrophobic and electrostatic interactions respectively due to the valine and the arginine in the Sos1 proline-rich motif PPVPPR.

. What might be the molecular basis of these two opposing thermodynamic forces dictating the Grb2-Sos1 interaction? Release of heat usually results from the formation of bonds. It is thus conceivable that the formation of an extensive network of non-covalent interactions due to hydrophobic contacts, electrostatic interactions and hydrogen bonding between SH3 domains and Sos1 may account for the highly favorable enthalpic changes observed here. The formation of inter-molecular hydrophobic contacts is most likely due

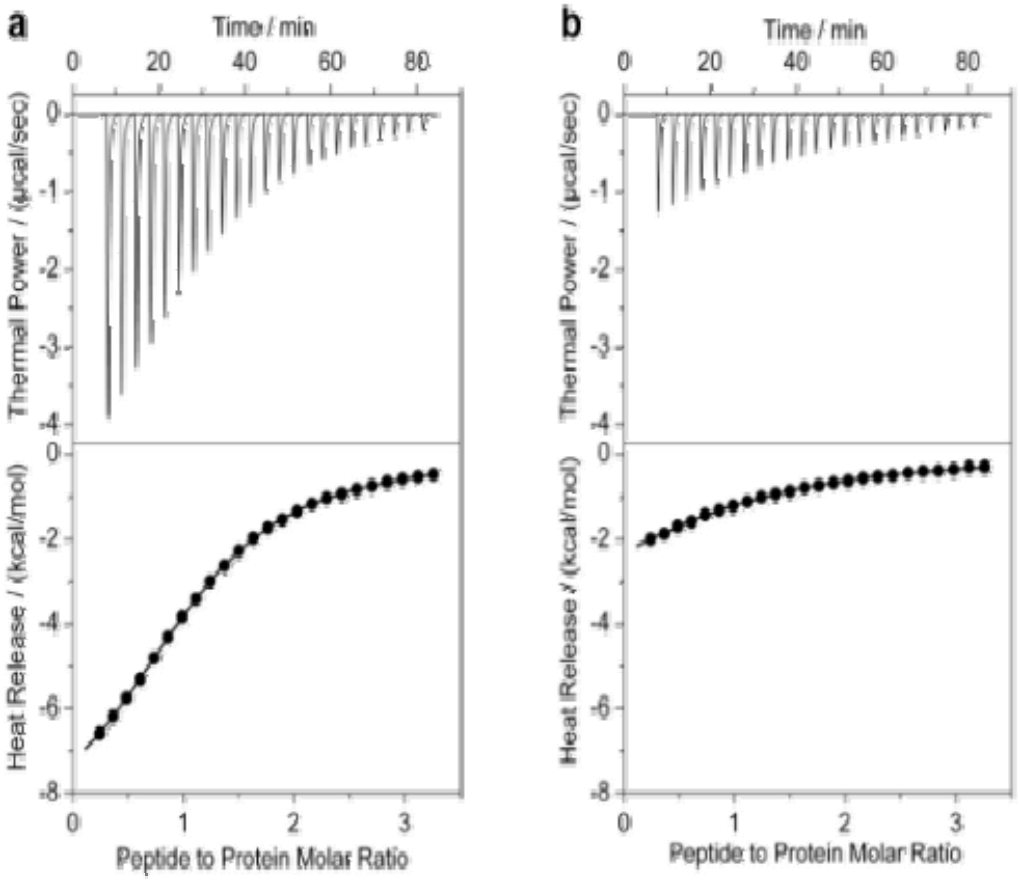

Figure 4-2: ITC analysis of the binding of wildtype nSH3 (a) and wildtype cSH3 (b) domains of Grb2 to the Sos1 peptide PVPPPVPPRRRP in Tris buffer. For each data set, the corresponding SH3 domain in the calorimetric cell was titrated with 25 x 10µl injections of the Sos1 peptide from the injection syringe at 25°C. The first injection and the corresponding heat release are not shown due to systematic uncertainties in the measurement. The top panels show the raw ITC data describing the change in thermal power as a function of time upon subsequent injections. The raw data were processed to generate the binding isotherms of heat release per injection as a function of increasing Sos1 peptide to SH3 domain molar ratio as shown in the bottom panels. The solid lines represent the fit of the data in the binding isotherms to equation [1] based on the binding of a ligand to a macromolecule using the Microcal ORIGIN software [88]. All data are shown to the same scale for direct comparison.

to the bringing together of hydrophobic residues such as P_0, P_{+1}, V_{+2}, P_{+3} and P_{+4} in the consensus motif PPVPPR within the close vicinity of specific residues constituting the binding cleft of the β-barrel upon complexation as observed in the 3D structure of the nSH3 domain bound to a Sos1 peptide [35, 38-40]. In contrast, the electrostatic interactions largely result from the formation of a salt bridge between R_{+5} in the consensus motif PPVPPR with D15 in the nSH3 domain or E171 in the cSH3 domain.

Additional electrostatic interactions may be afforded by further salt bridging between arginine residues R_{+6} and R_{+7} in the Sos1 peptide and specific acidic residues in the SH3 domains [35, 38]. However, these latter residues are likely to contribute little to the enthalpic gain observed due to the observation that their alanine substitution has little effect on the overall binding affinity of SH3 domains to Sos1 [35]. Finally, intermolecular hydrogen bonding between backbone carbonyl oxygens and amide hydrogens is also likely to contribute favorably to the enthalpic changes observed here. The overall entropic change accompanying molecular associations usually results from an interplay between two major entropic players in the form of solvation entropy and

Table 4-1

Experimentally determined thermodynamic parameters for the binding of various wildtype and mutant SH3 domains of Grb2 to the Sos1 peptide PVPPPVPPRRRP obtained from ITC measurements at 25°C and pH 8.0 in Tris and phosphate buffers

	Tris				Phosphate			
	K_d / μM	ΔH / kcalmol^{-1}	TΔS / kcalmol^{-1}	ΔG / kcalmol^{-1}	K_d / μM	ΔH / kcalmol^{-1}	TΔS / kcalmol^{-1}	ΔG / kcalmol^{-1}
nSH3_WT	38.64 ± 2.38	-9.45 ± 0.01	-3.42 ± 0.03	-6.03 ± 0.04	49.89 ± 8.90	-9.28 ± 0.18	-3.40 ± 0.29	-5.87 ± 0.11
nSH3_D15G	459.78 ± 2.49	-14.53 ± 0.42	-9.97 ± 0.42	-4.56 ± 0.01	444.07 ± 75.58	-15.09 ± 0.03	-10.51 ± 0.13	-4.58 ± 0.10
nSH3_A13E	41.76 ± 0.86	-11.66 ± 0.08	-5.68 ± 0.09	-5.98 ± 0.01	40.99 ± 0.71	-11.69 ± 0.11	-5.70 ± 0.10	-5.99 ± 0.01
cSH3_WT	117.10 ± 1.82	-4.60 ± 0.05	+0.77 ± 0.06	-5.37 ± 0.01	120.19 ± 4.62	-4.81 ± 0.14	+0.54 ± 0.12	-5.35 ± 0.02
cSH3_E171A	847.52 ± 10.15	-12.89 ± 0.40	-8.69 ± 0.41	-4.20 ± 0.01	521.30 ± 41.95	-13.55 ± 0.49	-9.07 ± 0.54	-4.48 ± 0.05
cSH3_G173D	56.50 ± 0.49	-7.03 ± 0.14	-1.23 ± 0.13	-5.80 ± 0.01	64.02 ± 0.47	-6.99 ± 0.06	-1.21 ± 0.05	-5.73 ± 0.01

The values for K_d and ΔH were obtained from the fit of expression [1] based on the binding of a ligand to a macromolecule using the law of mass action assuming a 1:1 binding stoichiometry to ITC isotherms. The values for TΔS were determined using equation [3]. The values for ΔG were calculated using equation [2]. The stoichiometries to the fits agreed to within ±10%. Errors were calculated from 3-4 independent measurements. All errors are given to one standard deviation.

conformational entropy [73-76]. The solvation entropy is due to the increase in the degrees of freedom of water molecules as a result of restructuring and displacement of water molecules from molecular surfaces, particularly from around the apolar groups, coming together. As such, the change in solvation entropy upon molecular associations contributes favorably to the overall entropic change. However, such favorable gain of entropy is largely offset and often overwhelmed by the unfavorable change in conformational entropy due to the loss in the degrees of freedom of backbone and sidechain atoms upon molecular associations. In light of the above-mentioned reasons, we attribute the entropic penalty observed for the binding of nSH3 domain to Sos1 largely to the loss in the degrees of freedom of backbone and sidechain atoms within both interacting partners, while the entropic gain observed for the binding of cSH3 domain to Sos1 is most likely due to the increase in the degrees of freedom of water molecules upon molecular association.

To gain further insights into the role of thermodynamic forces governing the binding of SH3 domains to Sos1, differential thermodynamic signatures for various pairs of wildtype and mutant SH3 domains are shown in Figure 4-3. In this analysis, the magnitude and the sign of each of the three major differential thermodynamic parameters $\Delta\Delta H$, $T\Delta\Delta S$ and $\Delta\Delta G$ provide a graphical output of the differences in the underlying thermodynamic forces for the Sos1-binding of one SH3 domain relative to the other SH3 domain. While the magnitude of a given differential parameter, as judged by the height of the bar along the vertical axis, is indicative of its significance, the positive or negative sign of a given differential parameter dictates whether it is favorable or unfavorable depending on the type of thermodynamic force under consideration for the Sos1-binding

of one SH3 domain relative to the other. Thus, a negative value of ΔΔH is indicative of enthalpy change being more favorable for the Sos1-binding of one SH3 domain relative to the other, while a positive value of TΔΔS is indicative of entropy change being more favorable for the Sos1-binding of one SH3 domain relative to the other. As shown in Figure 4-3a, it is evident that the Sos1-binding of nSH3_WT relative to cSH3_WT is enthalpically more favorable but entropically less favorable. Thus, the high affinity

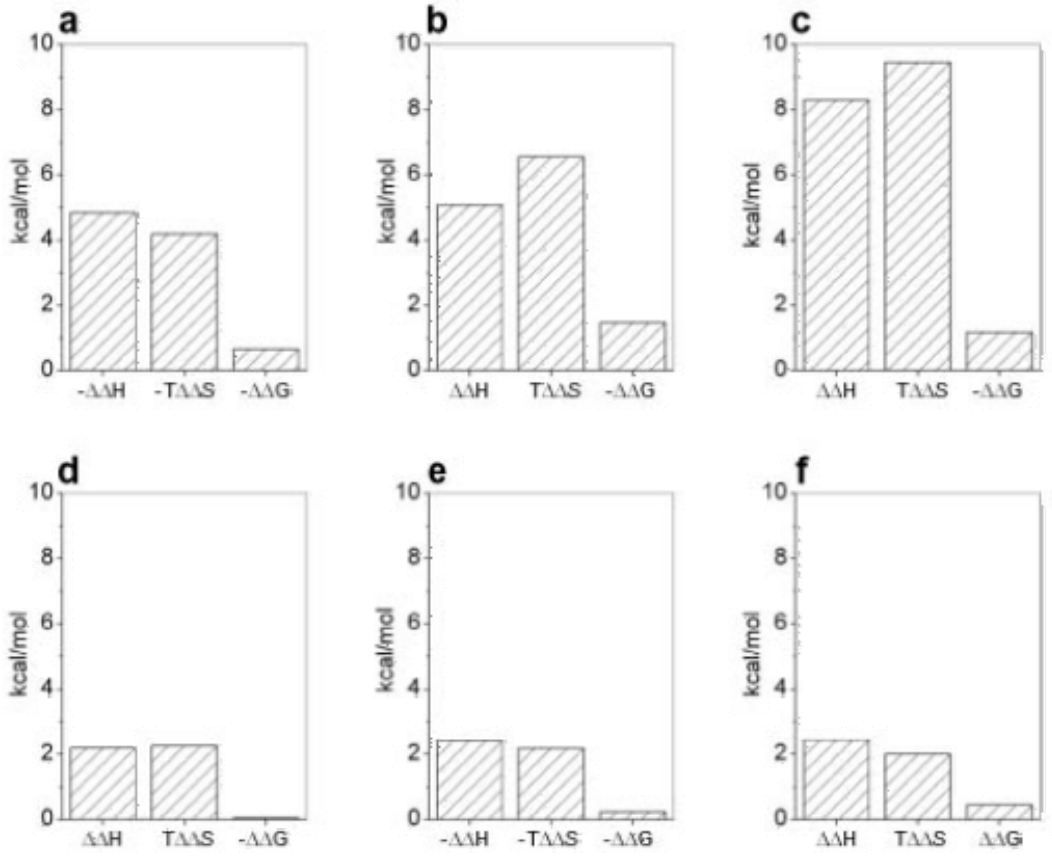

Figure 4-3: Differential energetics for the binding of various wildtype and mutant SH3 domains of Grb2 to the Sos1 peptide PVPPPVPPRRRP in Tris buffer. Shown are the differential thermodynamic signatures for the Sos1-binding of one SH3 domain relative to the other SH3 domain: (a) nSH3_WT relative to cSH3_WT; (b) nSH3_WT relative to nSH3_D15G; (c) cSH3_WT relative to cSH3_E171A; (d) nSH3_WT relative to nSH3_A13E; (e) nSH3_WT relative to cSH3_G173D; and (f) cSH3_WT relative to cSH3_G173D. ΔΔH, TΔΔS and ΔΔG were calculated from the relationships $\Delta\Delta H=\Delta H_X-\Delta H_Y$, $T\Delta\Delta S=T\Delta S_X-T\Delta S_Y$ and $\Delta\Delta G=\Delta G_X-\Delta G_Y$, where the subscripts X and Y denote the corresponding thermodynamic parameters for the binding of one SH3 domain (SH3_X) and the other SH3 domain (SH3_Y) to the Sos1 peptide, respectively (Figure 4-1). All plots are shown to the same scale for direct comparison.

binding of nSH3_WT to Sos1 appears to be largely attributable to favorable enthalpic changes in lieu of favorable entropic changes. In striking contrast, the enthalpy change is less favorable while entropy change is more favorable for the Sos1-binding of nSH3_WT relative to nSH3_D15G despite diminished affinity of the latter by more than an order of magnitude (Figure 4-3b). This salient observation implies that the formation of a salt bridge between R_{+5} in the consensus motif PPVPPR with D15 in the nSH3 domain is enthalpically unfavorable but entropically favorable, possibly due to the displacement of water molecules and the release of counterions from around the charged groups in R_{+5} and D15. That the formation of an intermolecular salt bridge may be accompanied by enthalpic penalty but entropic gain is further corroborated by the Sos1-binding of cSH3_WT relative to cSH3_E171A (Figure 4-3c). In this latter scenario, the alanine substitution of E171, which appears to engage in the formation of a salt bridge with R_{+5} in the consensus motif PPVPPR, is concomitant with a substantial release of enthalpy despite the reduction in binding to Sos1 by nearly an order of magnitude. However, the favorable enthalpy change is more than offset by a large entropic penalty. The above-mentioned observations thus indicate that the role of salt bridge formation in the SH3-Sos1 interaction is to lower the overall entropic loss due to binding.

The structurally equivalent residue to E171 in the nSH3 domain is A13 but, while the binding affinities of Sos1-binding of nSH3_WT relative to nSH3_A13E are very similar (Figure 4-1), the underlying energetics display some differences (Figure 4-3d). On the same token, nSH3_WT binds to Sos1 with a similar affinity to that observed for cSH3_G173D but the two display different thermodynamic signatures (Figure 4-3e). Interestingly, cSH3_G173D binds to Sos1 with an affinity that is over 2-fold greater than cSH3_WT but the differences in the underlying thermodynamic forces are no greater than

those observed for the Sos1-binding of nSH3_WT relative to nSH3_A13E and for the Sos1-binding of nSH3_WT relative to cSH3_G173D (Figures 3d-3f). That this is so emphasizes the rather highly under-appreciated fact that similar binding affinities may not necessarily arise from similar underlying thermodynamic forces and vice versa. In particular, substitution of specific amino acids may alter the thermodynamics of molecular associations without having any effect on the overall binding affinities. Such thermodynamic differences may be attributable to the differences in the solvation properties of the sidechains of specific residues and their ability to engage in specific interactions. Thus, although the substitution G173D in the cSH3 domain enables it to bind to Sos1 with an affinity that is virtually same as that observed for the binding of nSH3 domain, analysis of underlying thermodynamic forces suggests that the differential binding of these two SH3 domains to Sos1 is not merely attributable to the presence of a glycine residue at position 173 instead of an aspartate but that other residues are also likely to play a role in determining specific protein-protein interactions. For example, it is possible that specific acidic residues within nSH3 and cSH3 domains may stabilize positive charge on R_{+6} and/or R_{+7} in the Sos1 peptide. Further mutagenesis studies are thus warranted to map the role of additional residues that may underlie the differential binding of nSH3 and cSH3 domains to Sos1. It should also be noted here that the above thermodynamic arguments are based on the assumption that the wildtype and mutant SH3 domains retain the same conformation. Although our SEC and CD analysis demonstrate that this is likely the case, the possibility that subtle conformational changes could occur between the wildtype and mutant domains cannot be excluded and thus such conformational changes could partially contribute to the differential thermodynamics observed here.

4.5.3 Salt tightly modulates the binding of SH3 domains to Sos1 in a thermodynamically distinct manner

Elucidating the extent to which the thermodynamics are dependent on ambient salt concentration can provide novel insights into protein-protein interactions. Given that electrostatic interactions appear to play a key role in the formation of Grb2-Sos1 complex, the dependence of thermodynamics of this important interaction on salt concentration thus cannot be overemphasized.

Figure 4-4a shows the dependence of the equilibrium constant (K_d) for the binding of SH3 domains of Grb2 to the Sos1 peptide on NaCl concentration. It is evident from such data that the binding of both SH3 domains to Sos1 is highly sensitive to ambient salt concentration. Thus, while the K_d for the binding of nSH3 domain to Sos1 decreases by about 5-fold from around 10μM to over 50μM over the NaCl concentration in the range 0-300mM, the K_d for the binding of cSH3 domain to Sos1 decreases by about 3-fold from around 50μM to about 150μM over the same NaCl concentration range. The K_d values of about 10μM and 50μM observed for the binding of nSH3 and cSH3 domains to Sos1 in the absence of NaCl are in good agreement with the values previously reported for this interaction in low salt buffers [35, 37, 38]. That salt modulates the binding of cSH3 domain to Sos1 to a much lesser degree relative to that observed for the binding of nSH3 domain suggests strongly that the release of counterions plays a much greater role in the formation of the latter complex. To quantitatively measure the extent to which counterion release governs the binding of SH3 domains of Grb2 to Sos1, we generated the salt linkage plots of $\ln K_d$ versus ln[NaCl] and calculated the fractional degree of net counterion release (ψ) from the corresponding slopes (Figure 4-4a and Figure 4-2). Our analysis shows that ψ is nearly 2-fold greater for

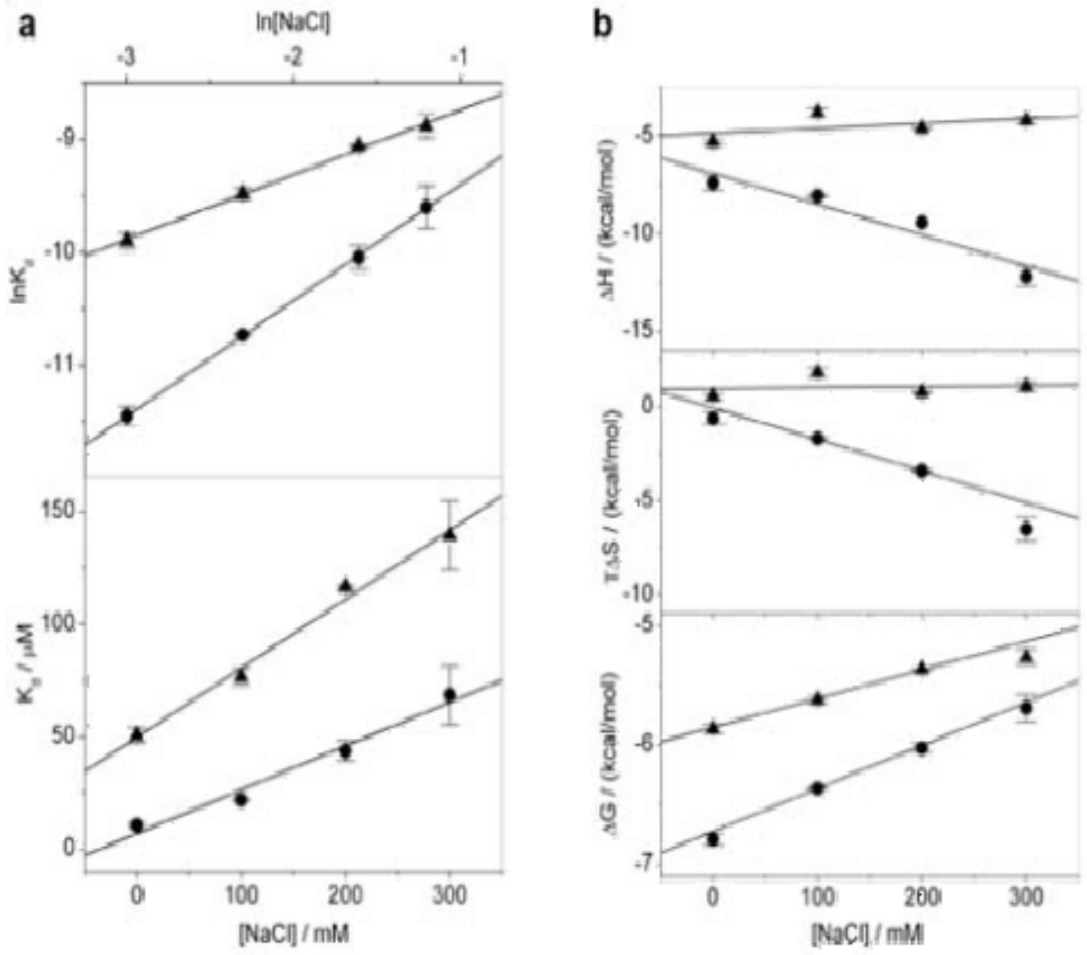

Figure 4-4: Effect of salt on the binding of wildtype SH3 domains of Grb2 to the Sos1 peptide PVPPPVPPRRRP in 50mM Tris, 1mM EDTA and 5mM β-mercaptoethanol containing 0-300mM NaCl at pH 8.0. Each SH3 domain in the calorimetric cell was titrated with 25 x 10μl injections of the Sos1 peptide from the injection syringe to obtain binding isotherms at NaCl concentrations in the range 0-300mM. To determine the various parameters, the binding isotherms at each NaCl concentration were fit to equation [1] based on the binding of a ligand to a macromolecule using the Microcal ORIGIN software. Each data point is the arithmetic mean of 3-4 experiments. All error bars are given to one standard deviation. (a) Dependence of K_d on NaCl concentration (lower panel) and the $\ln K_d$ versus ln[NaCl] plot (upper panel) used in the thermodynamic linkage analysis given by equation [6] for the binding of Sos1 peptide to nSH3 domain (●) and cSH3 domain (▲) of Grb2. [NaCl] and K_d in the upper panel were logarithmized in the standard units of mol/L. The solid lines show linear fits to the data points. (b) Dependence of thermodynamic parameters ΔH, TΔS and ΔG on NaCl concentration for the binding of Sos1 peptide to nSH3 domain (●) and cSH3 domain (▲) of Grb2. The solid lines show linear fits to the data points.

the binding of nSH3 domain versus the cSH3 domain to Sos1, arguing in favor of a much greater role of counterion release in driving the nSH3-Sos1 interaction. It is believed that the release of counterions upon protein-ligand interactions is entropically favorable and thus contributes to the overall free energy of binding. As indicated in Figure 4-2, the

counterion release contributes to the overall free energy of binding to Sos1 by nearly twice as much for nSH3 domain relative to the cSH3 domain at NaCl concentration of 200mM. In the absence of such favorable contributions, the binding of both SH3 domains to Sos1 would be expected to be lower by several folds.

That counterion release plays somewhat lesser role in dictating the Sos1-binding of cSH3 domain relative to nSH3 domain is further reflected in the salt-dependence of thermodynamic parameters ΔH and $T\Delta S$ (Figure 4-4b). Thus, ΔH and $T\Delta S$ are highly sensitive to changes in salt for the binding of nSH3 domain to Sos1 and experience a change of nearly equal but opposing 10 kcal/mol in their contribution to ΔG over the NaCl concentration in the range 0-300mM. In contrast, ΔH and $T\Delta S$ exhibit poor dependence on salt for the binding of cSH3 domain to Sos1 and undergo a change of only about 1 kcal/mol in their contribution to ΔG over the same NaCl concentration. Despite such dramatic differences in the behavior of underlying ΔH and $T\Delta S$ on ambient salt

Figure 4-2

Experimentally determined thermodynamic parameters underlying the energetic contributions resulting from the counterion release upon the binding of wildtype SH3 domains of Grb2 to the Sos1 peptide PVPPPVPPRRRP obtained from ITC measurements at 25°C and pH 8.0

	ψ	ΔG_{ion} / kcalmol^{-1}	ΔG_{lig} / kcalmol^{-1}	ΔG / kcalmol^{-1}
nSH3_WT	1.03 ± 0.01	-0.98 ± 0.01	-5.05 ± 0.05	-6.03 ± 0.04
cSH3_WT	0.57 ± 0.01	-0.55 ± 0.01	-4.82 ± 0.01	-5.37 ± 0.01

The ψ values were obtained from the slopes of linear fits to $\ln K_d$ versus ln[NaCl] plots in 50mM Tris, 1mM EDTA and 5mM β-mercaptoethanol containing 0-300mM NaCl at pH 8.0 (Figure 4-4a). The values for ΔG_{ion}, the free energy change due to counterion displacement, at 200mM NaCl were determined using expression [5]. The values for ΔG_{lig}, the free energy change exclusively due to ligand binding, at 200mM NaCl were calculated from equation [4]. The values for ΔG, the overall free energy change for binding, at 200mM NaCl were obtained from equation [2]. Errors were calculated from 3-4 independent measurements. All errors are given to one standard deviation.

concentration, ΔG appears to be tightly modulated in the binding of both SH3 domains to Sos1. That this is so further underlies the importance of thermodynamics to understanding protein-ligand interactions and emphasizes the fact that cellular processes may be modulated by salt through distinct thermodynamic mechanisms.

4.5.4 Thermodynamic data lead to structural refinement of SH3 domains bound to Sos1 peptide

In recent years, there has been growing interest in predicting the thermodynamics of protein-ligand interactions from structural information alone in what has come to be loosely defined as "structural thermodynamics" [76, 83, 94, 95]. Whether structural thermodynamics will deliver what it promises remains to be seen but few would doubt that the identification of key residues involved in protein-ligand interactions through a combination of thermodynamic analysis coupled with site-directed mutagenesis can often lead to refinement of structural data. Although the structures of nSH3 domain of Grb2 in complex with Sos1-derived peptides containing the consensus motif PPVPPR have been reported time and again [35, 38-40], the role of many residues critical to this protein-ligand recognition remains to be ascertained. Thus, for example, it has hitherto not been known whether D15 or E16 fulfilled the role of salt bridging partner for R_{+5} within the consensus motif PPVPPR. Due to lower binding affinity, structural analysis of cSH3 domain in complex with a Sos1-derived peptide has not been possible to date but NMR analysis suggests that Sos1 binds to the cSH3 domain in a manner akin to that observed for its interaction with the nSH3 domain [37]. In an attempt to refine the nSH3-Sos1 structure and to determine de novo structure of the cSH3 domain bound to Sos1 consistent with our thermodynamic data reported here, we used homology modeling in combination with various hydrogen bonding distance restraints to calculate new 3D structures of these two complexes (Figure 4-5).

As expected, the 3D structure of each SH3 domain in complex with the Sos1 peptide containing the consensus motif PPVPPR adopts a characteristic β-barrel fold comprised of a pair of nearly- orthogonal β-sheets with each β-sheet containing three anti-parallel β-strands (Figures 5a and 5b). The strands β1-β2-β6 constitute the first β-sheet, while the second β-sheet is comprised of strands β3-β4 -β5. The loop β1-β2 within the β-barrel is more widely referred to as the "RT loop" due to the observation that the mutations of arginine and threonine residues within this loop of the SH3 domain of Src tyrosine kinase are important determinants of its transforming potential [43]. It should be noted here that the curving of β-sheets around each other imparts on SH3 domains a more β-barrel-like shape in contrast to a β-sandwich in which the β-sheets tend to be straighter relative to each other. The incoming Sos1 peptide docks against a largely hydrophobic binding cleft located on one face of the β-barrel. Apart from the deep binding cleft, both SH3 domains adopt a near-spherical shape and appear to be somewhat electrostatically polarized — the negative charge is largely localized on the peptide binding face of each molecule with little or no negative charge on the opposite side (Figures 5c and 5d).

Upon binding to the SH3 domain, the Sos1 peptide adopts the relatively open left-handed polyproline type II helical conformation. Within the binding cleft, there are two key sub-sites that account for the binding specificity of SH3 domains of Grb2 to Sos1. Firstly, the triplet of residues constituted by F9/Y52/W36 in the nSH3 domain and F167/Y209/W193 in the cSH3 domain forms a "cradle" that exquisitely accommodates the V_{+2} residue in the consensus motif PPVPPR. While the alanine substitution of V_{+2} decreases the affinity of Sos1 peptide for the nSH3 domain by nearly an order of magnitude [35], the relative contribution of F9/F167, Y52/Y209 and W36/W193 to the binding energy has not been analyzed to date. While the tight modulation of SH3-Sos1

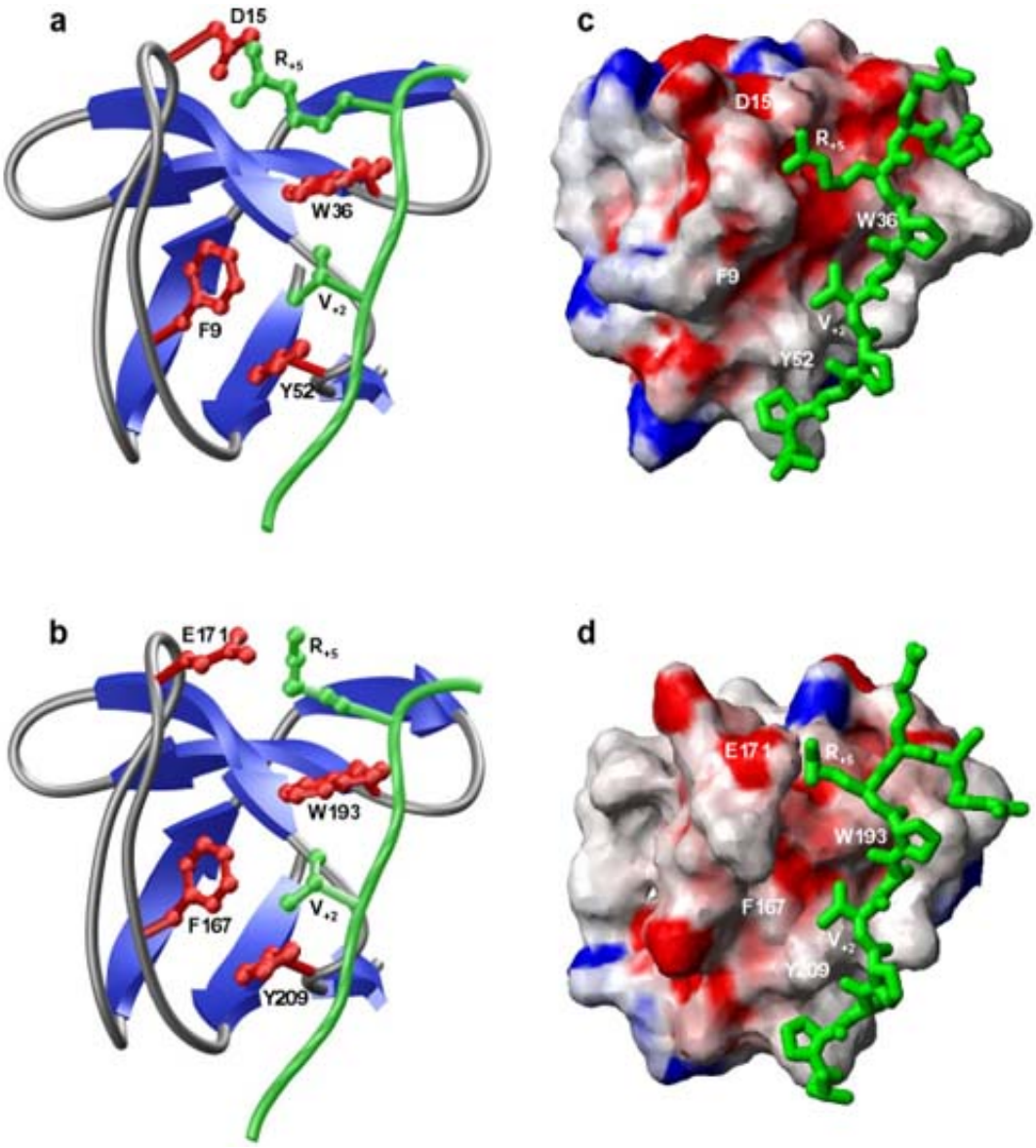

Figure 4-5: 3D structures of wildtype SH3 domains of Grb2 in complex with the Sos1 peptide PVPPPVPPRRRP obtained from homology modeling and using hydrogen bonding restraints consistent with thermodynamic data reported here. (a) Ribbon representation of nSH3 domain bound to Sos1 peptide. The nSH3 domain is shown in blue with loops depicted in gray and the sidechains of residues that stabilize the V_{+2} and R_{+5} residues in the Sos1 peptide are colored red. The Sos1 peptide, including the sidechains of V_{+2} and R_{+5} residues, is colored green. (b) Ribbon representation of cSH3 domain bound to Sos1 peptide. The cSH3 domain is shown in blue with loops depicted in gray and the sidechains of residues that stabilize the V_{+2} and R_{+5} residues in the Sos1 peptide are colored red. The Sos1 peptide, including the sidechains of V_{+2} and R_{+5} residues, is colored green. (c) Electrostatic surface potential view of nSH3 domain. The blue and red colors respectively denote the density of positive and negative charges, while the hydrophobic and neutral surfaces are indicated by white/gray color. The Sos1 peptide, including the sidechain of all residues, is shown in green. (d) Electrostatic surface potential view of cSH3 domain. The blue and red colors respectively denote the density of positive and negative charges, while the hydrophobic and neutral surfaces are indicated by white/gray color. The Sos1 peptide, including the sidechain of all residues, is shown in green.

interaction by changes in ambient salt concentrations as observed here is unlikely to be accounted for by the cradeling of V_{+2}, the stabilization of Sos1 peptide at a second sub-site via the formation of a salt bridge offers no better suspect. Here, the formation of ion pairs between D15 in the nSH3 domain and E171 in the cSH3 domain with the R_{+5} residue in the consensus motif PPVPPR generates much needed entropic contribution to the binding energy due to the release of counterions as supported by our thermodynamic data (Figure 4-2). Destabilization of these ion pairs reduces the binding affinity to Sos1 by nearly an order of magnitude in the case of cSH3 domain, while its impact on nSH3 domain is even more pronounced (Figure 4-1). It would be fitting to add here that the differential binding of nSH3 and cSH3 domains to Sos1 seems to be largely due to differences in the chemistry of the ion pair formation with the R_{+5} residue in the consensus motif PPVPPR. While this role is fulfilled by D15 in the nSH3 domain, the structurally equivalent residue in the cSH3 domain is G173. As a consequence of this, the cSH3 domain relies on the neighboring E171 to step up and although the role of E171 in neutralizing the charge on R_{+5} residue cannot be disputed, this interaction seems to be far from optimal and results in substantial reduction in the binding affinity of cSH3 domain relative to nSH3 domain. This view is supported by the fact that the G173D mutant of cSH3 domain binds to Sos1 with an affinity that is virtually indistinguishable from the binding of nSH3 domain (Figure 4-1).

Taken together, our 3D structural models of nSH3 and cSH3 domains in complex with Sos1 peptide shed new light on their binding specificity and structure-activity relationships. Unlike several previous studies [35, 38-40], in which various acidic residues have been suggested to participate in stabilizing the positive charge on the R_{+5} residue in the consensus motif PPVPPR, our thermodynamic data demonstrate here that

this role is exclusively fulfilled by D15 in the nSH3 domain and E171 in the cSH3 domain. Our structural data further argue that the spatial positioning of D15 and E171 in the β-barrel fold is consistent with their role in defining the differential binding of nSH3 and cSH3 domains to Sos1.

4.6 Concluding Remarks

Discovered over two decades ago as a non-catalytic component of various adaptors and enzymes [96], the SH3 domain is believed to be the most ubiquitous protein module amongst the vast arsenal employed by signaling machinery in mammalian cells. This notion is further supported by the fact that the human genome encodes for over 300 homologues of SH3 domains across a diverse plethora of proteins involved in a wide variety of activities from cell growth and proliferation through cell cycle regulation and developmental control to apoptosis and cancer. It then hardly comes as a surprise that Pubmed search of SH3 domain delivers nearly 5000 hits, more than for any other protein module, underlying extensive studies that have been carried out to explore the biological function and diversity of this important component of cellular signaling. Despite such wealth of knowledge, our understanding of the SH3-ligand specificity remains hitherto severely limited. Various attempts over the past decade to design computer algorithms to predict the specificity of SH3 domains against potential ligands have not only eluded theoreticians but also point to the need for further experiment.

In this study, we were driven by the curiosity to unravel the underlying structural basis for the differential binding of SH3 domains of Grb2 to Sos1 — a classical SH3-ligand interaction that has not only been widely studied but its role in determining the fate of a healthy from a diseased cell cannot be disputed. It was thus fitting that we chose this key protein-protein interaction to further expand our knowledge of SH3-ligand

specificity. Our data are consistent with the hypothesis that the residue D15 in the RT loop within the nSH3 domain is the major determinant of high affinity binding to Sos1 relative to the cSH3 domain by virtue of its ability to engage in the formation a salt bridge with R_{+5} residue in the consensus motif PPVPPR. In contrast, the residue analogous to D15 in the cSH3 domain is G173. Thus, the lack of a chemically and structurally equivalent residue at this key position in the RT loop of the β-barrel fold of cSH3 domain accounts for its low affinity binding to Sos1. That this is even possible is resurrected by the presence of a neighboring E171 in the cSH3 domain that appears to substitute for the role of D15 in the nSH3 domain. The differential binding affinities and differential thermodynamic mechanisms employed by the SH3 domains of Grb2 in their ability to recognize Sos1 may have evolved to provide a molecular switch necessary to regulate the interactions of Grb2 with a diverse array of downstream effectors of Grb2 in addition to Sos1 depending on the biological context and the nature of mitogenic stimuli [12-20].

It should be noted here that SH3 domains are generally believed to interact with their cognate ligands with an affinity in the 1-10μM range. However, this school of thought is largely based on studies carried out in buffers that show significant deviations from situations that are likely to be encountered within the complex milieu of the living cell. In particular, an increasing number of the SH3-ligand binding studies have been carried out in buffers that have tended to be devoid of salt. Our study here shows that salt tightly modulates the Grb2-Sos1 interaction and that this is likely to be the rule rather than an exception for the SH3-ligand interaction in general due to the universal requirement of one or more salt bridges that play a critical role in defining specificity between this pair of protein-protein interactions [42, 97-99]. Assuming that an aqueous

solution with ionic strength of around 200mM is a bona fide mimic of the physiological milieu of the living cell, our data presented here show that SH3 domains are more likely to bind to their cognate ligands with an affinity in the 10-100μM range in lieu of 1-10μM. What we have not argued thus far is the realization that a vast number of SH3-proteins contain SH3 domains in multiple copies and often in tandem. Complementing this exquisite multiple-domain architecture is the design of SH3 ligands which also tend to boast multiple proline-rich motifs within the same stretch of a polypeptide chain, with Sos1 being a classical example of this class of polydentate SH3 ligands. Thus, it seems likely that the simultaneous binding of multiple SH3 domains to multiple ligand sites may result in pronounced binding affinities, due to entropic advantage, instead of those inferred from the analysis of isolated SH3 domains with their cognate ligands. Sos1 indeed contains multiple proline-rich sequences containing the consensus motif PPVPPR. It is thus conceivable that the SH3 domains of Grb2 bind to Sos1 simultaneously and thereby leading to enhancement of Grb2-Sos1 interaction.

In short, our data reported here provide key insights into the structural basis of the differential binding of SH3 domains of Grb2 to Sos1 and significantly contribute to our understanding of the molecular determinants of SH3-ligand specificity. Because of our poor understanding of the biophysical principles that underlie this specificity, our attempts to design novel inhibitors to disrupt this key protein-protein interaction pertinent to cellular signaling and cancer have met little success to date. Further biophysical analysis of SH3-ligand interactions is thus clearly warranted to expand our knowledge of the biology of SH3 domains and to help pave the way for the design of novel and more effective anti-SH3 inhibitors.

5 Chapter 5: SH3 Domains of Grb2 Adaptor Bind to PXψPXR Motifs Within the Sos1 Nucleotide Exchange Factor in a Discriminate Manner

5.1 Summary

Ubiquitously encountered in a wide variety of cellular processes, the Grb2-Sos1 interaction is mediated through the combinatorial binding of nSH3 and cSH3 domains of Grb2 to various sites containing PXψPXR motifs within Sos1. Here, using isothermal titration calorimetry, we demonstrate that while the nSH3 domain binds with affinities in the physiological range to all four sites containing PXψPXR motifs, designated S1, S2, S3 and S4, the cSH3 domain can only do so at S1 site. Further scrutiny of these sites yields rationale for the recognition of various PXψPXR motifs by the SH3 domains in a discriminate manner. Unlike the PXψPXR motifs at S2, S3 and S4 sites, the PXψPXR motif at S1 site is flanked at its C-terminus with two additional arginine residues that are absolutely required for high-affinity binding of cSH3 domain. In striking contrast, these two additional arginine residues augment the binding of nSH3 domain to S1 site but their role is not critical for the recognition of S2, S3 and S4 sites. Site-directed mutagenesis suggests that the two additional arginine residues flanking the PXψPXR motif at S1 site contribute to free energy of binding via the formation of salt bridges with specific acidic residues in SH3 domains. Molecular modeling is employed to project these novel findings into the 3D structures of SH3 domains in complex with a peptide containing the PXψPXR motif and flanking arginine residues at S1 site. Taken together, this study furthers our understanding of the assembly of a key signaling complex central to cellular machinery.

5.2 Abbreviations

CD	Circular dichroism
EGF	Epidermal Growth Factor
Grb2	Growth factor Receptor Binder 2
ITC	Isothermal Titration Calorimetry
MAP	Mitogen-Activated Protein
NMR	Nuclear Magnetic Resonance
PDGF	Platelet-Derived Growth Factor
RTK	Receptor Tyrosine Kinase
SH2	Src Homology 2
SH3	Src Homology 3
Sos1	Son of Sevenless 1

5.3 Background

Grb2-Sos1 interaction, mediated by the canonical binding of N-terminal SH3 (nSH3) and C-terminal SH3 (cSH3) domains of Grb2 to proline-rich motifs within Sos1, plays a central role in relaying external signals from receptor tyrosine kinases (RTKs) at the cell surface to downstream effectors and regulators such as Ras within the cytosol [2, 13, 36, 50]. Comprised of a central SH2 domain flanked between nSH3 and cSH3 domains (Figure 5-1a), Grb2 recognizes activated RTKs by virtue of its SH2 domain to bind to tyrosine-phosphorylated (pY) sequences in the context of pYXN motif located within the cytoplasmic tails of a diverse array of receptors, including EGF and PDGF receptors [3, 4]. Upon binding to RTKs, the SH3 domains live up to Grb2's reputation and grab a wide variety of proteins, containing proline-rich sequences, in an attempt to

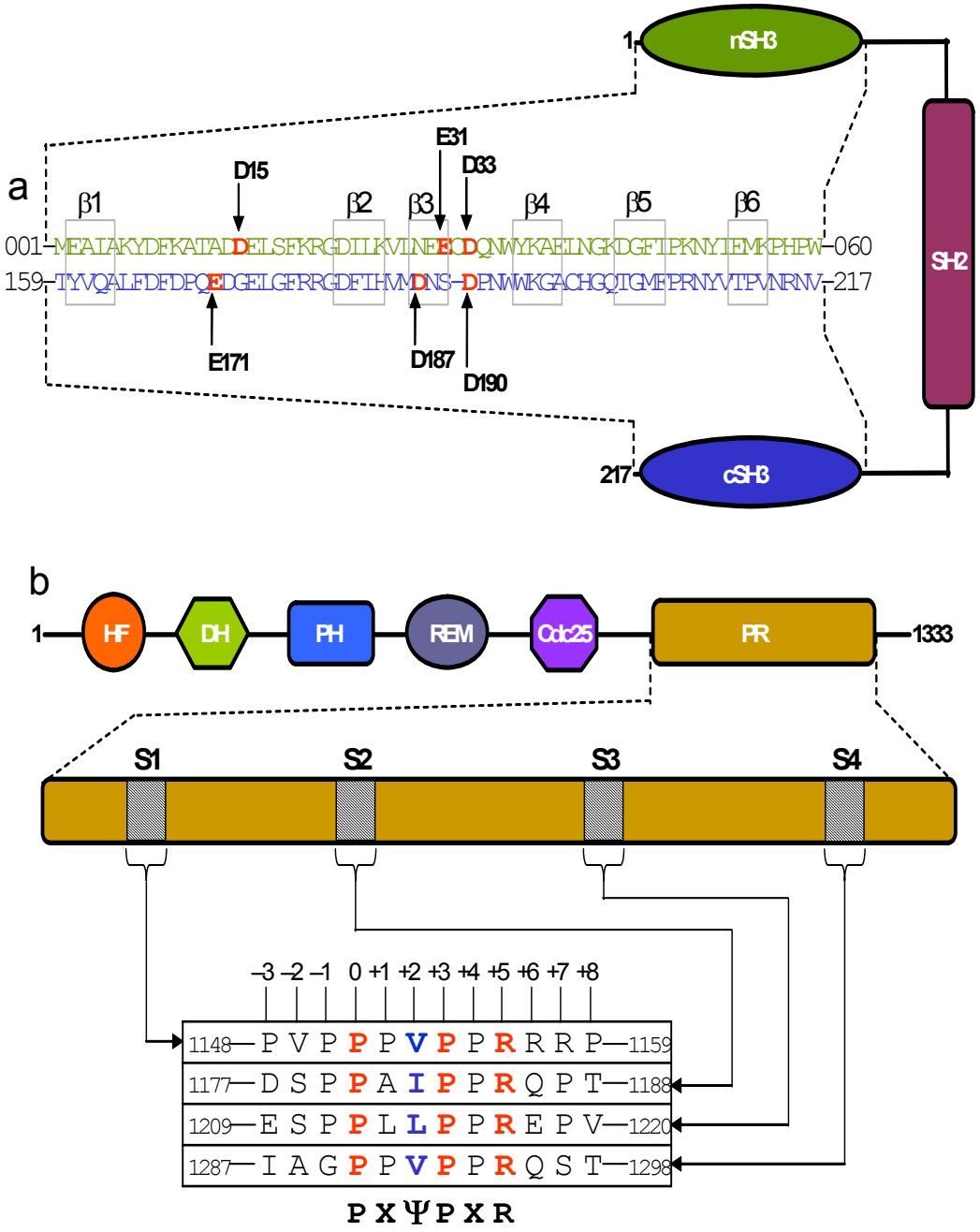

Figure 5-1: Domain organization and sequence analysis of Grb2 and Sos1. (a) Grb2 is comprised of a central SH2 (Src homology 2) domain flanked between SH3 (Src homology 3) domains. The sequence alignment of nSH3 and cSH3 domains highlights various structurally equivalent residues within the β-barrel fold. The residues constituting the β1-β6 strands are boxed. Vertical arrows indicate acidic residues whose roles in recognizing Sos1 are being investigated in this study. (b) The proline-rich (PR) domain of Sos1 lies at the extreme C-terminal end. The PR domain contains four distinct sites (designated S1, S2, S3 and S4) characterized by the PXψPXR consensus motif. The complete sequences of these sites are shown. The position of various residues relative to the first proline within the PXψPX motif, which is designated zero, is also indicated. Other domains within Sos1 shown are HF (histone fold), DH (Dbl homology), PH (pleckstrin homology), REM (Ras exchange motif) and Cdc25.

recruit them to the inner membrane surface — the site of initiation of a plethora of signaling cascades [12-20]. Among them, the guanine nucleotide exchange factor Sos1 is by far the best characterized downstream partner of Grb2 [12, 13]. Upon recruitment to the inner membrane surface, Sos1 catalyzes the GDP-GTP exchange within the membrane-bound GTPase Ras and thereby switches on a key signaling circuit that involves the activation of MAP kinase cascade central to cellular proliferation, survival and differentiation [21, 22].

Sos1 contains four distinct sites within its proline-rich (PR) domain for binding to the SH3 domains of Grb2 (Figure 5-1b). These sites, designated S1, S2, S3 and S4, conform to the PXψPXR consensus motif, where X is any residue and ψ is valine, leucine or isoleucine. In accordance with the nomenclature suggested by Schreiber and co-workers [42], the residues within the PXψPXR motif are assigned 0 for the N-terminal proline through to +5 for the C-terminal arginine. Although site-directed mutagenesis studies suggest that PXψPXR is the minimal motif (with the prolines at 0 and +3 positions, ψ at +2 position and arginine at +5 position) required for high-affinity binding to nSH3 domain [35], the extent to which residues flanking this motif may be non-redundant for binding to the cSH3 domain is not understood. On the basis of structural studies of the nSH3 domain of Grb2 in complex with peptides derived from S1 site in Sos1 [35, 38-40], the nSH3 domain folds into a characteristic β-barrel architecture resulting in the formation of a hydrophobic cleft on one face of the domain for accommodating the incoming peptide. While the β-barrel is comprised of a pair of nearly-orthogonal β-sheets, with each β-sheet containing three anti-parallel β-strands, the peptide adapts a relatively open left-handed polyproline type II (PPII) helical conformation upon binding. Our previous studies suggest that the cSH3 domain of Grb2

is likely to bind to S1 peptide in a manner akin to that observed for the nSH3 domain [41].

Although biophysical and structural analysis of the binding of SH3 domains to peptides derived from S1 site has been extensively carried out [35, 37, 38, 41], little is understood about Grb2-Sos1 interaction at S2, S3 and S4 sites. In an effort to fully address Grb2-Sos1 interaction in biophysical terms, we have employed here isothermal titration calorimetry (ITC) to study the binding of SH3 domains of Grb2 to peptides derived from S1-S4 sites within Sos1. Our data demonstrate that while the nSH3 domain binds with affinities in the physiological range to all four sites containing PXψPXR motifs, the cSH3 domain can only do so at S1 site. Further scrutiny of these sites yields rationale for the recognition of various PXψPXR motifs by the SH3 domains in a discriminate manner. Unlike the PXψPXR motifs at S2, S3 and S4 sites, the PXψPXR motif at S1 site is flanked at its C-terminus with two additional arginine residues that are absolutely required for high-affinity binding of cSH3 domain. In striking contrast, these two additional arginine residues augment the binding of nSH3 domain to S1 site but their role is not critical for the recognition of S2, S3 and S4 sites. Site-directed mutagenesis suggests that the two additional arginine residues flanking the PXψPXR motif at S1 site contribute to free energy of binding via the formation of salt bridges with specific acidic residues in SH3 domains. Molecular modeling is employed to project these novel findings into the 3D structures of SH3 domains in complex with a peptide containing the PXψPXR motif and flanking arginine residues at S1 site. Taken together, this study furthers our understanding of the assembly of a key signaling complex central to cellular machinery.

5.4 Experimental Procedures

5.4.1 Sample preparation

Wildtype and mutant SH3 domains of human Grb2 were expressed, purified and characterized as described earlier [41]. HPLC-grade 12-residue peptides spanning S1, S2, S3 and S4 sites within the human Sos1 were commercially obtained from GenScript Corporation. The sequences of these peptides are shown in Figure 5-1b. The peptide concentrations were measured gravimetrically. Circular dichroism (CD) analysis of SH3 domains and Sos1 peptides revealed that the introduction of various alanine substitutions at specific positions had no observable effect on their secondary structural conformations.

5.4.2 ITC measurements

Isothermal titration calorimetry (ITC) experiments were performed on Microcal VP-ITC instrument and data were acquired and processed using fully automized features in Microcal ORIGIN software. All measurements were repeated 2-3 times. Briefly, SH3 domain samples were prepared in 50mM Tris, 200mM NaCl, 1mM EDTA and 5mM β-mercaptoethanol at pH 8.0. The experiments were initiated by injecting 25 x 10μl aliquots of 2-8mM of each peptide from the syringe into the calorimetric cell containing 1.8ml of 50-200μM of an SH3 domain solution at 25°C. The binding affinity (K_d) and the enthalpy change (ΔH) were extracted from the data by the fit of a one-site model, derived from the binding of a ligand to a macromolecule [88], using Microcal Origin. All other control experiments and data processing were performed as described earlier [41].

5.4.3 Molecular modeling

3D structures of SH3 domains of Grb2 in complex with S1 peptide were modeled using the MODELLER software based on homology modeling [62]. In each case, the NMR structure of nSH3 domain of Grb2 in complex with a peptide corresponding to S1

site in Sos1 (with a PDB code of 4GBQ) was used as a template. Briefly, MODELLER employs molecular dynamics and simulated annealing protocols to optimize the modeled structure through satisfaction of spatial restraints derived from amino acid sequence alignment with a corresponding template in Cartesian space. For amino acid sequence identity between 25-50% between the template and target, MODELLER can generate 3D structures with accuracy comparable to NMR and X-ray structures for small proteins such as SH3 domains of around 50 amino acids. It is of worthy note that the nSH3 domain shares 35% sequence identity with the cSH3 domain, while the peptide ligand is identical between the template and modeled structures. Thus, the modeled structures of SH3 domains of Grb2 in complex with S1 peptide should be expected to adapt 3D folds similar to the template structure except for the sidechain conformations of specific amino acids due to the introduction of specific hydrogen bonding restraints between specific pairs of basic residues in the S1 peptide and acidic residues in the SH3 domains. Such hydrogen bonding restraints being introduced herein are necessary to bring the sidechain atoms of respective residues within optimal hydrogen bonding distance in agreement with our thermodynamic data reported here and in the previous study [41]. The atomic distances set for hydrogen bonding restrains between a specific pair of oxygen and nitrogen atoms were 2.8±0.5Å. Thus, MODELLER will force the sidechain oxygen and nitrogen atoms of specific hydrogen bonding partners to lie within approximately 2.8Å of each other through the rotation of backbone N-Cα and Cα-C' bonds with little effect on the overall global fold of S1 peptide and SH3 domains. To generate the 3D structural model of nSH3 domain in complex with S1 peptide, hydrogen bonding restraints were added between the OD1 and OD2 atoms of D15 in the nSH3 domain and NH1 and NH2 atoms of R+5 in S1 peptide, and between the OD1 and OD2 atoms of D33 in the nSH3

domain and NH1 and NH2 atoms of R+7 in the S1 peptide. To generate the 3D structural model of cSH3 domain in complex with S1 peptide, hydrogen bonding restraints were added between the OE1 and OE2 atoms of E171 in the cSH3 domain and NH1 and NH2 of R+5 in the S1 peptide, between the OD1 and OD2 atoms of D187 in the cSH3 domain and NH1 and NH2 atoms of R+6 in the S1 peptide, and between the OD1 and OD2 atoms of D190 in the cSH3 domain and NH1 and NH2 atoms of R+7 in the S1 peptide. To generate the 3D structural model of the cSH3_G173D mutant domain (that behaves like nSH3-mimetic) in complex with S1 peptide, hydrogen bonding restraints were added between the OE1 and OE2 atoms of E171 in the cSH3_G173D domain and NH1 and NH2 of R+5 in the S1 peptide, between the OD1 and OD2 atoms of G173D in the cSH3_G173D domain and NH1 and NH2 atoms of R+5 in the S1 peptide, between the OD1 and OD2 atoms of D187 in the cSH3_G173D domain and NH1 and NH2 atoms of R+6 in the S1 peptide, and between the OD1 and OD2 atoms of D190 in the cSH3_G173D domain and NH1 and NH2 atoms of R+7 in the S1 peptide. In each case, a total of 100 structural models were calculated and the structure with the lowest energy, as judged by the MODELLER Objective Function, was selected for further energy minimization in MODELLER prior to analysis. The modeled structures were rendered using RIBBONS [63]. All calculations were performed on the lowest energy structural model.

5.4.4 Motif search

The PXψPXR and PXψPXRRR motifs within the human proteome were searched using the ScanProsite software available at Expasy online server. X was set to any residue while ψ was set to valine, leucine or isoleucine. The protein database searched contained a total of 402,482 entries.

5.5 Results and discussion

5.5.1 nSH3 and cSH3 domains pose distinct requirements for binding to PXψPXR motifs within Sos1

To further characterize the Grb2-Sos1 interaction in biophysical terms, we measured the binding of nSH3 and cSH3 domains to peptides derived from S1-S4 sites containing the PXψPXR motifs using ITC. Figures 2 and 3 show representative data obtained upon conducting such measurements, while corresponding thermodynamic parameters are reported in Table 5-1. It is clearly evident from our data that the binding

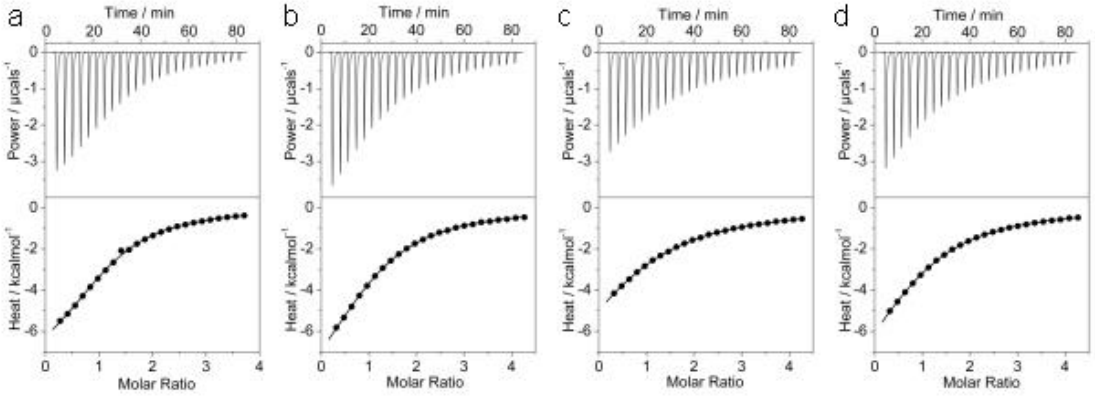

Figure 5-2: ITC analysis for the binding of nSH3 domain of Grb2 to Sos1-derived peptides S1 (a), S2 (b), S3 (c) and S4 (d). The solid lines show the fit of data to a one-site model based on the binding of a ligand to a macromolecule as incorporated in the Microcal Origin software.

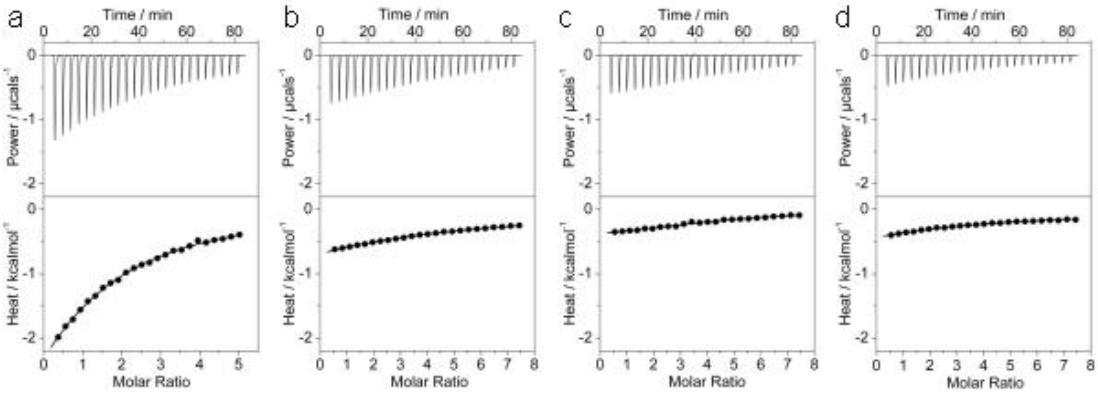

Figure 5-3: ITC analysis for the binding of cSH3 domain of Grb2 to Sos1-derived peptides S1 (a), S2 (b), S3 (c) and S4 (d). The solid lines show the fit of data to a one-site model based on the binding of a ligand to a macromolecule as incorporated in the Microcal Origin software.

of both SH3 domains at S1-S4 sites within Sos1 is exclusively under enthalpic control and, with the exception of binding of cSH3 domain to S1 site as noted previously [41], binding at all other sites is also accompanied by entropic penalty as is often observed in enthalpically-driven biological processes. This observation is consistent with the notion that enthalpy drives SH3-ligand interactions in general, while entropic changes provide unfavorable contributions to the free energy [38, 100-105]. That enthalpy drives the SH3-

Table 5-1

Experimentally determined thermodynamic parameters for the binding of wildtype nSH3 and cSH3 domains of Grb2 to various Sos1 peptides obtained from ITC measurements at 25°C and pH 8.0

		nSH3				cSH3			
Peptide	Sequence	K_d / μM	ΔH / kcalmol^{-1}	TΔS / kcalmol^{-1}	ΔG / kcalmol^{-1}	K_d / μM	ΔH / kcalmol^{-1}	TΔS / kcalmol^{-1}	ΔG / kcalmol^{-1}
S1	PVPPPVPPRRRP	39 ± 1	-9.41 ± 0.02	-3.39 ± 0.03	-6.02 ± 0.01	125 ± 13	-4.45 ± 0.15	+0.88 ± 0.09	-5.29 ± 0.06
S2	DSPPAIPPRQPT	56 ± 5	-11.63 ± 0.94	-5.83 ± 0.88	-5.80 ± 0.05	1396 ± 87	-9.94 ± 0.84	-6.04 ± 0.88	-3.87 ± 0.04
S3	ESPPLLPPREPV	117 ± 2	-11.38 ± 0.24	-6.01 ± 0.25	-5.36 ± 0.01	1718 ± 33	-16.63 ± 0.16	-12.85 ± 0.17	-3.78 ± 0.01
S4	IAGPPVPPRQST	82 ± 1	-11.45 ± 0.09	-5.87 ± 0.10	-5.58 ± 0.01	1318 ± 44	-11.52 ± 0.41	-7.59 ± 0.43	-3.92 ± 0.02
S1_AAA	PVPPPVPPAAAP	2557 ± 335	-89.13 ± 7.02	-85.58 ± 7.10	-3.54 ± 0.08	3089 ± 121	-35.66 ± 0.21	-32.23 ± 0.19	-3.42 ± 0.02
S1_AA	PVPPPVPPRAAP	84 ± 1	-11.42 ± 0.35	-5.85 ± 0.36	-5.57 ± 0.01	1574 ± 27	-20.75 ± 1.70	-16.92 ± 1.73	-3.82 ± 0.03
S1_R+5A	PVPPPVPPARRP	490 ± 20	-9.42 ± 0.61	-4.90 ± 0.59	-4.52 ± 0.02	962 ± 26	-2.92 ± 0.12	+1.20 ± 0.13	-4.12 ± 0.02
S1_R+6A	PVPPPVPPRARP	53 ± 1	-9.10 ± 0.25	-3.26 ± 0.27	-5.84 ± 0.02	331 ± 2	-3.96 ± 0.41	+0.80 ± 0.42	-4.75 ± 0.01
S1_R+7A	PVPPPVPPRRAP	72 ± 1	-9.50 ± 0.05	-3.84 ± 0.05	-5.66 ± 0.01	318 ± 23	-3.53 ± 0.56	+1.25 ± 0.52	-4.78 ± 0.04

The residues within the S1 peptide subjected to alanine substitution are underlined for clarity. The values for the binding affinity (K_d) and the enthalpy change (ΔH) were obtained from the fit of a function, based on the binding of a ligand to a macromolecule [88], to the ITC isotherms. Free energy of binding (ΔG) was calculated from the relationship $\Delta G=RT\ln K_d$, where R is the universal molar gas constant (1.99 cal/mol/K) and T is the absolute temperature (K). Entropic contribution (TΔS) to binding was calculated from the relationship $T\Delta S=\Delta H-\Delta G$. The binding stoichiometries to the fits agreed to within ±10%. Errors were calculated from 2-3 independent measurements. All errors are given to one standard deviation. All parameters are reported to no more than four significant figures.

peptide interaction implies that both hydrophobic forces and electrostatic interactions play a key role in the assembly of this signaling complex. However, the dominance of entropic penalty accompanying the SH3-peptide interaction is most likely attributable to the greater loss of degrees of motions available to these molecules when free in solution but becoming more compact upon binding. Close scrutiny of data presented in Table 5-1 indicates that both SH3 domains have a preference for binding to S1 site. However, while the nSH3 domain binds to S1-S4 sites with very similar affinities that extend over nearly three folds, the cSH3 domain not only binds to S1 site in an exclusive manner but also with an affinity that is weaker that that observed for the binding of nSH3 domain to any of these sites. The binding of cSH3 domain to S2, S3 and S4 sites occurs with affinities in the millimolar range, implying that the interaction of cSH3 domain with these sites is not likely to be physiologically relevant. It should be noted here that the affinities observed for the binding of nSH3 domain to S1-S4 sites and cSH3 domain to S1 site within Sos1 are consistent with the binding of SH3 domains to their cognate ligands with affinities typically in the 10-100μM range [42, 97-99, 106-112]. However, in some cases, SH3 domains have also been shown to bind to their ligands with affinities in the sub-μM range [15, 113-119]. Given the ubiquitous nature of SH3 domains within the mammalian proteome, it is believed that the rather weak SH3-ligand interactions are central to the temporal and spatial regulation of signaling pathways that constitute the bedrock of cellular communication.

The differential behavior of SH3 domains toward their putative sites within Sos1 must correlate with amino acids residing within or flanking the PXψPXR motifs. In view of the fact that one or more basic residues flanking consensus proline-rich motifs provide an additional level of modulating their binding affinity and specificity toward SH3

domains, we reasoned that the differential behavior of nSH3 and cSH3 domains toward S1-S4 sites might be attributable to the presence of arginine residues at positions +6 (R+6) and +7 (R+7) within the S1 site but absent in other sites (Figure 5-1b). Supporting this credence is the observation that the affinity of S1 peptide lacking all three arginine residues at positions +5, +6 and +7 (S1_AAA) is significantly compromised toward both SH3 domains (Table 5-1). To directly test that the high affinity and specific binding of cSH3 domain to S1 site is largely afforded by the presence of R+6 and R+7, we measured the binding of S1 peptide containing alanine substitutions at these two arginine positions (S1_AA) to SH3 domains. Our results reveal that while the binding of S1_AA peptide to nSH3 domain is only slightly weaker than the S1 peptide, it binds to the cSH3 domain with an affinity that is over an order of magnitude weaker relative to S1 peptide (Table 5-1). This salient observation unequivocally demonstrates that R+6 and R+7 flanking the C-terminal of the PXψPXR motif at S1 site are absolutely required for the binding of cSH3 domain within the physiological context. In a leap of further curiosity, we also analyzed the extent to which R+5, R+6 and R+7 within the S1 site were individually critical for binding to SH3 domains (Table 5-1). The substitution of R+5 to alanine within S1 peptide (S1_R+5A) reduced the binding affinities to both the nSH3 and cSH3 domains by an order of magnitude, implying that R+5 is critical for the binding of both SH3 domains to S1 site. In the case of substitution of R+6 to alanine within S1 peptide (S1_R+6A), the binding to nSH3 domain was virtually indistinguishable from that observed for the S1 peptide but underwent a close to three-fold reduction in affinity upon binding to the cSH3 domain relative to S1 peptide.

On the basis of these observations, the most straightforward conclusion is that while R+6 is important for the binding of cSH3 domain to S1 site, it is redundant in the

case of nSH3 domain. Finally, in the case of the S1 peptide containing an alanine substitution at R+7 (S1_R+7A), the binding to both SH3 domains suffers between two-to-three fold reduction, implying that R+7 plays a non-redundant role in the binding of both the nSH3 and cSH3 domains to S1 site. Taken together, our data demonstrate that while all three R+5, R+6 and R+7 arginine residues are critical for the binding of cSH3 domain to S1 site, the nSH3 domain only strictly requires R+5 and R+7.

5.5.2 D33-R+7 salt bridge enhances the binding of nSH3 domain to S1 site

Our data presented above suggest strongly that both R+5 and R+7 arginine residues within S1 site are required for optimal binding of the nSH3 domain. The simplest mechanism by which these basic residues in the S1 peptide are likely to contribute to the free energy of binding is by virtue of their ability to engage in the formation of ion pairs or salt bridges with specific acidic residues in the nSH3 domain. It should be noted that such charged residues do not exist in solitude but in a symbiotic relationship with counterions when free in solution. Upon the formation of ion pairs with oppositely charged residues, usually through intermolecular association, the release of counterions into solution contributes to the free energy of binding through entropic gain. We have previously shown that R+5 ion pairs with D15 in the nSH3 domain [41]. But which acidic residue in the nSH3 domain does R+7 ion pair with?

Analysis of available 3D atomic coordinates of nSH3 domain in complex with a Sos1-derived peptide flanking the S1 site reveals that the two most likely suspects for this role could be either E31 or D33 (Figure 5-1a) [35, 38-40]. Both of these acidic residues are located close to the exit of the hydrophobic groove in the nSH3 domain that accommodates the peptide and lie within stretching distance of R+7. To determine which

Table 5-2

Experimentally determined thermodynamic parameters for the binding of mutant nSH3 domains of Grb2 to various Sos1 peptides obtained from ITC measurements at 25°C and pH 8.0

		nSH3_E31A				nSH3_D33A			
Peptide	Sequence	K_d / μM	ΔH / $kcalmol^{-1}$	TΔS / $kcalmol^{-1}$	ΔG / $kcalmol^{-1}$	K_d / μM	ΔH / $kcalmol^{-1}$	TΔS / $kcalmol^{-1}$	ΔG / $kcalmol^{-1}$
S1	PVPPPVPPRRRP	56 ± 0.1	-7.49 ± 0.13	-1.69 ± 0.12	-5.80 ± 0.01	157 ± 0.1	-8.15 ± 0.07	-2.96 ± 0.07	-5.19 ± 0.01
S1_R+6A	PVPPPVPPR<u>A</u>RP	67 ± 0.3	-8.10 ± 0.14	-2.40 ± 0.14	-5.70 ± 0.01	137 ± 7.6	-8.54 ± 0.18	-3.27 ± 0.21	-5.28 ± 0.03
S1_R+7A	PVPPPVPPRR<u>A</u>P	91 ± 1.2	-7.99 ± 0.12	-2.47 ± 0.11	-5.52 ± 0.01	169 ± 4.5	-8.62 ± 0.19	-3.47 ± 0.20	-5.15 ± 0.02

The residues within the S1 peptide subjected to alanine substitution are underlined for clarity. The values for the binding affinity (K_d) and the enthalpy change (ΔH) were obtained from the fit of a function, based on the binding of a ligand to a macromolecule [88], to the ITC isotherms. Free energy of binding (ΔG) was calculated from the relationship $\Delta G=RTlnK_d$, where R is the universal molar gas constant (1.99 cal/mol/K) and T is the absolute temperature (K). Entropic contribution (TΔS) to binding was calculated from the relationship TΔS=ΔH-ΔG. The binding stoichiometries to the fits agreed to within ±10%. Errors were calculated from 2-3 independent measurements. All errors are given to one standard deviation. All parameters are reported to no more than four significant figures.

of these two potential acidic residues is actually responsible for neutralizing the positive charge on R+7, we measured the binding of mutant nSH3 domains containing either an alanine substitution at E31 (nSH3_E31A) or at D33 (nSH3_D33A) to S1 peptide using ITC (Table 5-2). Our data reveal that while nSH3_E31A binds to S1 peptide with an affinity that is very similar to that observed for the binding of wild-type nSH3 domain, the binding of nSH3_D33A to S1 peptide occurs with an affinity that is over four-fold weaker relative to nSH3 domain. This finding suggests that it is D33 and not E31 that engages in the formation of a salt bridge with R+7. To further demonstrate that this is so, we also measured the binding of S1_R+6A and S1_R+7A peptides to nSH3_E31A and nSH3_D33A mutant domains (Table 5-2). The fact that the S1_R+6A peptide binds to nSH3_E31A and nSH3_D33A mutant domains with affinities that are similar to those observed for the binding of S1 peptide implies that R+6 is not involved in the formation

of an ion pair as noted above. In contrast, the S1_R+7A peptide binds to nSH3_E31A with an affinity that is nearly two-fold weaker than that observed for the binding of S1 peptide, implying that this reduction in affinity is most likely due to the disruption of an ion pair involving R+7 with an acidic residue in the nSH3_E31A domain other than E31. This mysterious acidic residue involved in the formation of an ion pair with R+7 is thus likely to be D33 due to the fact that the nSH3_D33A mutant domain binds with very similar affinities to both the S1 and S1_R+7A peptides.

In light of these considerations and data reported previously [41], the binding of nSH3 domain to S1 site in Sos1 is driven by the formation of D15-R+5 and D33-R+7 salt bridges. However, the D33-R+7 salt bridge is not critical allowing the nSH3 domain to also bind to S2, S3 and S4 sites in Sos1 that are devoid of R+7.

5.5.3 D187-R+6 and D190-R+7 salt bridges cooperate to drive the binding of cSH3 domain to S1 site

While the nSH3 domain only requires the ion pairing of R+5 and R+7 in binding to S1 site, R+6 also appears to be necessary for the binding of cSH3 domain (Table 5-1). In a previous study, we demonstrated that R+5 forms a salt bridge with E171 in the cSH3 domain [41]. Here we set out to identify the potential partners of R+6 and R+7 in the cSH3 domain. The most likely candidates for this role are D187 and D190 within the cSH3 domain in agreement with structure-based sequence alignment with nSH3 domain (Figure 5-1a). To test this hypothesis, we introduced alanine substitutions within the cSH3 domain at D187 (cSH3_D187A) and D190 (cSH3_D190A) and measured the binding of these mutant domains to S1 peptide (Table 5-3). The fact that both cSH3_D187A and SH3_D190A mutant domains bind to S1 peptide with about two-fold reduction in binding affinity relative to the wildtype cSH3 domain suggests strongly that both D187 and D190 are involved in forming ion pairs with R+6 and R+7.

Table 5-3

Experimentally determined thermodynamic parameters for the binding of mutant cSH3 domains of Grb2 to various Sos1 peptides obtained from ITC measurements at 25°C and pH 8.0

		cSH3_D187A				cSH3_D190A			
Peptide	Sequence	K_d / μM	ΔH / $kcalmol^{-1}$	TΔS / $kcalmol^{-1}$	ΔG / $kcalmol^{-1}$	K_d / μM	ΔH / $kcalmol^{-1}$	TΔS / $kcalmol^{-1}$	ΔG / $kcalmol^{-1}$
S1	PVPPPVPPRRRP	230 ± 4	-4.55 ± 0.11	+0.42 ± 0.12	-4.97 ± 0.01	272 ± 11	-4.24 ± 0.42	+0.63 ± 0.45	-4.87 ± 0.02
S1_R+6A	PVPPPVPPRARP	544 ± 102	-3.35 ± 0.03	+1.12 ± 0.08	-4.46 ± 0.11	910 ± 57	-14.80 ± 0.27	-10.65 ± 0.23	-4.15 ± 0.04
S1_R+7A	PVPPPVPPRRAP	2388 ± 73	-9.94 ± 0.11	-6.36 ± 0.09	-3.58 ± 0.02	482 ± 47	-5.12 ± 0.41	-0.59 ± 0.47	-4.53 ± 0.06

The residues within the S1 peptide subjected to alanine substitution are underlined for clarity.The values for the binding affinity (K_d) and the enthalpy change (ΔH) were obtained from the fit of a function, based on the binding of a ligand to a macromolecule [88], to the ITC isotherms. Free energy of binding (ΔG) was calculated from the relationship $\Delta G=RT\ln K_d$, where R is the universal molar gas constant (1.99 cal/mol/K) and T is the absolute temperature (K). Entropic contribution (TΔS) to binding was calculated from the relationship TΔS=ΔH-ΔG. The binding stoichiometries to the fits agreed to within ±10%. Errors were calculated from 2-3 independent measurements. All errors are given to one standard deviation. All parameters are reported to no more than four significant figures.

To identify the specific residues involved in the formation of these ion pairs, we also measured the binding of cSH3_D187A and cSH3_D190A mutant domains to S1_R+6A and S1_R+7A peptides (Table 5-3). The fact that the cSH3_D187A binds to the S1_R+7A peptide with an affinity that is over four-fold weaker than that observed for its binding to the S1_R+6A peptide implies that it is R+6 and not R+7 that must ion pair with D187. This observation is further corroborated upon the binding of cSH3_D190A to S1_R+6A peptide with an affinity that is nearly two-fold weaker than that observed for its binding to S1_R+7A, implying that it is R+7 and not R+6 that forms an ion pair with D190. Taking these observations together in light of the previous data [41], the binding of cSH3 domain to S1 site in Sos1 is driven by the formation of E171-R+5, D187-R+6 and

D190-R+7 salt bridges. Given that all of these three salt bridges are critical for the binding of nSH3 domain to S1 site implies that it cannot bind to S2, S3 and S4 sites in Sos1 devoid of R+6 and R+7.

5.5.4 Arginine residues within S1 site contribute differentially to the free energy of binding of nSH3 and cSH3 domains

The foregoing argument suggests strongly that the arginine residues R+5, R+6 and R+7 within the S1 site play a key role in driving the Grb2-Sos1 interaction. As illustrated in Figure 5-4, it can be further seen that these arginine residues contribute between 30-40% of the total free energy available to drive the binding of nSH3 and cSH3 domains to S1 site in a distinct manner. Thus, while R+5 is the major contributor to the overall free energy of binding of nSH3 domain to S1 site, R+7 and R+6 play lesser roles, with the contribution of the latter falling within the experimental error of the measurements being reported here. In contrast, while R+5 also heavily contributes to the overall free energy of binding of cSH3 domain to S1 site, R+6 and R+7 clearly play significant roles and, together, the energetic contributions of R+6 and R+7 almost match those of R+5. The specificity of nSH3 and cSH3 domains toward Sos1 thus seems to be largely due to the distinct contributions of arginine residues R+5, R+6 and R+7 to the free energy of binding. In other words, electrostatic interactions in lieu of hydrophobic contacts appear to define the distinguishing features of the binding of nSH3 and cSH3 domains to Sos1. This is further corroborated by the fact that the S1_AAA peptide, in which all three arginine residues are substituted by alanine, binds to both nSH3 and cSH3 domains with very similar affinities, albeit in a non-physiologically-relevant manner (Table 5-1).

5.5.5 D15 underscores the high-affinity binding of nSH3 domain to PXψPXR motifs within Sos1

Our data presented above provide the rationale underlying the binding of nSH3 domain to all four S1-S4 sites with Sos1, while the cSH3 domain can only bind to S1 site. But what features within the nSH3 domain enable it to only strictly require R+5, while the cSH3 domain has an obligate requirement of all three R+5, R+6 and R+7 arginine residues within the putative binding sites in Sos1? Given that the binding affinity of S1_R+5A peptide to nSH3 domain is reduced by more than an order of magnitude relative to S1 peptide (Table 5-1), we reasoned that the energetic contribution resulting from the formation of D15-R+5 salt bridge may be largely responsible for driving the binding of nSH3 domain to all four S1-S4 sites in contrast to cSH3 domain that can only bind to S1 site. This seems logical in light of the fact that the cSH3 domain contains a glycine (G173) instead of an acidic residue, let alone an aspartate, at the structurally equivalent position occupied by D15 in the nSH3 domain (Figure 5-1a). The cSH3 domain rather relies on a neighboring glutamate (E171) to engage in the formation of a salt bridge with R+5. Because D15 and E171 are structurally and chemically non-equivalent, it is very likely that such differences also translate into D15-R+5 and E171-R+5 salt bridges being energetically non-equivalent and thus may underlie the distinct behavior of nSH3 and cSH3 domains toward S1-S4 sites. As discussed above and illustrated in Figure 5-4, this is indeed the case. To further test the extent to which the ability of nSH3 domain to bind to all four S1-S4 sites is attributable to D15, we introduced alanine substitution at G173 in the cSH3 domain (cSH3_G173D) and measured the binding of cSH3_G173D mutant domain to S1-S4 peptides containing PXψPXR motifs. Comparison of affinities and various associated thermodynamic

parameters for the binding of nSH3 and cSH3_G173D domains to S1-S4 peptides is provided in Figure 5-5. It is clearly apparent from our data that the G173D substitution renders the cSH3 domain to behave very much like the nSH3

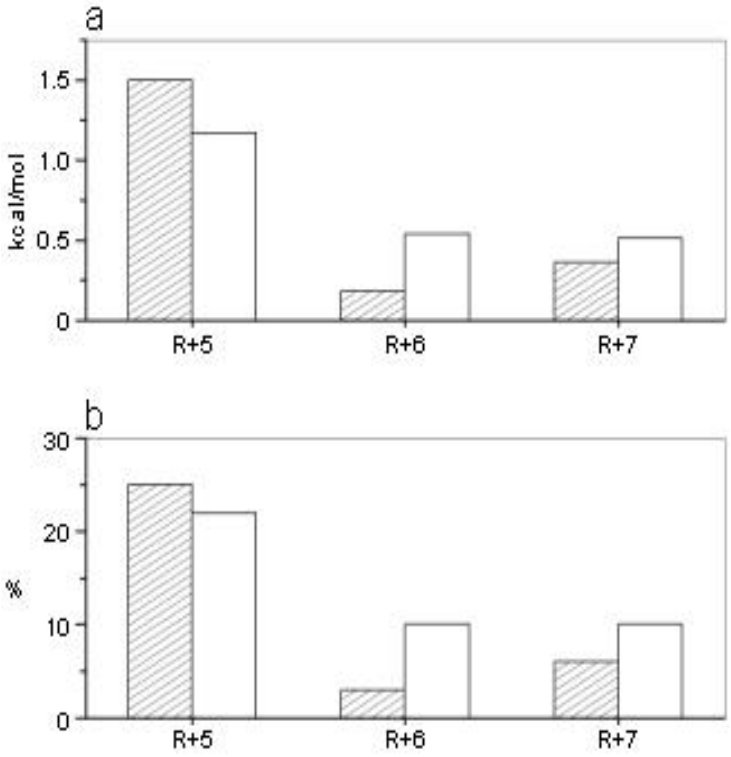

Figure 5-4: Comparison of energetic contributions of arginine residues R+5, R+6 and R+7 within the S1 site to the free energy of binding of nSH3 (shaded columns) and cSH3 (unshaded columns) domains. (a) Energetic contributions relative to the total free energy (ΔG_{Total}) of binding of nSH3 and cSH3 domains to S1 peptide expressed in absolute terms (kcal/mol). The energetic contribution of R+5 (ΔG_{R+5}) was calculated from the relationship $\Delta G_{R+5}=\Delta G_{R+5A}-\Delta G_{Total}$, where ΔG_{R+5A} is the free energy of binding of S1_R+5A peptide to the nSH3 or the cSH3 domain. The energetic contribution of R+6 (ΔG_{R+6}) was calculated from the relationship $\Delta G_{R+6}=\Delta G_{R+6A}-\Delta G_{Total}$, where ΔG_{R+6A} is the free energy of binding of S1_R+6A peptide to the nSH3 or the cSH3 domain. The energetic contribution of R+7 (ΔG_{R+7}) was calculated from the relationship $\Delta G_{R+7}=\Delta G_{R+7A}-\Delta G_{Total}$, where ΔG_{R+7A} is the free energy of binding of S1_R+7A peptide to the nSH3 or the cSH3 domain. (b) Energetic contributions relative to the total free energy (ΔG_{Total}) of binding of nSH3 and cSH3 domains to S1 peptide expressed as a percentage (%). The energetic contribution of R+5 ($\%_{R+5}$) was calculated from the relationship $\%_{R+5}=[(\Delta G_{R+5A}/\Delta G_{Total})x100]$, where ΔG_{R+5A} is the free energy of binding of S1_R+5A peptide to the nSH3 or the cSH3 domain. The energetic contribution of R+6 ($\%_{R+6}$) was calculated from the relationship $\%_{R+6}=[(\Delta G_{R+6A}/\Delta G_{Total})x100]$, where ΔG_{R+6A} is the free energy of binding of S1_R+6A peptide to the nSH3 or the cSH3 domain. The energetic contribution of R+7 ($\%_{R+7}$) was calculated from the relationship $\%_{R+7}=[(\Delta G_{R+7A}/\Delta G_{Total})x100]$, where ΔG_{R+7A} is the free energy of binding of S1_R+7A peptide to the nSH3 or the cSH3 domain. All energetic contributions were calculated using data provided in Table 5-1.

domain in its ability to recognize all four S1-S4 sites with binding affinities in the physiologically relevant range. This suggests strongly that D15 is largely responsible for the ability of nSH3 domain to recognize all four S1-S4 sites, while the placement of a glycine residue at this structurally equivalent position within the cSH3 domain deprives it of recognizing S2, S3 and S4 sites.

It is of worthy note that although the nSH3-mimetic cSH3_G173D may appear to exhibit similar binding energetics (Figures 5a and 5d), the underlying thermodynamic forces are quite distinct (Figures 5b and 5c). Thus, while the binding of nSH3 domain to all four S1-S4 sites is under enthalpic control accompanied by entropic penalty, this only holds true in the case of cSH3_G173D binding to S1 site, whereas binding of cSH3_G173D to S2, S3 and S4 sites is accompanied by favorable entropic contributions. This is indicative of the fact that although D15 may be largely responsible for the ability of nSH3 domain to bind to all four S1-S4 sites, other residues may also play a role in defining its binding specificity.

5.5.6 3D atomic models offer structural insights into the distinct mechanisms employed by SH3 domains in binding to Sos1

In an attempt to rationalize the distinct mechanisms employed by SH3 domains of Grb2 in recognizing Sos1, we modeled 3D structures of nSH3, cSH3 and cSH3_G173D domains in complex with S1 peptide (Figure 5-6). In these models, the SH3 domains adapt the characteristic β-barrel fold and the peptide is accommodated into a hydrophobic groove with a relatively open left-handed polyproline type II (PPII) helical conformation. Although the nature of intermolecular hydrophobic forces stabilizing nSH3-peptide and cSH3-peptide complexes is virtually identical, as discussed earlier [41], the major

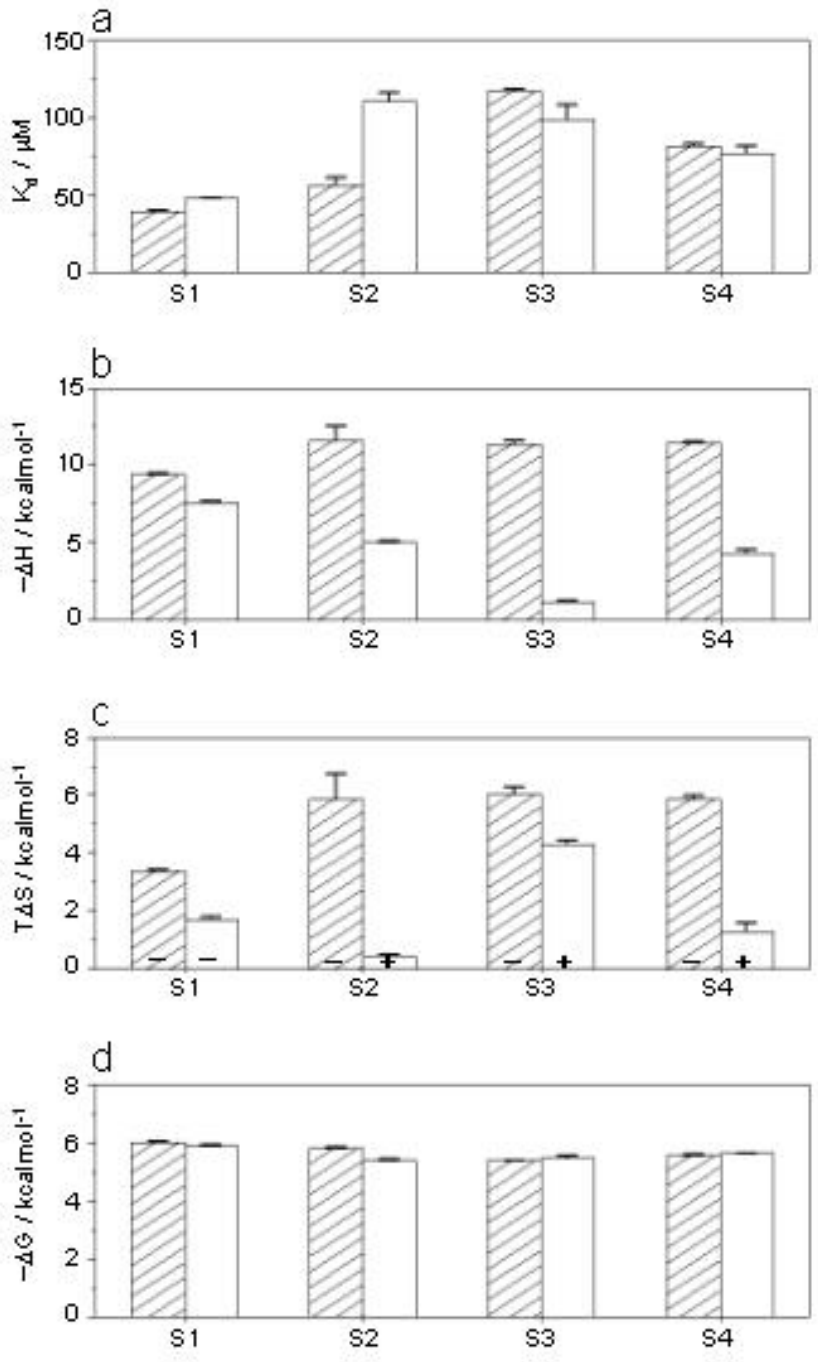

Figure 5-5: Comparison of energetics of binding of Sos1-derived peptides S1-S4 to wildtype nSH3 domain (shaded columns) and cSH3_G173D mutant domain (unshaded columns). (a) Binding affinity (K_d); (b) Enthalpic contribution to binding (ΔH); (c) Entropic contribution to binding (TΔS) with the + and − signs indicating entropic gain and entropic penalty, respectively; and (d) Overall free energy of binding (ΔG). All parameters were directly determined from ITC analysis. Error bars were calculated from 2-3 independent measurements. All error bars are given to one standard deviation.

differences surface in the nature of intermolecular electrostatic forces. Thus, while the nSH3 domain employs respectively D15 and D33 in the formation of ion pairs with R+5 and R+7 in the peptide (Figure 5-6a), the cSH3 domain relies on E171 and D190 in accomplishing what may seem to be the same feat but it is far from that (Figure 5-6b). The reason being that while D190 is structurally and chemically equivalent to D33 with the effect that the D33-R+7 and D190-R+7 salt bridges are more or less energetically equivalent, D15 and E171 are structurally non-equivalent and chemically distinct, with G173 in the cSH3 domain being structurally equivalent to D15. Such differences within the two SH3 domains result in the D15-R+5 and E171-R+5 salt bridges being energetically non-equivalent and therefore being the major source of the differential behavior of these two domains toward various potential binding sites within Sos1. As if these residues were insufficient to distinguish their biological roles, the cSH3 domain entertains one additional trick to further differentiate its behavior from the nSH3 domain. Such coup de grace is delivered in the form of D187 involved in the formation of a third salt bridge with R+6 in the peptide (Figure 5-6b).

Taking these considerations into account, it would suffice to add that the nSH3 and cSH3 domains employ two-prong and three-prong mechanisms to engage in electrostatic interactions with S1 site in Sos1, respectively. Clearly, the lack of R+6 and R+7 at S2, S3 and S4 sites in Sos1 would imply that not only nSH3 would bind to these sites in an exclusive manner but that it would do so through the engagement of a single D15-R+5 salt bridge, albeit with no effect on the nature of intermolecular hydrophobic forces. It is also of worthy note that while the nSH3 domain and its mimetic cSH3_G173D mutant domain bind to S1-S4 peptides with very similar affinities, the latter displays distinct contributions from the underlying enthalpic and entropic

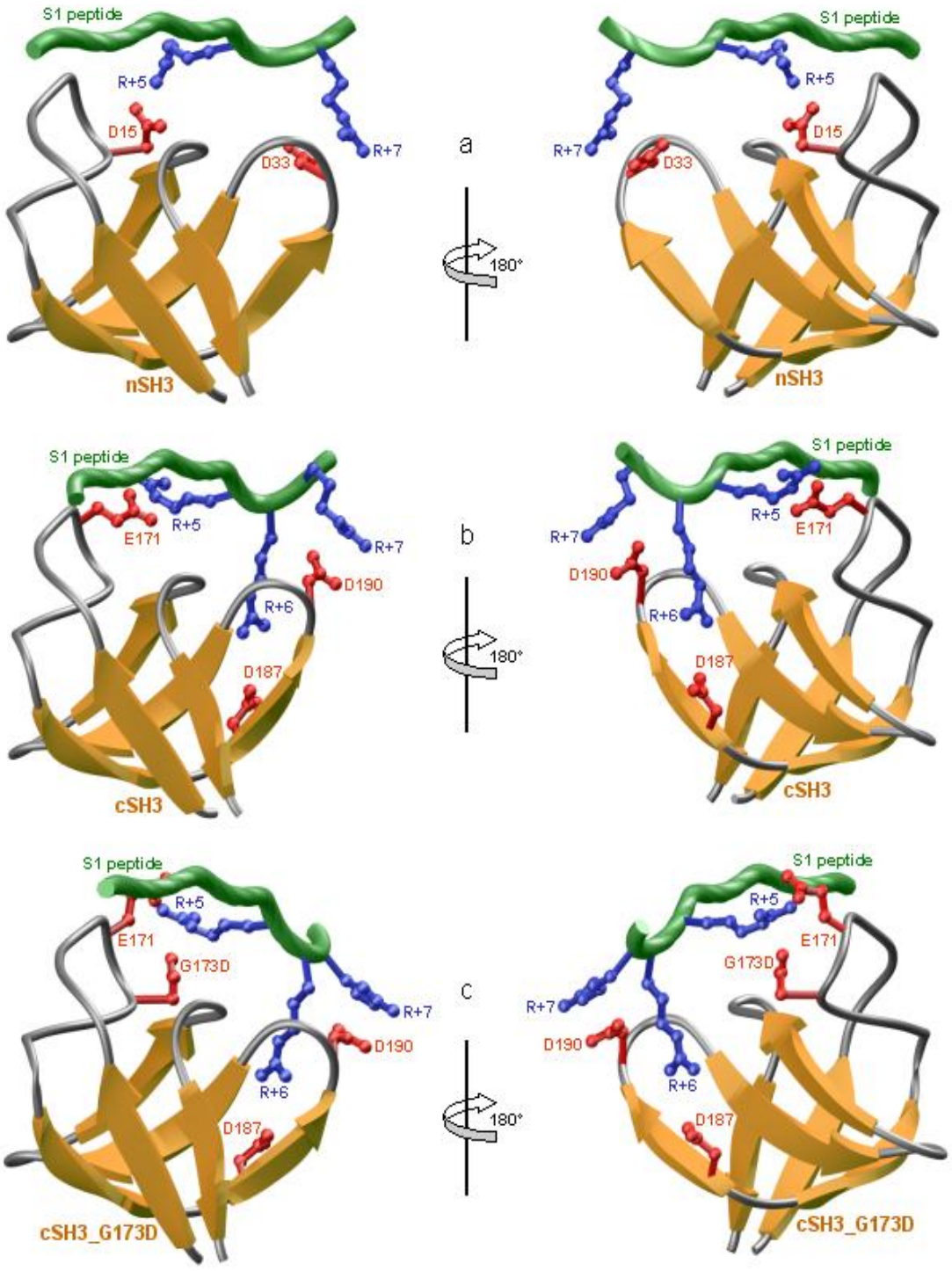

Figure 5-6: 3D structural models of S1 peptide in complex with nSH3 (a), cSH3 (b), and cSH3_G173D (c) domains of Grb2. The β-strands in SH3 domains are shown in yellow with loops depicted in gray and the sidechains of acidic residues involved in salt bridging with the peptide in red. The backbone of Sos1 peptide is colored green with the sidechains of arginine residues involved in salt bridging with SH3 domains in blue. Two alternative orientations, related by an 180°-rotation about the vertical axis, are shown for clarity and close scrutiny.

components (Figure 5-5). Although structural thermodynamics is still in its infancy, it is interesting to note that such differences in the underlying thermodynamic components may be due to the fact that while nSH3 domain engages in only two intermolecular salt bridges (Figure 5-6a), the cSH3_G173D mutant domain employs three (Figure 5-6c). Additionally, the R+5 residue in S1 peptide likely bifurcates the E171 and G173D ion pairs within the cSH3_G173D mutant domain, while R+5 merely engages in the formation of an ion pair with D15 — the residue that is structurally equivalent to G173D — due to the substitution of an alanine (A13) at the structurally equivalent position occupied by E171 in the cSH3_G173D mutant domain. In short, our 3D atomic models offer a closer glimpse into the structural basis of the exclusivity of S1 site for binding to cSH3 domain, while the nSH3 domain can bind to all S1-S4 sites indiscriminately.

5.5.7 SH3 domains appear to combine fidelity and promiscuity under the flagship of Grb2 in cellular signaling

The data presented herein suggest strongly that the cSH3 domain strictly requires the PXψPXRRR motif for binding to Sos1, while the nSH3 domain will do so only upon the presentation of PXψPXR motif under physiological context. In light of these observations, it is tempting to add that the SH3 domains may have evolved to bring the best of both worlds to Grb2. Thus, while nSH3 domain may be ideally suited for signaling promiscuity due to requirement of only one arginine residue within its proline-rich ligands, the cSH3 domain most certainly imparts signaling fidelity upon Grb2. To further confirm this notion, we searched the human proteome for the occurrence of PXψPXR and PXψPXRRR motifs. Our findings reveal that while there are 753 PXψPXR motifs within the human proteome across nearly as many proteins, only six of

				P	X	Ψ	P	X	R	R	R		
SOS1	1148-P	V	P	P	P	V	P	P	R	R	R	P-1159	Q07889
GPC2	0460-A	S	G	P	D	V	P	T	R	R	R	R-0471	Q8N158
MDM1	0431-V	S	A	P	T	I	P	V	R	R	R	L-0442	Q8TC05
OBSL1	0282-E	G	R	P	L	L	P	D	R	R	R	L-0293	O75147
SETD5	0758-F	G	S	P	F	I	P	E	R	R	R	R-0769	Q9C0A6
SPTA1	1037-D	E	F	P	M	L	P	Q	R	R	R	E-1048	P02549

Figure 5-7: Amino acid sequence alignment showing the cccurrence of PXψPXRRR motif in human proteome. Absolutely conserved residues within the PXψPXRRR motif are shown in red, the ψ residue is depicted in blue and all other residues are colored black. The proteins containing this motif are listed in the far left column, while the far right column provides the corresponding Expasy codes. The numerals hyphenated to amino acid sequence at each end denote the residue number within the protein sequence.

them contain the PXψPXRRR motif (Figure 5-7). In addition to Sos1, these include GPC2, MDM1, OBSL1, SETD5 and SPTA1 [120-124]. With the exception of Sos1, none of these proteins contain the PXψPXR motif, implying that the cSH3 domain of Grb2 may bind to them in an exclusive manner and thereby leading to build-up of weak interactions. Such a design may be an important aspect of transient signaling allowing Grb2 to fine-tune various overlapping cascades via its interaction with the aforementioned partners.

Our analysis presented above clearly suggests that while the interaction of Grb2 with other cellular partners through its nSH3 domain may be highly promiscuous, the cSH3 domain provides a striking contrast by virtue of its ability to bind to only a handful of partners adding much needed fidelity to signaling via Grb2. It should be borne in mind that while the proteins containing the PXψPXRRR motif should be expected to bind to the cSH3 domain, the lack of such motif in cellular proteins may not necessarily rule out their interaction with Grb2. This is due to the fact that SH3 domains have also adapted an alternative mechanism independent of the consensus proline-rich sequence PXXP for recognizing some of their partners. In particular, the cSH3 domain of Grb2 has been shown to bind to key signaling modulators Gab1 and SLP76 via the recognition of a non-

consensus PXXXRXXKP motif [15, 117]. Structural analysis reveals that the PXXXRXXKP motif binds to the cSH3 domain in a manner akin to the binding of PXψPXRRR motif, with the both motifs sharing the same binding groove and orientation [118, 119]. However, there are some discernable differences. While the PXψPXRRR motif adapts a relatively open left-handed polyproline type II (PPII) helical conformation, the PXXXRXXKP motif adapts a 3_{10}-helical conformation upon binding to the cSH3 domain. The respective conformations are required to orient the critical residues within each motif for optimal interactions within the binding groove of the cSH3 domain. Overall, the PXXXRXXKP motif engages in additional contacts within the binding groove of cSH3 domain relative to the PXψPXRRR motif and, by virtue of these distinguishing interactions, the cSH3 domain binds to Gab1 and SLP76 with higher affinity than Sos1. Such differential binding of cSH3 domain to Gab1 and SLP76 versus Sos1 may be an important determinant of monitoring the ratios of Grb2-Sos1 pool versus Grb2-Gab1 and Grb2-SLP76 pools with consequences for activation of Ras versus other signaling pathways.

5.6 Concluding Remarks

Although the central role of Grb2-Sos1 signaling complex in mitogenic signaling was first demonstrated over a decade ago [6, 13, 36, 125], the precise mechanism by which it is assembled remains largely obscure. The prevailing view for the past decade has been that Grb2 recognizes Sos1 by virtue of its SH3 domains to bind to various PXψPXR motifs within Sos1. Our present study suggests that although there are four such putative sites within Sos1 (S1-S4), they may not all be used indiscriminately to recognize the SH3 domains of Grb2. Thus, while the nSH3 domain binds to all four sites with very similar affinities in the physiological range, the cSH3 domain can only do so at

S1 site. The reason for such high specificity for the cSH3 domain is not clear but it may be an important feature of Grb2 in signaling cascades that demand high fidelity. Nonetheless, the mechanism by which the cSH3 domain has acquired such a high level of specificity appears to be remarkably simple. The substitution of D15 within the RT loop of nSH3 domain to a glycine at the structurally equivalent position in the cSH3 domain seems to be all that is required to specifically direct the cSH3 domain to S1 site and prevent it from binding to other potential sites containing the PXψPXR motifs. Because of this substitution, the cSH3 domain employs a distinct mechanism in recognizing the S1 site compared with the nSH3 domain. Thus, while the nSH3 domain employs only two intermolecular salt bridges for binding to S1 site, the cSH3 domain relies on three. Electrostatic interactions are a general feature of SH3-ligand specificity due to the presence of one or more charged residues flanking the PXXP motif as well as those lining the binding groove within the SH3 domains [42, 97-99]. In fact, substitution of these charged residues with alanine almost always abrogates SH3-ligand interactions. Consistent with these observations, our present data epitomize the role of multiple salt bridges in the assembly of Grb2-Sos1 complex. In particular, our data suggest that the salt bridges contribute between 30-40% of the total free energy available to drive the binding of nSH3 and cSH3 domains to S1 site. The specificity of nSH3 and cSH3 domains toward Sos1 thus largely appears to be due to the distinct contributions of arginine residues R+5, R+6 and R+7 to the free energy of binding. In other words, electrostatic interactions in lieu of hydrophobic contacts appear to define the distinguishing features of the binding of nSH3 and cSH3 domains to Sos1. That this is so implies that intracellular salt concentrations may be an important determinant of Grb2-

Sos1 assembly. We have indeed previously shown that salt tightly modulates the binding of nSH3 and cSH3 domains of Grb2 to Sos1 [41].

It has been previously suggested that Grb2 binds to Sos1 with a 1:1 stoichiometry [126]. In light of this observation coupled with our data presented herein, we propose a model of how Grb2 and Sos1 might assemble at the inner membrane surface upon growth factor receptor stimulation. The exclusivity of binding of cSH3 domain to S1 site would allow the nSH3 domain to bind to one of the other available S2-S4 sites with little or no preference. In this manner, the binding of cSH3 domain to S1 site could restrict the orientation of Grb2 relative to Sos1, while the binding of nSH3 domain to one of the three available S2-S4 sites may result in the formation of various structurally and conformationally distinct Grb2-Sos1 complexes. Such orientational constraint imposed upon Grb2-Sos1 assembly by the cSH3 domain coupled with conformational heterogeneity resulting from the promiscuity of nSH3 domain may be an important determinant of regulating the activation of downstream molecules such as Ras. For example, the preference of cSH3 domain toward S1 site may orient Grb2 in such a manner that it does not interfere with the GDP-GTP nucleotide exchange function of Sos1 required for the activation of membrane-bound Ras [55, 127]. Given that Sos1 competes with a diverse array of other downstream effectors for binding to Grb2, including the adaptor proteins Gab1 and SLP76 [14, 15], the endocytic GTPase dynamin1 [16, 17], the ubiquitin ligase Cbl [15, 18, 19] and the cell cycle inhibitor p27kip1 [20], the ability of cSH3 domain to dictate the binding of Grb2 to Sos1 in an oriented manner may also play an important role in determining the fraction of Grb2-Sos1 pool. It should be noted that the role of molecular orientation and conformational heterogeneity of protein-protein complexes is largely under-appreciated in the temporal and spatial

regulation of signaling complexes. Our present study thus sets a precedent for the design and guidance of further experiments to unravel the regulatory role of molecular orientation and conformational heterogeneity in the assembly of signaling complexes.

6 Chapter 6: Conclusion

Elucidating protein-protein interactions in thermodynamic terms offers molecular insights into the mechanisms of life at a level second to none. Although Grb2 has been perceived as a central player in cellular signaling since its discovery over a decade ago [2, 4, 10], little is known about the role of oligomerization in the biological function of Grb2. In this thesis, using an array of biophysical methods, we have shown that Grb2 exists in a dynamic equilibrium between dimer and monomer with the equilibrium well in favor of the latter species under low protein concentrations that are likely to be encountered under normal functioning of the cellular machinery. Although the Grb2 monomer-dimer equilibrium is likely to be in favor of the monomer in quiescent cells, rapid expression and rise in Grb2 concentration upon mitogenic stimulation is likely to shift this equilibrium in favor of the dimer. Other factors within the cell are also likely to affect the Grb2 monomer-dimer equilibrium. Studies on cultured mammalian cells indicate that phosphorylation of both Y239 and Y317 in p52Shc is required for efficient formation of p52Shc-Grb2-Sos complex [11]. Thus, the requirement of two rather than one phosphorylation sites in p52Shc for Grb2 recruitment may shift the Grb2 monomer-dimer equilibrium in favor of the dimer due to the fact that SH2 domains in dimeric Grb2 are likely to bind to two phosphorylation sites in p52Shc with much greater affinity and specificity than a single SH2 domain in monomeric Grb2. As a consequence of this differential binding, the existence of Grb2 dimer over monomers will be highly favored over both thermodynamic and kinetic grounds not to mention the functional advantages that such a mechanism may impart upon cellular signaling.

This thesis also demonstrates exquisitely how thermodynamic information can be employed to corroborate or refute structural data. Although Grb2 crystallizes as a dimer

with a two-fold axis of symmetry [10], the assumption that the monomers within this dimer may retain the same conformation in isolation is unlikely to bear fruit due to the large and flexible inter-domain loops. Our thermodynamic data indeed suggest strongly that the monomers are likely to undergo cSH3-SH2 domain swapping and thus adopt a more compact structure than that observed in the Grb2 dimer. Given that the structure of Grb2 in its monomeric state is not available and that it may not be practically surmountable in the foreseeable future due to the requirement of protein at high concentrations, conditions under which it predominantly exists as a dimer, for structural analysis by both the X-ray and NMR methodologies, the relevance of our thermodynamic studies presented here could not be overemphasized.

Furthermore, we were driven by the curiosity to unravel the underlying structural basis for the differential binding of SH3 domains of Grb2 to Sos1 — a classical SH3-ligand interaction that has not only been widely studied but its role in determining the fate of a healthy from a diseased cell cannot be disputed. It was thus fitting that we chose this key protein-protein interaction to further expand our knowledge of SH3-ligand specificity. Our data are consistent with the hypothesis that the residue D15 in the RT loop within the nSH3 domain is the major determinant of high affinity binding to Sos1 relative to the cSH3 domain by virtue of its ability to engage in the formation of a salt bridge with R_{+5} residue in the consensus motif PXψPXR. In contrast, the residue analogous to D15 in the cSH3 domain is G173. Thus, the lack of a chemically and structurally equivalent residue at this key position in the RT loop of the β-barrel fold of cSH3 domain accounts for its low affinity binding to Sos1. That this is even possible is resurrected by the presence of a neighboring E171 in the cSH3 domain that appears to substitute for the role of D15 in the nSH3 domain. The differential binding affinities and

differential thermodynamic mechanisms employed by the SH3 domains of Grb2 in their ability to recognize Sos1 may have evolved to provide a molecular switch necessary to regulate the interactions of Grb2 with a diverse array of downstream effectors of Grb2 in addition to Sos1 depending on the biological context and the nature of mitogenic stimuli [12-20].

An increasing number of the SH3-ligand binding studies have been carried out in buffers that have tended to be devoid of salt. This thesis shows that salt tightly modulates the Grb2-Sos1 interaction and that this is likely to be the rule rather than an exception for the SH3-ligand interaction in general due to the universal requirement of one or more salt bridges that play a critical role in defining specificity between this pair of protein-protein interactions [42, 97-99]. What we have not argued thus far is the realization that a vast number of SH3-proteins contain SH3 domains in multiple copies and often in tandem. Complementing this exquisite multiple-domain architecture is the design of SH3 ligands which also tend to boast multiple proline-rich motifs within the same stretch of a polypeptide chain, with Sos1 being a classical example of this class of polydentate SH3 ligands. Thus, it seems likely that the simultaneous binding of multiple SH3 domains to multiple ligand sites may result in pronounced binding affinities, due to entropic advantage, instead of those inferred from the analysis of isolated SH3 domains with their cognate ligands. Sos1 indeed contains multiple proline-rich sequences containing the consensus motif PXψPXR. It is thus conceivable that the SH3 domains of Grb2 bind to Sos1 simultaneously and thereby leading to enhancement of Grb2-Sos1 interaction.

The prevailing view for the past decade has been that Grb2 recognizes Sos1 by virtue of its SH3 domains to bind to various PXψPXR motifs within Sos1. This thesis suggests that although there are four such putative sites within Sos1 (S1-S4), they may

not all be used indiscriminately to recognize the SH3 domains of Grb2. Thus, while the nSH3 domain binds to all four sites with very similar affinities in the physiological range, the cSH3 domain can only do so at S1 site. The reason for such high specificity for the cSH3 domain is not clear but it may be an important feature of Grb2 in signaling cascades that demand high fidelity. Nonetheless, the mechanism by which the cSH3 domain has acquired such a high level of specificity appears to be remarkably simple. The substitution of D15 within the RT loop of nSH3 domain to a glycine at the structurally equivalent position in the cSH3 domain seems to be all that is required to specifically direct the cSH3 domain to S1 site and prevent it from binding to other potential sites containing the PXψPXR motifs. Because of this substitution, the cSH3 domain employs a distinct mechanism in recognizing the S1 site compared with the nSH3 domain. Thus, while the nSH3 domain employs only two intermolecular salt bridges for binding to S1 site, the cSH3 domain relies on three. Electrostatic interactions are a general feature of SH3-ligand specificity due to the presence of one or more charged residues flanking the PXXP motif as well as those lining the binding groove within the SH3 domains [42, 97-99]. In fact, substitution of these charged residues with alanine almost always abrogates SH3-ligand interactions. Consistent with these observations, our present data epitomize the role of multiple salt bridges in the assembly of Grb2-Sos1 complex. In particular, our data suggest that the salt bridges contribute between 30-40% of the total free energy available to drive the binding of nSH3 and cSH3 domains to S1 site. The specificity of nSH3 and cSH3 domains toward Sos1 thus largely appears to be due to the distinct contributions of arginine residues R+5, R+6 and R+7 to the free energy of binding. In other words, electrostatic interactions in lieu of hydrophobic contacts appear to define the distinguishing features of the binding of nSH3 and cSH3 domains to

Sos1. That this is so implies that intracellular salt concentrations may be an important determinant of Grb2-Sos1 assembly.

It has been previously suggested that Grb2 binds to Sos1 with a 1:1 stoichiometry [126]. In light of this observation coupled with our data presented herein, we propose a model of how Grb2 and Sos1 might assemble at the inner membrane surface upon growth factor receptor stimulation. The exclusivity of binding of cSH3 domain to S1 site would allow the nSH3 domain to bind to one of the other available S2-S4 sites with little or no preference. In this manner, the binding of cSH3 domain to S1 site could restrict the orientation of Grb2 relative to Sos1, while the binding of nSH3 domain to one of the three available S2-S4 sites may result in the formation of various structurally and conformationally distinct Grb2-Sos1 complexes. Such orientational constraint imposed upon Grb2-Sos1 assembly by the cSH3 domain coupled with conformational heterogeneity resulting from the promiscuity of nSH3 domain may be an important determinant of regulating the activation of downstream molecules such as Ras. For example, the preference of cSH3 domain toward S1 site may orient Grb2 in such a manner that it does not interfere with the GDP-GTP nucleotide exchange function of Sos1 required for the activation of membrane-bound Ras [55, 127]. Given that Sos1 competes with a diverse array of other downstream effectors for binding to Grb2, the ability of cSH3 domain to dictate the binding of Grb2 to Sos1 in an oriented manner may also play an important role in determining the fraction of Grb2-Sos1 pool. It should be noted that the role of molecular orientation and conformational heterogeneity of protein-protein complexes is largely under-appreciated in the temporal and spatial regulation of signaling complexes. This thesis thus sets a precedent for the design and guidance of

further experiments to unravel the regulatory role of molecular orientation and conformational heterogeneity in the assembly of signaling complexes.

In conclusion, our data reported here provide key insights into the structural basis of the differential binding of SH3 domains of Grb2 to Sos1 and significantly contribute to our understanding of the molecular determinants of SH3-ligand specificity. However, there is still much work to be done. Our preliminary data indicate, that in the context of full-length Grb2 the binding of one molecule of Sos1 to the nSH3 domain allosterically induces a conformational change within Grb2 such that the loading of a second molecule of Sos1 onto the cSH3 domain is blocked and, in so doing, allowing the Gab1 adaptor access to the cSH3 domain in an exclusively non-competitive manner to generate the Sos1-Grb2-Gab1 ternary complex. Furthermore, preliminary data suggest that the S4 site may play a previously unappreciated critical role in the ability of Grb2 to interact as a dimer with Sos1. However, further studies must be done to confirm these results and finish elucidating the details of this crucial protein-protein interaction. Furthermore, to unravel the physical basis of the formation of Sos1-Grb2 complex, the 3D structure of full-length Grb2 in complex with the PR domain of Sos1 using X-ray crystallography should be determined. Because of our poor understanding of the biophysical principles that underlie this specificity, our attempts to design novel inhibitors to disrupt this key protein-protein interaction pertinent to cellular signaling and cancer have met little success to date. Further biophysical analysis of SH3-ligand interactions is thus clearly warranted to expand our knowledge of the biology of SH3 domains and to help pave the way for the design of novel and more effective anti-SH3 inhibitors.

WORKS CITED

1. Cheng, A.M., Saxton, T.M., Sakai, R., Kulkarni, S., Mbamalu, G., Vogel, W., Tortorice, C.G., Cardiff, R.D., Cross, J.C., Muller, W.J., and Pawson, T. (1998). Mammalian Grb2 regulates multiple steps in embryonic development and malignant transformation. Cell *95*, 793-803.

2. Chardin, P., Cussac, D., Maignan, S., and Ducruix, A. (1995). The Grb2 adaptor. FEBS Lett *369*, 47-51.

3. Rozakis-Adcock, M., McGlade, J., Mbamalu, G., Pelicci, G., Daly, R., Li, W., Batzer, A., Thoma, S., Brugge, J., Pelicci, P.G., Schlessinger, J., and Pawson, T. (1992). Association of the Shc and Grb2/Sem5 SH2-containing proteins is implicated in activation of the Ras pathway by tyrosine kinases. Nature *360*, 689-692.

4. Lowenstein, E.J., Daly, R.J., Batzer, A.G., Li, W., Margolis, B., Lammers, R., Ullrich, A., Skolnik, E.Y., Bar-Sagi, D., and Schlessinger, J. (1992). The SH2 and SH3 domain-containing protein Grb2 links receptor tyrosine kinases to Ras signaling. Cell *70*, 431-442.

5. Rozakis-Adcock, M., McGlade, J., Mbamalu, G., Pelicci, G., Daly, R., Li, W., Batzer, A., Thomas, S., Brugge, J., Pelicci, P.G., and et al. (1992). Association of the Shc and Grb2/Sem5 SH2-containing proteins is implicated in activation of the Ras pathway by tyrosine kinases. Nature *360*, 689-692.

6. Rozakis-Adcock, M., Fernley, R., Wade, J., Pawson, T., and Bowtell, D. (1993). The SH2 and SH3 domains of mammalian Grb2 couple the EGF receptor to the Ras activator mSos1. Nature *363*, 83-85.

7. Walk, S.F., March, M.E., and Ravichandran, K.S. (1998). Roles of Lck, Syk and ZAP-70 tyrosine kinases in TCR-mediated phosphorylation of the adapter protein Shc. Eur J Immunol *28*, 2265-2275.

8. Blake, R.A., Broome, M.A., Liu, X., Wu, J., Gishizky, M., Sun, L., and Courtneidge, S.A. (2000). SU6656, a selective Src family kinase inhibitor, used to probe growth factor signaling. Mol Cell Biol *20*, 9018-9027.

9. McGlade, J., Cheng, A., Pelicci, G., Pelicci, P.G., and Pawson, T. (1992). Shc proteins are phosphorylated and regulated by the v-Src and v-Fps protein-tyrosine kinases. Proc Natl Acad Sci U S A *89*, 8869-8873.

10. Maignan, S., Guilloteau, J.P., Fromage, N., Arnoux, B., Becquart, J., and Ducruix, A. (1995). Crystal structure of the mammalian Grb2 adaptor. Science *268*, 291-293.

11. Harmer, S.L., and DeFranco, A.L. (1997). Shc contains two Grb2 binding sites needed for efficient formation of complexes with Sos in B lymphocytes. Mol Cell Biol *17*, 4087-4095.

12. Chardin, P., Camonis, J.H., Gale, N.W., van Aelst, L., Schlessinger, J., Wigler, M.H., and Bar-Sagi, D. (1993). Human Sos1: a guanine nucleotide exchange factor for Ras that binds to Grb2. Science *260*, 1338-1343.

13. Li, N., Batzer, A., Daly, R., Yajnik, V., Skolnik, E., Chardin, P., Bar-Sagi, D., Margolis, B., and Schlessinger, J. (1993). Guanine-nucleotide-releasing factor hSos1 binds to Grb2 and links receptor tyrosine kinases to Ras signalling. Nature *363*, 85-88.

14. Schaeper, U., Gehring, N.H., Fuchs, K.P., Sachs, M., Kempkes, B., and Birchmeier, W. (2000). Coupling of Gab1 to c-Met, Grb2, and Shp2 mediates biological responses. J Cell Biol *149*, 1419-1432.

15. Lewitzky, M., Kardinal, C., Gehring, N.H., Schmidt, E.K., Konkol, B., Eulitz, M., Birchmeier, W., Schaeper, U., and Feller, S.M. (2001). The C-terminal SH3 domain of the adapter protein Grb2 binds with high affinity to sequences in Gab1 and SLP-76 which lack the SH3-typical P-x-x-P core motif. Oncogene *20*, 1052-1062.

16. Seedorf, K., Kostka, G., Lammers, R., Bashkin, P., Daly, R., Burgess, W.H., van der Bliek, A.M., Schlessinger, J., and Ullrich, A. (1994). Dynamin binds to SH3 domains of phospholipase C gamma and Grb2. J Biol Chem *269*, 16009-16014.

17. Vidal, M., Montiel, J.L., Cussac, D., Cornille, F., Duchesne, M., Parker, F., Tocque, B., Roques, B.P., and Garbay, C. (1998). Differential interactions of the growth factor receptor-bound protein 2 N-SH3 domain with son of sevenless and dynamin. Potential role in the Ras-dependent signaling pathway. J Biol Chem *273*, 5343-5348.

18. Odai, H., Sasaki, K., Iwamatsu, A., Hanazono, Y., Tanaka, T., Mitani, K., Yazaki, Y., and Hirai, H. (1995). The proto-oncogene product c-Cbl becomes tyrosine phosphorylated by stimulation with GM-CSF or Epo and constitutively binds to the SH3 domain of Grb2/Ash in human hematopoietic cells. J Biol Chem *270*, 10800-10805.

19. Park, R.K., Kyono, W.T., Liu, Y., and Durden, D.L. (1998). Cbl-Grb2 interaction in myeloid immunoreceptor tyrosine activation motif signaling. J Immunol *160*, 5018-5027.

20. Moeller, S.J., Head, E.D., and Sheaff, R.J. (2003). p27Kip1 inhibition of Grb2-Sos formation can regulate Ras activation. Mol Cell Biol *23*, 3735-3752.

21. Reuther, G.W., and Der, C.J. (2000). The Ras branch of small GTPases: Ras family members don't fall far from the tree. Curr Opin Cell Biol *12*, 157-165.

22. Robinson, M.J., and Cobb, M.H. (1997). Mitogen-activated protein kinase pathways. Curr Opin Cell Biol *9*, 180-186.

23. Cunnick, J.M., Meng, S., Ren, Y., Desponts, C., Wang, H.G., Djeu, J.Y., and Wu, J. (2002). Regulation of the mitogen-activated protein kinase signaling pathway by Shp2. J Biol Chem *277*, 9498-9504.

24. Gu, H., and Neel, B.G. (2003). The "Gab" in signal transduction. Trends Cell Biol *13*, 122-130.

25. Araki, T., Nawa, H., and Neel, B.G. (2003). Tyrosyl phosphorylation of Shp2 is required for normal ERK activation in response to some, but not all, growth factors. J Biol Chem *278*, 41677-41684.

26. Kim, D., and Chung, J. (2002). Akt: versatile mediator of cell survival and beyond. J Biochem Mol Biol *35*, 106-115.

27. Vallee, R.B., Herskovits, J.S., Aghajanian, J.G., Burgess, C.C., and Shpetner, H.S. (1993). Dynamin, a GTPase involved in the initial stages of endocytosis. Ciba Found Symp *176*, 185-193; discussion 193-187.

28. Herskovits, J.S., Burgess, C.C., Obar, R.A., and Vallee, R.B. (1993). Effects of mutant rat dynamin on endocytosis. J Cell Biol *122*, 565-578.

29. Ravid, T., Heidinger, J.M., Gee, P., Khan, E.M., and Goldkorn, T. (2004). c-Cbl-mediated ubiquitinylation is required for epidermal growth factor receptor exit from the early endosomes. J Biol Chem *279*, 37153-37162.

30. Buday, L., and Downward, J. (1993). Epidermal growth factor regulates p21ras through the formation of a complex of receptor, Grb2 adapter protein, and Sos nucleotide exchange factor. Cell *73*, 611-620.

31. Aronheim, A., Engelberg, D., Li, N., al-Alawi, N., Schlessinger, J., and Karin, M. (1994). Membrane targeting of the nucleotide exchange factor Sos is sufficient for activating the Ras signaling pathway. Cell *78*, 949-961.

32. Holsinger, L.J., Spencer, D.M., Austin, D.J., Schreiber, S.L., and Crabtree, G.R. (1995). Signal transduction in T lymphocytes using a conditional allele of Sos. Proc Natl Acad Sci USA *92*, 9810-9814.

33. Quilliam, L.A., Huff, S.Y., Rabun, K.M., Wei, W., Park, W., Broek, D., and Der, C.J. (1994). Membrane-targeting potentiates guanine nucleotide exchange factor CDC25 and Sos1 activation of Ras transforming activity. Proc Natl Acad Sci USA *91*, 8512-8516.

34. Zhao, C., Du, G., Skowronek, K., Frohman, M.A., and Bar-Sagi, D. (2007). Phospholipase D2-generated phosphatidic acid couples EGFR stimulation to Ras activation by Sos. Nat Cell Biol *9*, 706-712.

35. Wittekind, M., Mapelli, C., Lee, V., Goldfarb, V., Friedrichs, M.S., Meyers, C.A., and Mueller, L. (1997). Solution structure of the Grb2 N-terminal SH3 domain complexed with a ten-residue peptide derived from Sos: direct refinement against NOEs, J-couplings and 1H and 13C chemical shifts. J Mol Biol *267*, 933-952.

36. Gale, N.W., Kaplan, S., Lowenstein, E.J., Schlessinger, J., and Bar-Sagi, D. (1993). Grb2 mediates the EGF-dependent activation of guanine nucleotide exchange on Ras. Nature *363*, 88-92.

37. Kohda, D., Terasawa, H., Ichikawa, S., Ogura, K., Hatanaka, H., Mandiyan, V., Ullrich, A., Schlessinger, J., and Inagaki, F. (1994). Solution structure and ligand-binding site of the carboxy-terminal SH3 domain of Grb2. Structure *2*, 1029-1040.

38. Wittekind, M., Mapelli, C., Farmer, B.T., 2nd, Suen, K.L., Goldfarb, V., Tsao, J., Lavoie, T., Barbacid, M., Meyers, C.A., and Mueller, L. (1994). Orientation of peptide fragments from Sos proteins bound to the N-terminal SH3 domain of Grb2 determined by NMR spectroscopy. Biochemistry *33*, 13531-13539.

39. Goudreau, N., Cornille, F., Duchesne, M., Parker, F., Tocque, B., Garbay, C., and Roques, B.P. (1994). NMR structure of the N-terminal SH3 domain of Grb2 and its complex with a proline-rich peptide from Sos. Nat Struct Biol *1*, 898-907.

40. Terasawa, H., Kohda, D., Hatanaka, H., Tsuchiya, S., Ogura, K., Nagata, K., Ishii, S., Mandiyan, V., Ullrich, A., Schlessinger, J., and et al. (1994). Structure of the N-terminal SH3 domain of Grb2 complexed with a peptide from the guanine nucleotide releasing factor Sos. Nat Struct Biol *1*, 891-897.

41. McDonald, C.B., Seldeen, K.L., Deegan, B.J., and Farooq, A. (2008). Structural basis of the differential binding of the SH3 domains of Grb2 adaptor to the guanine nucleotide exchange factor Sos1. Arch Biochem Biophys *479*, 52-62.

42. Yu, H., Chen, J.K., Feng, S., Dalgarno, D.C., Brauer, A.W., and Schreiber, S.L. (1994). Structural basis for the binding of proline-rich peptides to SH3 domains. Cell *76*, 933-945.

43. Kato, J.Y., Takeya, T., Grandori, C., Iba, H., Levy, J.B., and Hanafusa, H. (1986). Amino acid substitutions sufficient to convert the nontransforming p60c-src protein to a transforming protein. Mol Cell Biol *6*, 4155-4160.

44. Li, S., Couvillon, A.D., Brasher, B.B., and Van Etten, R.A. (2001). Tyrosine phosphorylation of Grb2 by Bcr/Abl and epidermal growth factor receptor: a novel regulatory mechanism for tyrosine kinase signaling. Embo J *20*, 6793-6804.

45. Broek, D., Toda, T., Michaeli, T., Levin, L., Birchmeier, C., Zoller, M., Powers, S., and Wigler, M. (1987). The S. Cerevisiae CDC25 gene product regulates the Ras/adenylate cyclase pathway. Cell *48*, 789-799.

46. Boguski, M.S., and McCormick, F. (1993). Proteins regulating Ras and its relatives. Nature *366*, 643-654.

47. Lai, C.C., Boguski, M., Broek, D., and Powers, S. (1993). Influence of guanine nucleotides on complex formation between Ras and CDC25 proteins. Mol Cell Biol *13*, 1345-1352.

48. Nimnual, A.S., Yatsula, B.A., and Bar-Sagi, D. (1998). Coupling of Ras and Rac guanosine triphosphatases through the Ras exchanger Sos. Science *279*, 560-563.

49. Sondermann, H., Nagar, B., Bar-Sagi, D., and Kuriyan, J. (2005). Computational docking and solution x-ray scattering predict a membrane-interacting role for the histone domain of the Ras activator son of sevenless. Proc Natl Acad Sci USA *102*, 16632-16637.

50. Nimnual, A., and Bar-Sagi, D. (2002). The two hats of Sos. Sci STKE *2002*, PE36.

51. Scita, G., Nordstrom, J., Carbone, R., Tenca, P., Giardina, G., Gutkind, S., Bjarnegard, M., Betsholtz, C., and Di Fiore, P.P. (1999). EPS8 and E3B1 transduce signals from Ras to Rac. Nature *401*, 290-293.

52. Mettouchi, A., Klein, S., Guo, W., Lopez-Lago, M., Lemichez, E., Westwick, J.K., and Giancotti, F.G. (2001). Integrin-specific activation of Rac controls progression through the G(1) phase of the cell cycle. Mol Cell *8*, 115-127.

53. Quilliam, L.A., Rebhun, J.F., and Castro, A.F. (2002). A growing family of guanine nucleotide exchange factors is responsible for activation of Ras-family GTPases. Prog Nucleic Acid Res Mol Biol *71*, 391-444.

54. Boriack-Sjodin, P.A., Margarit, S.M., Bar-Sagi, D., and Kuriyan, J. (1998). The structural basis of the activation of Ras by Sos. Nature *394*, 337-343.

55. Margarit, S.M., Sondermann, H., Hall, B.E., Nagar, B., Hoelz, A., Pirruccello, M., Bar-Sagi, D., and Kuriyan, J. (2003). Structural evidence for feedback activation by Ras.GTP of the Ras-specific nucleotide exchange factor Sos. Cell *112*, 685-695.

56. Freedman, T.S., Sondermann, H., Friedland, G.D., Kortemme, T., Bar-Sagi, D., Marqusee, S., and Kuriyan, J. (2006). A Ras-induced conformational switch in the Ras activator Son of sevenless. Proc Natl Acad Sci USA *103*, 16692-16697.

57. Li, Y., Asuri, S., Rebhun, J.F., Castro, A.F., Paranavitana, N.C., and Quilliam, L.A. (2006). The RAP1 guanine nucleotide exchange factor Epac2 couples cyclic AMP and Ras signals at the plasma membrane. J Biol Chem *281*, 2506-2514.

58. Liao, Y., Satoh, T., Gao, X., Jin, T.G., Hu, C.D., and Kataoka, T. (2001). RA-GEF-1, a guanine nucleotide exchange factor for Rap1, is activated by translocation induced by association with Rap1*GTP and enhances Rap1-dependent B-Raf activation. J Biol Chem *276*, 28478-28483.

59. Gasteiger, E., Hoogland, C., Gattiker, A., Duvaud, S., Wilkins, M.R., Appel, R.D., and Bairoch, A. (2005). Protein Identification and Analysis Tools on the ExPASy Server. In The Proteomics Protocols Handbook, J.M. Walker, ed. (Humana Press), pp. 571-607.

60. Leavitt, S., and Freire, E. (2001). Direct measurement of protein binding energetics by isothermal titration calorimetry. Curr Opin Struct Biol *11*, 560-566.

61. Cliff, M.J., and Ladbury, J.E. (2003). A survey of the year 2002 literature on applications of isothermal titration calorimetry. J Mol Recognit *16*, 383-391.

62. Marti-Renom, M.A., Stuart, A.C., Fiser, A., Sanchez, R., Melo, F., and Sali, A. (2000). Comparative protein structure modeling of genes and genomes. Annu Rev Biophys Biomol Struct *29*, 291-325.

63. Carson, M. (1991). Ribbons 2.0. J Appl Crystallogr *24*, 958-961.

64. Lebowitz, J., Lewis, M.S., and Schuck, P. (2002). Modern analytical ultracentrifugation in protein science: a tutorial review. Protein Sci *11*, 2067-2079.

65. Edgcomb, S.P., and Murphy, K.P. (2000). Structural energetics of protein folding and binding. Curr Opin Biotechnol *11*, 62-66.

66. Murphy, K.P., and Freire, E. (1992). Thermodynamics of structural stability and cooperative folding behavior in proteins. Adv Protein Chem *43*, 313-361.

67. Xie, D., and Freire, E. (1994). Molecular basis of cooperativity in protein folding. V. Thermodynamic and structural conditions for the stabilization of compact denatured states. Proteins *19*, 291-301.

68. Spolar, R.S., and Record, M.T., Jr. (1994). Coupling of local folding to site-specific binding of proteins to DNA. Science *263*, 777-784.

69. Fraczkiewicz, R., and Braun, W. (1998). Exact and efficient analytical calculation of the accesible surface area and their gradients for macromolecules. J Comp Chem *19*, 319-333.

70. McPhail, D., and Cooper, A. (1997). Thermodynamics and kinetics of dissociation of ligand-induced dimers of vancomycin antibiotics. J Chem Soc Faraday Trans *93*, 2283-2289.

71. Burrows, S.D., Doyle, M.L., Murphy, K.P., Franklin, S.G., White, J.R., Brooks, I., McNulty, D.E., Scott, M.O., Knutson, J.R., Porter, D., and et al. (1994). Determination of the monomer-dimer equilibrium of interleukin-8 reveals it is a monomer at physiological concentrations. Biochemistry *33*, 12741-12745.

72. Cooper, A. (1998). Microcalorimetry of protein-protein interactions. In biocalorimetry: applications of calorimetry in the biological sciences, B.Z. Chowdhry, ed. (New York: John Wiley & Sons Ltd), pp. 103-111.

73. Siebert, X., and Amzel, L.M. (2004). Loss of translational entropy in molecular associations. Proteins *54*, 104-115.

74. Murphy, K.P., Xie, D., Thompson, K.S., Amzel, L.M., and Freire, E. (1994). Entropy in biological binding processes: estimation of translational entropy loss. Proteins *18*, 63-67.

75. Tamura, A., and Privalov, P.L. (1997). The entropy cost of protein association. J Mol Biol *273*, 1048-1060.

76. Murphy, K.P. (1999). Predicting binding energetics from structure: looking beyond DeltaG degrees. Med Res Rev *19*, 333-339.

77. Murphy, K.P., Bhakuni, V., Xie, D., and Freire, E. (1992). Molecular basis of co-operativity in protein folding. III. Structural identification of cooperative folding units and folding intermediates. J Mol Biol *227*, 293-306.

78. Privalov, P.L., and Gill, S.J. (1988). Stability of protein structure and hydrophobic interaction. Adv Protein Chem *39*, 191-234.

79. Spolar, R.S., Ha, J.H., and Record, M.T., Jr. (1989). Hydrophobic effect in protein folding and other noncovalent processes involving proteins. Proc Natl Acad Sci U S A *86*, 8382-8385.

80. Ladbury, J.E., Wright, J.G., Sturtevant, J.M., and Sigler, P.B. (1994). A thermodynamic study of the trp repressor-operator interaction. J. Mol. Biol. *238*, 669-681.

81. Privalov, P.L., and Makhatadze, G.I. (1992). Contribution of hydration and non-covalent interactions to the heat capacity effect on protein unfolding. J Mol Biol *224*, 715-723.

82. Spolar, R.S., Livingstone, J.R., and Record, M.T., Jr. (1992). Use of liquid hydrocarbon and amide transfer data to estimate contributions to thermodynamic functions of protein folding from the removal of nonpolar and polar surface from water. Biochemistry *31*, 3947-3955.

83. Freire, E. (1993). Structural thermodynamics: prediction of protein stability and protein binding affinities. Arch Biochem Biophys *303*, 181-184.

84. Yuzawa, S., Yokochi, M., Hatanaka, H., Ogura, K., Kataoka, M., Miura, K., Mandiyan, V., Schlessinger, J., and Inagaki, F. (2001). Solution structure of Grb2 reveals extensive flexibility necessary for target recognition. J Mol Biol *306*, 527-537.

85. Schiering, N., Casale, E., Caccia, P., Giordano, P., and Battistini, C. (2000). Dimer formation through domain swapping in the crystal structure of the Grb2-SH2-Ac-pYVNV complex. Biochemistry *39*, 13376-13382.

86. Nioche, P., Liu, W.Q., Broutin, I., Charbonnier, F., Latreille, M.T., Vidal, M., Roques, B., Garbay, C., and Ducruix, A. (2002). Crystal structures of the SH2 domain of Grb2: highlight on the binding of a new high-affinity inhibitor. J Mol Biol *315*, 1167-1177.

87. Benfield, A.P., Whiddon, B.B., Clements, J.H., and Martin, S.F. (2007). Structural and energetic aspects of Grb2-SH2 domain-swapping. Arch Biochem Biophys *462*, 47-53.

88. Wiseman, T., Williston, S., Brandts, J.F., and Lin, L.N. (1989). Rapid measurement of binding constants and heats of binding using a new titration calorimeter. Anal. Biochem. *179*, 131-137.

89. Chaires, J.B. (1996). Dissecting the free energy of drug binding to DNA. Anticancer Drug Des *11*, 569-580.

90. Record, M.T., Jr., Lohman, M.L., and De Haseth, P. (1976). Ion effects on ligand-nucleic acid interactions. J Mol Biol *107*, 145-158.

91. Wyman, J., Jr. (1964). Linked functions and reciprocal effects in hemoglobin: a second look. Adv Protein Chem *19*, 223-286.

92. Lohman, T.M., and Mascotti, D.P. (1992). Thermodynamics of ligand-nucleic acid interactions. Methods Enzymol *212*, 400-424.

93. Koradi, R., Billeter, M., and Wuthrich, K. (1996). MOLMOL: a program for display and analysis of macromolecular structures. J Mol Graph *14*, 51-55.

94. Baker, B.M., and Murphy, K.P. (1998). Prediction of binding energetics from structure using empirical parameterization. Methods Enzymol *295*, 294-315.

95. Lee, K.H., Xie, D., Freire, E., and Amzel, L.M. (1994). Estimation of changes in side chain configurational entropy in binding and folding: general methods and application to helix formation. Proteins *20*, 68-84.

96. Mayer, B.J., Hamaguchi, M., and Hanafusa, H. (1988). A novel viral oncogene with structural similarity to phospholipase C. Nature *332*, 272-275.

97. Lim, W.A., Richards, F.M., and Fox, R.O. (1994). Structural determinants of peptide-binding orientation and of sequence specificity in SH3 domains. Nature *372*, 375-379.

98. Sparks, A.B., Rider, J.E., Hoffman, N.G., Fowlkes, D.M., Quillam, L.A., and Kay, B.K. (1996). Distinct ligand preferences of Src homology 3 domains from Src, Yes, Abl, Cortactin, p53bp2, PLCgamma, Crk, and Grb2. Proc Natl Acad Sci U S A *93*, 1540-1544.

99. Cesareni, G., Panni, S., Nardelli, G., and Castagnoli, L. (2002). Can we infer peptide recognition specificity mediated by SH3 domains? FEBS Lett *513*, 38-44.

100. Arold, S., O'Brien, R., Franken, P., Strub, M.P., Hoh, F., Dumas, C., and Ladbury, J.E. (1998). RT loop flexibility enhances the specificity of Src family SH3 domains for HIV-1 Nef. Biochemistry *37*, 14683-14691.

101. Wang, C., Pawley, N.H., and Nicholson, L.K. (2001). The role of backbone motions in ligand binding to the c-Src SH3 domain. J Mol Biol *313*, 873-887.

102. Renzoni, D.A., Pugh, D.J., Siligardi, G., Das, P., Morton, C.J., Rossi, C., Waterfield, M.D., Campbell, I.D., and Ladbury, J.E. (1996). Structural and thermodynamic characterization of the interaction of the SH3 domain from Fyn with the proline-rich binding site on the p85 subunit of PI3-kinase. Biochemistry *35*, 15646-15653.

103. Ferreon, J.C., and Hilser, V.J. (2003). The effect of the polyproline II (PPII) conformation on the denatured state entropy. Protein Sci *12*, 447-457.

104. Ferreon, J.C., and Hilser, V.J. (2003). Ligand-induced changes in dynamics in the RT loop of the C-terminal SH3 domain of Sem-5 indicate cooperative conformational coupling. Protein Sci *12*, 982-996.

105. Ferreon, J.C., and Hilser, V.J. (2004). Thermodynamics of binding to SH3 domains: the energetic impact of polyproline II (PII) helix formation. Biochemistry *43*, 7787-7797.

106. Tong, A.H., Drees, B., Nardelli, G., Bader, G.D., Brannetti, B., Castagnoli, L., Evangelista, M., Ferracuti, S., Nelson, B., Paoluzi, S., Quondam, M., Zucconi, A., Hogue, C.W., Fields, S., Boone, C., and Cesareni, G. (2002). A combined experimental and computational strategy to define protein interaction networks for peptide recognition modules. Science *295*, 321-324.

107. Panni, S., Dente, L., and Cesareni, G. (2002). In vitro evolution of recognition specificity mediated by SH3 domains reveals target recognition rules. J Biol Chem *277*, 21666-21674.

108. Brannetti, B., Via, A., Cestra, G., Cesareni, G., and Helmer-Citterich, M. (2000). SH3-SPOT: an algorithm to predict preferred ligands to different members of the SH3 gene family. J Mol Biol *298*, 313-328.

109. Ghose, R., Shekhtman, A., Goger, M.J., Ji, H., and Cowburn, D. (2001). A novel, specific interaction involving the Csk SH3 domain and its natural ligand. Nat Struct Biol *8*, 998-1004.

110. Mayer, B.J. (2001). SH3 domains: complexity in moderation. J Cell Sci *114*, 1253-1263.

111. Zarrinpar, A., Bhattacharyya, R.P., and Lim, W.A. (2003). The structure and function of proline recognition domains. Sci STKE *2003*, RE8.

112. Feng, S., Chen, J.K., Yu, H., Simon, J.A., and Schreiber, S.L. (1994). Two binding orientations for peptides to the Src SH3 domain: development of a general model for SH3-ligand interactions. Science *266*, 1241-1247.

113. Kami, K., Takeya, R., Sumimoto, H., and Kohda, D. (2002). Diverse recognition of non-PxxP peptide ligands by the SH3 domains from p67(phox), Grb2 and Pex13p. Embo J *21*, 4268-4276.

114. Lee, C.H., Leung, B., Lemmon, M.A., Zheng, J., Cowburn, D., Kuriyan, J., and Saksela, K. (1995). A single amino acid in the SH3 domain of Hck determines its high affinity and specificity in binding to HIV-1 Nef protein. Embo J *14*, 5006-5015.

115. Lee, C.H., Saksela, K., Mirza, U.A., Chait, B.T., and Kuriyan, J. (1996). Crystal structure of the conserved core of HIV-1 Nef complexed with a Src family SH3 domain. Cell *85*, 931-942.

116. Moarefi, I., LaFevre-Bernt, M., Sicheri, F., Huse, M., Lee, C.H., Kuriyan, J., and Miller, W.T. (1997). Activation of the Src-family tyrosine kinase Hck by SH3 domain displacement. Nature *385*, 650-653.

117. Berry, D.M., Nash, P., Liu, S.K., Pawson, T., and McGlade, C.J. (2002). A high-affinity Arg-X-X-Lys SH3 binding motif confers specificity for the interaction between Gads and SLP-76 in T cell signaling. Curr Biol *12*, 1336-1341.

118. Harkiolaki, M., Lewitzky, M., Gilbert, R.J., Jones, E.Y., Bourette, R.P., Mouchiroud, G., Sondermann, H., Moarefi, I., and Feller, S.M. (2003). Structural basis for SH3 domain-mediated high-affinity binding between Mona/Gads and SLP-76. Embo J *22*, 2571-2582.

119. Liu, Q., Berry, D., Nash, P., Pawson, T., McGlade, C.J., and Li, S.S. (2003). Structural basis for specific binding of the Gads SH3 domain to an RxxK motif-containing SLP-76 peptide: a novel mode of peptide recognition. Mol Cell *11*, 471-481.

120. Geisler, S.B., Robinson, D., Hauringa, M., Raeker, M.O., Borisov, A.B., Westfall, M.V., and Russell, M.W. (2007). Obscurin-like 1, OBSL1, is a novel cytoskeletal protein related to obscurin. Genomics *89*, 521-531.

121. Chang, B., Mandal, M.N., Chavali, V.R., Hawes, N.L., Khan, N.W., Hurd, R.E., Smith, R.S., Davisson, M.L., Kopplin, L., Klein, B.E., Klein, R., Iyengar, S.K., Heckenlively, J.R., and Ayyagari, R. (2008). Age-related retinal degeneration (arrd2) in a novel mouse model due to a nonsense mutation in the Mdm1 gene. Hum Mol Genet *17*, 3929-3941.

122. Bodfish, P., Warne, D., Nyberg, K., and Spurr, N.K. (1992). Dinucleotide repeat polymorphism at the human erythroid alpha-spectrin (SPTA1) mRNA gene detected using PCR. Hum Mol Genet *1*, 287.

123. Hentati, A., Hu, P., Asgharzadeh, S., and Siddique, T. (1992). Dinucleotide repeat polymorphism at the human erythroid alpha spectrin (SPTA1) locus. Hum Mol Genet *1*, 218.

124. Kurosawa, N., Chen, G.Y., Kadomatsu, K., Ikematsu, S., Sakuma, S., and Muramatsu, T. (2001). Glypican-2 binds to midkine: the role of glypican-2 in neuronal cell adhesion and neurite outgrowth. Glycoconj J *18*, 499-507.

125. Schlaepfer, D.D., Hanks, S.K., Hunter, T., and van der Geer, P. (1994). Integrin-mediated signal transduction linked to Ras pathway by Grb2 binding to focal adhesion kinase. Nature *372*, 786-791.

126. Chook, Y.M., Gish, G.D., Kay, C.M., Pai, E.F., and Pawson, T. (1996). The Grb2-mSos1 complex binds phosphopeptides with higher affinity than Grb2. J Biol Chem *271*, 30472-30478.

127. Sondermann, H., Soisson, S.M., Boykevisch, S., Yang, S.S., Bar-Sagi, D., and Kuriyan, J. (2004). Structural analysis of autoinhibition in the Ras activator Son of sevenless. Cell *119*, 393-405.